AD-A106 733 AIR FORCE INST OF TECH WRIGHT-PATTERSON AFB OH F/G 4/1
A CLIMATE INDEX DERIVED FROM SATELLITE MEASURED SPECTRAL INFRAR--ETC(U)
APR 81 M D ABEL
UNCLASSIFIED AFIT-CI-81-46D NL

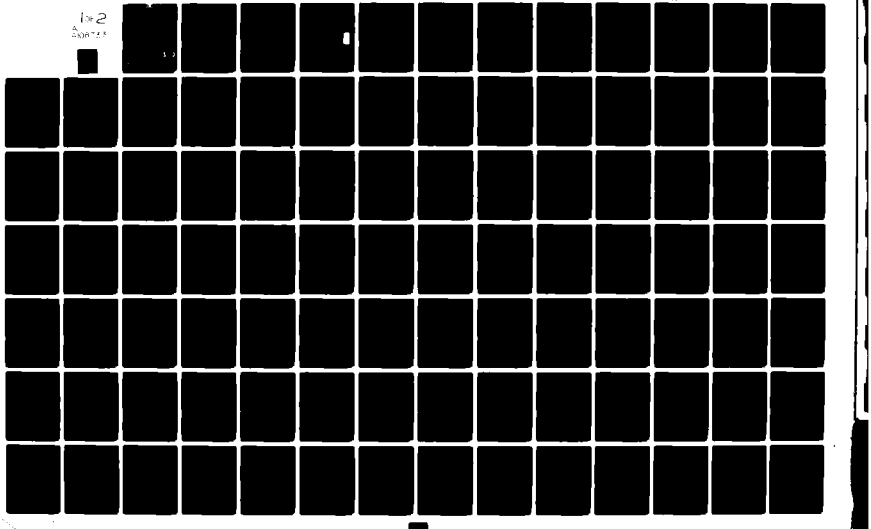

AD A106733

LEVEL II

UNCLASS
SECURITY CLASSIFICATION OF THIS PAGE (When Data Entered)

REPORT DOCUMENTATION PAGE

READ INSTRUCTIONS BEFORE COMPLETING FORM

1. REPORT NUMBER: 81-46D	2. GOVT ACCESSION NO.: AD-A106733
3. RECIPIENT'S CATALOG NUMBER:	
4. TITLE (and Subtitle): A Climate Index Derived From Satellite Measured Spectral Infrared Radiation (14) AFIT-CI-81-46D	5. TYPE OF REPORT & PERIOD COVERED: THESIS/DISSERTATION
	6. PERFORMING ORG. REPORT NUMBER:
7. AUTHOR(s): (10) Michael David/Abel	8. CONTRACT OR GRANT NUMBER(s): (9) Doctoral thesis
9. PERFORMING ORGANIZATION NAME AND ADDRESS: AFIT STUDENT AT: Colorado State University	10. PROGRAM ELEMENT, PROJECT, TASK AREA & WORK UNIT NUMBERS: 2917601
11. CONTROLLING OFFICE NAME AND ADDRESS: AFIT/NR, WPAFB OH 45433	12. REPORT DATE: (11) Apr 1981
	13. NUMBER OF PAGES: 142
14. MONITORING AGENCY NAME & ADDRESS (if different from Controlling Office):	15. SECURITY CLASS. (of this report): UNCLASS
	15a. DECLASSIFICATION DOWNGRADING SCHEDULE:

16. DISTRIBUTION STATEMENT (of this Report)

APPROVED FOR PUBLIC RELEASE; DISTRIBUTION UNLIMITED

17. DISTRIBUTION STATEMENT (of the abstract entered in Block 20, if different from Report)

16 OCT 1981

Air Force Institute of Technology (ATC)
Wright-Patterson AFB, OH 45433

Fredric C. Lynch

FREDRIC C. LYNCH, Major, USAF
Director of Public Affairs

18. SUPPLEMENTARY NOTES

APPROVED FOR PUBLIC RELEASE: IAW AFR 190-17

19. KEY WORDS (Continue on reverse side if necessary and identify by block number)

DTIC ELECTE S NOV 6 1981 D

20. ABSTRACT (Continue on reverse side if necessary and identify by block number)

ATTACHED

A

81 10 27 259

012200 JOB

DD FORM 1 JAN 73 1473 EDITION OF 1 NOV 65 IS OBSOLETE

UNCLASS
SECURITY CLASSIFICATION OF THIS PAGE (When Data Entered)

DTIC FILE COPY

ABSTRACT

Michael David Abel; A Climate Index Derived from Satellite Measured Spectral Infrared Radiation, Captain, USAF, Air Weather Service, 1981, 143 pp., Ph.D. Thesis, Dept. of Atmos. Sci., Colo. State Univ. Sources: Main Library or Atmos. Science Dept. Library, Colo. State Univ., Ft. Collins, CO.; Air Weather Service Technical Library, Scott, AFB, IL.

This thesis introduces a climate index based on radiative transfer theory and derived from the spectral radiances typically used to retrieve temperature profiles. It is assumed that clouds and climate are closely related and a change in one will result in a change in the other. Because the index developed in this paper is primarily a function of the cloud distribution and also dependent upon temperature and moisture distributions, it may be used as a climate index. The advantage is that the index is more accurately retrieved from satellite data than cloudiness per se. This index, hereafter referred to as the VIRES index (for Vertical Infrared Radiative Emitting Structure), is based upon the shape and relative magnitude of the broadband weighting function of the infrared radiative transfer equation. The broadband weighting curves (VIRES curves) are retrieved from simulated satellite infrared sounder data (spectral radiances). The VIRES index is a useful means of classifying the VIRES curves. This thesis describes the retrieval procedure and investigates error sensitivities of this method. Advantages of the approach include; day and night capability, no need to know cloud radiative properties, retrieval ability when cloud fraction or cloud emittance is less than 1.0, retrieved information below sensor resolution, minimum influence on the index from low tropospheric retrieval errors, and the ability to statistically discriminate between VIRES curves retrieved from different scenes. Operational VIRES index retrieval strategies and a number of specific applications are also proposed.

AFIT RESEARCH ASSESSMENT

The purpose of this questionnaire is to ascertain the value and/or contribution of research accomplished by students or faculty of the Air Force Institute of Technology (ATC). It would be greatly appreciated if you would complete the following questionnaire and return it to:

AFIT/NR
Wright-Patterson AFB OH 45433

RESEARCH TITLE: A Climate Index Derived From Satellite Measured Spectral Infrared Radiation

AUTHOR: Michael David Abel

RESEARCH ASSESSMENT QUESTIONS:

1. Did this research contribute to a current Air Force project?

( ) a. YES ( ) b. NO

2. Do you believe this research topic is significant enough that it would have been researched (or contracted) by your organization or another agency if AFIT had not?

( ) a. YES ( ) b. NO

3. The benefits of AFIT research can often be expressed by the equivalent value that your agency achieved/received by virtue of AFIT performing the research. Can you estimate what this research would have cost if it had been accomplished under contract or if it had been done in-house in terms of manpower and/or dollars?

( ) a. MAN-YEARS _____ ( ) b. $_____

4. Often it is not possible to attach equivalent dollar values to research, although the results of the research may, in fact, be important. Whether or not you were able to establish an equivalent value for this research (3. above), what is your estimate of its significance?

( ) a. HIGHLY SIGNIFICANT ( ) b. SIGNIFICANT ( ) c. SLIGHTLY SIGNIFICANT ( ) d. OF NO SIGNIFICANCE

5. AFIT welcomes any further comments you may have on the above questions, or any additional details concerning the current application, future potential, or other value of this research. Please use the bottom part of this questionnaire for your statement(s).

NAME GRADE POSITION

ORGANIZATION LOCATION

STATEMENT(s):

FOLD DOWN ON OUTSIDE - SEAL WITH TAPE

AFIT/NR
WRIGHT-PATTERSON AFB OH 45433

OFFICIAL BUSINESS
PENALTY FOR PRIVATE USE. $300

NO POSTAGE
NECESSARY
IF MAILED
IN THE
UNITED STATES

BUSINESS REPLY MAIL
FIRST CLASS PERMIT NO. 73236 WASHINGTON D.C.

POSTAGE WILL BE PAID BY ADDRESSEE

AFIT/ DAA
Wright-Patterson AFB OH 45433

FOLD IN

81-46D

THESIS

A CLIMATE INDEX DERIVED FROM SATELLITE MEASURED SPECTRAL INFRARED RADIATION

Submitted by

Michael David Abel

Department of Atmospheric Science

In partial fulfillment of the requirements

for the Degree of Doctor of Philosophy

Colorado State University

Fort Collins, Colorado

Spring, 1981

COLORADO STATE UNIVERSITY

April 1 , 1981

WE HEREBY RECOMMEND THAT THE THESIS PREPARED UNDER OUR SUPERVISION

BY Michael David Abel

ENTITLED A CLIMATE INDEX DERIVED FROM SATELLITE MEASURED SPECTRAL INFRARED RADIATION

BE ACCEPTED AS FULFILLING IN PART REQUIREMENTS FOR THE DEGREE OF

Doctor of Philosophy

Committee on Graduate Work

Thomas H. Vonder Haar

Paul W. Mueller

Peter C. Sinclair

Stephen K. Cox

Adviser

ABSTRACT OF THESIS

A CLIMATE INDEX DERIVED FROM SATELLITE MEASURED SPECTRAL INFRARED RADIATION

This thesis introduces a climate index based on radiative transfer theory and derived from the spectral radiances typically used to retrieve temperature profiles. It is assumed that clouds and climate are closely related and a change in one will result in a change in the other. Because the index developed in this paper is a function of the cloud, temperature, and moisture distributions, it may be used as a climate index. The advantage is that the index is more accurately retrieved from satellite data than cloudiness per se. This index, hereafter referred to as the VIRES index (for Vertical Infrared Radiative Emitting Structure), is based upon the shape and relative magnitude of the broadband weighting function of the infrared radiative transfer equation. The broadband weighting curves are retrieved from simulated satellite infrared sounder data (spectral radiances). This thesis describes the retrieval procedure and investigates error sensitivities of this method. It also proposes index measuring options and possible applications of the VIRES index.

Results indicate that the VIRES approach is a very effective use of satellite radiometer measurements. Retrieval advantages include; day and night capability, no need to know cloud radiative properties, retrieval ability when cloud fraction or cloud emittance is less than 1.0, minimal geometric assumptions, retrieved information below sensor resolution, and minimum influence on the index from low tropospheric retrieval errors. These advantages along with the approach of compositing scenes for an average VIRES curve greatly reduce the retrieval

sensitivity to the kind of errors found under assumed normal operating conditions. A detailed error analysis indicated that the most important error sources are instrument system noise, and ill specified temperature and humidity profiles. Accurate VIRES retrievals are illustrated under a number of different error and atmospheric conditions. Furthermore, a statistical technique used to successfully discriminate between VIRES curves derived for different atmospheric conditions is discussed.

Operational VIRES index retrieval strategies and a number of specific applications are proposed. It is suggested that the index be derived from geostationary satellite data and averaged to provide weekly regional values. These index values would be used in a regional climate monitoring mode. They would also be useful for verification of climate model generated infrared radiation to space values.

Michael David Abel, Captain USAF
Atmospheric Science Department
Colorado State University
Fort Collins, Colorado 80523
Spring, 1981

ACKNOWLEDGMENTS

This dissertation is dedicated to the idea that faith and science are logically complementary and not mutually exclusive as implied by the psalmist who wrote; "Great are the works of the Lord, studied by all those who have pleasure in them". Ps 111:2 RSV. In order to do justice to a set of events, the author believes that it is often necessary to give more than one account of it, in terms of more than one conceptual framework. Thus, scientific convictions can be constructively related to Christian beliefs.

The author wishes to extend his sincere thanks to his advisor Dr. Stephen K. Cox who provided patient guidance and advice, and who arranged for the financial means to support this research. The author also wishes to thank his graudate committee Drs. Paul Mielke, Peter Sinclair and Thomas H. Vonder Haar for their assistance and thoughtful review of this research. The author has also greatly benefitted from discussions with the members of Dr. Cox's research group, especially during project review meetings. Special thanks are due to Ms. Sandy Wunch for typing many drafts of this paper as well as the final manuscript, to Ms. Judy Sorbie for drafting the figures, and to Ms. Pauline Martin for proofreading the final manuscript.

This work has been supported in part by NASA Contract NSG 5357. The author would also like to thank the Air Force Institute of Technology for sponsoring this assignment. Finally, the author happily acknowledges the support, sacrifices, and understanding of his wife Linda and our family during this time of graduate study.

TABLE OF CONTENTS

TABLE OF CONTENTS (Continued)

LIST OF TABLES

LIST OF FIGURES

LIST OF FIGURES (Continued)

LIST OF FIGURES (Continued)

LIST OF SYMBOLS AND ACRONYMS

$B(\nu,T)$	Planck Function
b	Equation coefficient, ln b is the y intercept
c_1, c_2	Plank Function constants
C, D	Empirical constants for retrieval relationship (Equations 6 and 7)
CH_4	Methane
CO_2	Carbon dioxide
CCRC	Clear column radiance correction
COSPAR	Committee on Space Research
d.f.	Degrees of freedom
g	Acceleration due to gravity, 9.8 m s^{-2}
GARP	Global Atmospheric Research Program
GATE	GARP Atlantic Tropical Experiment
GCM	General Circulation Model
H_2O	Water vapor
H_0	Null hypothesis
HIRS	High Resolution Infrared Sounder
IR	Infrared radiation
IRIS	Infrared interferometer spectrometer
ITPR	Infrared temperature profile radiometer
k	Number of like signs, used in the Sign Test
$K(\nu,p)$	Gas mass absorption coefficient, m^2 g^{-1}
$L(\nu,\theta)$	Spectral radiance
L_{cld}	Satellite level spectral radiance from atmosphere above cloud top
L_{cs}	Satellite level spectral radiance due to clear atmosphere

LIST OF SYMBOLS AND ACRONYMS

LWC	Liquid water content, g m^{-3}
m	Equation coefficient, line's slope
N	Fraction of the sky which is cloudy
n	Total number of non zero signs, used in Sign Test
N_2O	Nitrous oxide
NCRP	National Climate Research Program
O_3	Ozone
P	Probability, used in the Sign Test
p	Pressure, mb
p_c	Cloud top pressure level
p_o	Pressure at top of atmosphere
p_s	Surface pressure
p_{wf}	Pressure at weighting function peak level
q	Gas mass mixing ratio
R	Universal gas constant
r^2	Coefficient of determination
RMS	Root mean square
RTE	Radiative transfer equation
SIRS	Satellite IR spectrometer
SW	Shortwave radiation
T	Fisher's combined probability Sign Test statistic
$T_{[p]}$	Ambient temperature profile
TD	Infrared temperature difference between surface and cloud top
VIRES	Vertical Infrared Radiative Emitting Structure
VTPR	Vertical Temperature Profile Radiometer

LIST OF SYMBOLS AND ACRONYMS

W	Gas mixing ratio
χ^2	Chi-Squared distribution
x	Independent variable
y	Dependent variable
z	Vertical distance
α	Effective fractional weighting (clear vs effective cloudy)
$\varepsilon(\nu)$	Spectral infrared emittance
ε_s	Effective infrared broadband surface emittance
θ	Solar zenith angle
λ	Wavelength, μm
ν	Wavenumber, cm^{-1}
σ	Stefan-Boltzman constant
$\tau(\nu)$	Spectral infrared transmittance
$\frac{\partial \tau}{\partial\, \ell np}$	Infrared radiative transfer equation weighting function

LIST OF SUBSCRIPTS

c	at cloud top level
cld	above cloud
cs	clear sky
o	top of atmosphere
s	surface
ν	wavenumber

I. INTRODUCTION

This paper introduces and describes a climate index called the VIRES index. VIRES (pronounced vī·rēs) is the acronym for Vertical Infrared Radiative Emitting Structure and quite by chance it is also the plural form of the Latin word vis, meaning forces or powers. Thus, the acronym seems especially appropriate since the atmosphere's VIRES is one of the major forcing factors behind the earth's climate. The VIRES index is related to the earth's climate through the earth's radiation budget and therefore, can be considered a climate index. The logic of this may be stated as follows. The climate system is determined by the energy input to the system and the distribution, transformation, and storage of energy in various forms within the system. These processes are mirrored in the components of the earth's radiation budget, one of which is the outgoing emitted thermal radiation (COSPAR Report to ICSU and JOC, 1978b). This cooling to space is described by the VIRES which is primarily a function of cloud distribution.

Atmospheric observation has been and continues to be central to the progress of atmospheric science. Better observations remain one of the needs of the discipline. The recent introduction of meteorological satellite systems has contributed significantly to the growing need of monitoring world-wide weather variables. Satellites not only have world-wide coverage capability with good horizontal and time resolution, they also have a second advantage. Large numbers of observations are made with the same instrument increasing the integrity and comparability of such measurements (Houghton, 1979). The relative if not the absolute accuracy of the satellite measurement is high. More attention

to absolute accuracy has been paid to the sounding type instruments than to any other satellite instrument, (i.e. ITPR, SIRS, IRIS).

The scientific community is still seeking the best ways to use and apply satellite data. Most of the recent successes in using satellite data in a quantitative global way in the atmospheric sciences have come in the areas of solar constant measurement and radiation budget measurements (Heath, 1973; Smith et al. 1977; Vonder Haar and Oort, 1973). Application of satellite data to these problems is fairly straightforward since the principal satellite instrument is a radiometer and the measurement is a spectral or broadband irradiance. Other important areas of research include inference of temperature and humidity profiles, as well as cloud and wind determinations from satellite radiance values. The suitability of satellite observations is reduced since the required information must be inferred from the radiance values measured remotely at the satellite and from the appropriate geometric and radiative transfer principles.

The objective of this study is to describe the Vertical Infrared Radiative Emitting Structure (VIRES) of the atmosphere by using simulated satellite spectral radiation measurements. A process is described that accomplishes this objective using specified cloud radiative properties and mean temperature and gaseous atmospheric profiles. These findings are used to examine the feasibility of using infrared radiative transfer weighting curves (which describe the atmosphere's VIRES by defining how the atmosphere cools to space) as a climate index. This index would be principally dependent on climatological cloudiness, and its variability could be regarded as an indicator of climate variance. The strength of this approach is that it deals

directly with the radiative aspect of the problem thus circumventing the need to infer specific individual clouds directly using the typical parameters of height, base, and amount. The distinction of this technique is that computationally one may be able to simply, accurately, and quickly archive the atmospheric VIRES as a manifestation of global cloudiness in a form that is useful for monitoring climate change, or for validating the statistical characteristics of cooling to space computed by climate models. Many factors account for the strong potential of this approach.

Day to day variations as well as longer period variations in the atmospheres VIRES (which is reflected in satellite measured earth radiances) are primarily caused by clouds. Many techniques using satellite data, some of which are discussed in the next section, have been developed to infer cloudiness in the standard sense. Of course any inference of clouds using such data will by definition be a kind of radiative measure of cloudiness with the drawback that specific radiative cloud properties must be assumed before results are possible. Of course it is desirable to make as few a priori assumptions as possible when analyzing the data for the purpose of obtaining reliable cloud information. By using a radiance measure of cloudiness as proposed in this paper one increases the compatibility between the satellite measurement and the quantity labeled cloudiness. Furthermore, by using a unique form of the technique commonly called the infrared sounder cloud retrieval method for a single field of view, we minimize the assumptions about the spatial scales and geometry, and about the cloud radiative properties while avoiding many time consuming calculations involving iterations through the radiative transfer equation. This new

method is used to find two curve shape parameters which define the atmosphere's VIRES in terms of the infrared weighting curve.

Following the chapter on background information, the specifics of the approach are described. For orientation purposes Figures 1a,b are provided. As described in Figure 1a the procedure starts with satellite spectral data (in this case simulated data) in the 15 μm CO_2 absorption bands and the 10-12 μm window band. These radiances contain information on the VIRES of the atmosphere. Computationally, relative importance is placed on the radiances depending upon where in the vertical most of its energy originates. By assuming known or measured gaseous and temperature profiles one may interpret the scene radiatively by solving for the weighting function peak due to radiatively specified effective clouds and the fractional weighting of a totally overcast effective cloud scene versus a totally clear scene. This scheme results in a spectral weighting curve shape specified by the two variables mentioned in Figure 1a. By design the curve shape is not dependent on the cloud radiative properties specified. For example, if a cloud covering the entire satellite-sensed scene is specified as opaque (black) when its emittance is only 0.5, the routine will compute a proper weighting function peak height (p_{wf}) due to the cloud with 0.5 fractional weighting (α). These two curve shape variables will give the correct weighting function curve, the same curve one gets from an overcast case and cloud emittance of 0.5. Of course, if one insists on interpreting the weighting function peak and fractional weighting as cloud top height and cloud fraction, the accuracy of the cloud fraction value is strongly dependent on how close the assigned cloud emittance is to the true cloud emittance.

Start with satellite spectral radiance values at 12 and 15 μm (in this paper simulated values).	Interpret a single scene radiatively. solve for Wt. Fun. Pk. Level and Fractional Wt. (clear vs. effective clouds), the two curve shape parameters.	Using the cloud shape parameters, compute the IR broadband Wt. curve (how atm. cools to space). Composite many curves for a measure of climatological cloud structure.	Statistically discriminate between curves and calculate a four number climate index, (the VIRES index).
$L_{\nu 1}, L_{\nu 2}, \ldots$	→ p_{wf}, α	→ $(\frac{\partial \bar{\tau}}{\partial \ln p}, p)$	→ 250-450-690-1

Figure 1a. Schematic diagram showing computational steps leading to the proposed atmospheric VIRES climate index.

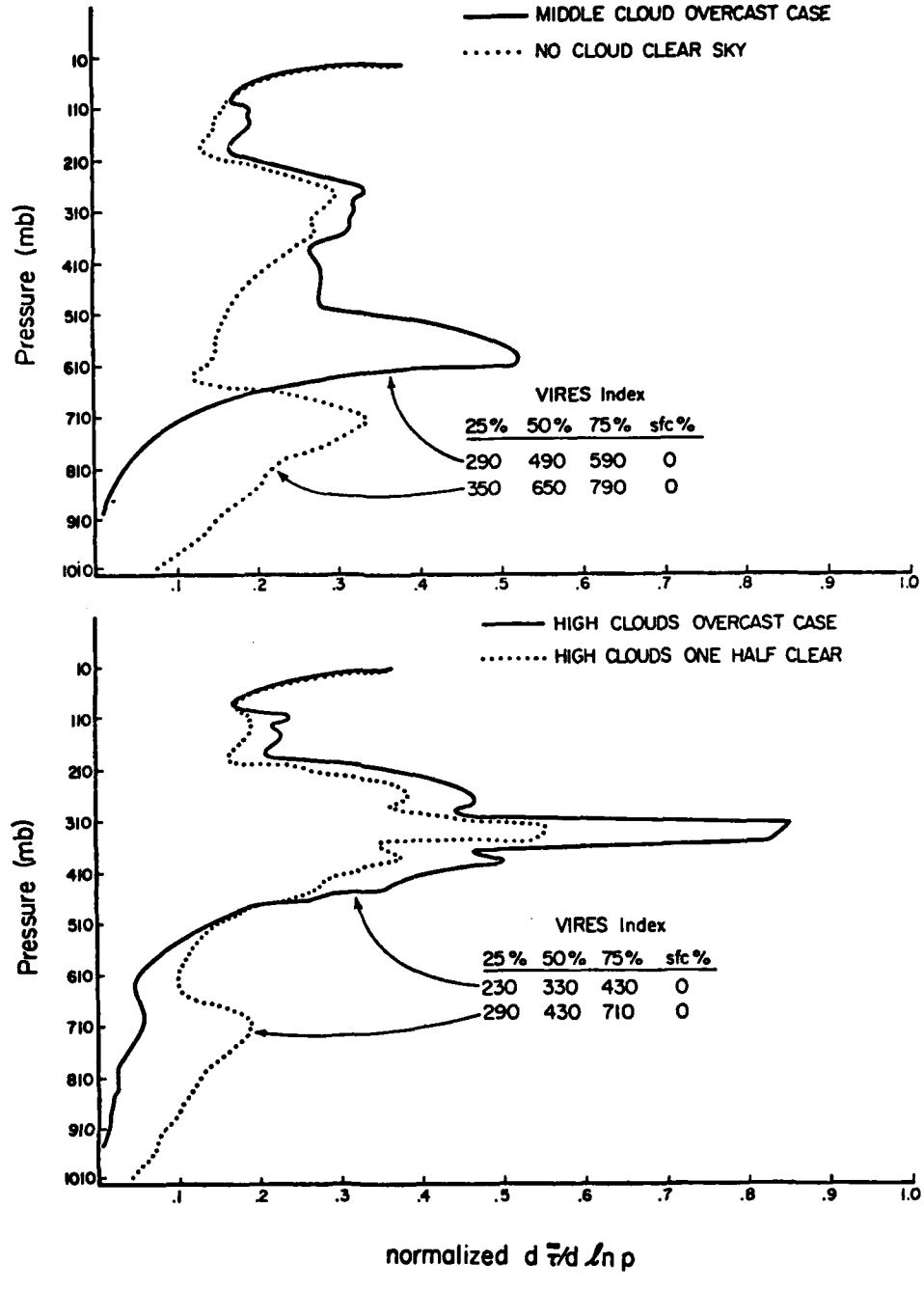

Figure 1b. Schematic diagram showing the relationship between four atmospheric cloud scenarios and the resulting VIRES curves and VIRES indices (reference Chapter VI-B).

Once the two variables determining weighting curve shape are found they may be used in a broadband transfer equation to give a broadband weighting curve (see Figure 1b). This curve combined with the respective temperature profile describes the vertical structure of atmospheric cooling to space. As a test, the value of the earth's emittance to space calculated from the derived weighting curve may be compared to a satellite measured value of the same quantity. As part of this study an error analysis is done to evaluate the influence of several assumptions on the results. In addition, the important question of time and space averaging of the quantities discussed above is also addressed. A technique for discriminating between weighting function curves, and a related climate index is discussed. Finally, the strengths and limitations of using IR broadband weighting curves as a climatic index and representation of cloudiness will be examined.

II. BACKGROUND INFORMATION

There have been many attempts to deduce cloud cover, structure, and radiative properties from satellite data. Table 1 is an outline of most of the approaches, all of which seek to define inferred cloudiness in standard terms. A short summary of the more notable research follows. However, a critique of specific approach shortcomings is not attempted.

Using visible wavelength values Miller and Feddes (1971), have related brightness measurements to cloud amount. Analysis of cloud amount and type from satellite pictures (nephanalysis) has been done using the 'eyeball' method (Clapp, 1964). Another more objective method combines pictures from two geostationary satellites to give a steroscopic view and measure of cloud height (Dalton et al. 1979). Of course these methods are limited to daylight observations and are degraded by variable and cloud look-a-like surface reflectance.

Infra-red window data combined with simplifying assumptions (which greatly reduce the accuracy and applicability) and a 'known' temperature profile when used with appropriate radiation laws will give estimates of cloud height or cloud fraction (Koffler et al. 1973). One also needs to know or estimate cloud radiative characteristics. An example of a technique that uses this type of data is the adjacent field of view method described by Smith et al. (1970). They use the derived cloud information to construct clear column radiance profiles as part of a temperature profile retrieval process. Exact cloud location is still temperature profile dependent. Another totally different approach is described by Rao (1970). He statistically relates

METHODS OF OBSERVING CLOUDS FROM SATELLITES

I. Visible Wavelength Observations

- A. Reflected Solar Radiances
  - 1. Threshold
  - 2. Weighted histogram
- B. Nephanalysis
- C. Stereoscopic

II. Infra-red Wavelength Observations

- A. Window Measurements
  - 1. Threshold
  - 2. TD
- B. CO_2 Gas Band Measurements
  - 1. Single field of view - RTE iterations
    - a. Radiance ratioing
    - b. Minimization
  - 2. Single field of view - empirical RTE*

III. Vis/IR Combined Observations

- A. Dual channel
- B. Bi-spectral
- C. 2-D histogram

*Developed and employed in this paper

Table 1. An outline of satellite cloud retrieval methods.

radiative values to differences between surface and cloud top temperatures (TD) over ocean areas. However, the most straightforward approach is to simply relate cloud top temperature and a known or assumed temperature profile (assuming one measures a single overcast cloud layer). An example of this threshold approach is the work of Cox and Griffith (1978) using GATE data. More recently Campbell et al. (1980) have used geosynchronous satellite IR window observations to produce area cloud top distribution profiles. They wish to assess the impact of the diurnal and spatial changes of these distributions on the earth-atmosphere radiation budget.

Other methods seek to improve accuracy by combining solar brightness and IR window information. However, while improving the accuracy over taking each method separately, one must be content with the limitations of both methods. A good example of this is the bi-spectral technique of Reynolds and Vonder Haar (1977) and expanded upon by Mendola and Cox (1978). They solve simultaneously a set of budget type radiative equations. They also use a method described by Shenk and Curran (1973) to improve retrieval of cirrus clouds. Other methods are often referred to as dual channel. For example, in another paper Reynolds et al. (1978) describe a technique for discriminating different cloud types by visible and IR image subtraction. A similar approach, called the 2-D histogram method, is outlined by Smith (1978). This last technique is designed to handle large quantities of data very quickly. Of course result accuracy is sacrificed for speed. However, for climatological applications the results may be useful.

Because this paper presents a technique using CO_2 gas band measurements, this approach will be discussed in greater detail below.

First it should be mentioned that there are other techniques for determining cloud characteristics from satellite measurements that do not fit neatly into the categories outlined in Table 1. For example, it may be possible in the future to use lidar techniques from space like those described by Platt (1979) for ground based units. Microwave measurements may be used with SW and/or IR measurements in a tri-channel or dual channel approach (Yeh and Liou, 1980). Following this reasoning a 3-D histogram technique has been suggested. A method using IR window and water vapor channels is being pursued by Chen et al. (1980). Finally, a technique that uses spectral infrared measurements from limb scanning is described by Taylor (1974) and by Remsberg et al. (1980).

To conclude this section the single field of view CO_2 gas band measurement technique will now be discussed. It is also referred to as the infrared sounder cloud retrieval method. This approach has many advantages. It requires the fewest a priori assumptions while providing day and night capability. However, it does have problems detecting low clouds. More details on the assumptions involved and limitations will be given later.

The IR RTE in integro-differential form represents the backbone of this method and is given below.

$$L(\nu,\theta) = \varepsilon_s(\nu)\, B(\nu, T_s)\, \tau(\nu, \theta, p_s) + \int_{\ln p_s}^{\ln p_o} B(\nu, T_{[p]}) \frac{\partial \tau(\nu, \theta, p)}{\partial \ln p}\, d \ln p \qquad (1)$$

where L is spectral radiance in W/m^2 sr cm^{-1}, θ is solar zenith angle and ε_s is surface spectral emittance usually taken to be 1 for 10-15 μm wavelengths. The Planck Function B is given below.

$$B(\nu, T) = c_1 \nu^3/[\exp(c_2\nu/T)-1]$$

where ν is wavenumber in cm^{-1}, T is temperature in °K, and c_1 and c_2 are constants. The equation for transmittance τ is given below.

$$\tau(\nu, \theta, p) = \exp[-\frac{q}{g}\int_{p_o}^{p} K(\nu,p) \sec\theta \, dp]$$

where q is the gas mass mixing ratio, g is the acceleration due to gravity, p is pressure with p_o being pressure at the top of the atmosphere and p_s being pressure at the surface, and K is the gas absorption coefficient. Also, $\frac{\partial\tau}{\partial \ln p}$ is commonly referred to as the weighting function. Equation 1 may be rewritten as Eq. (2) for the case of opaque clouds with cloud top height at p_c for cloud fraction N, and 1-N clear sky (cs).

$$L(\nu, \theta) = N\left\{B(\nu, T_c)\,\tau(\nu, \theta, p_c) + \int_{\ln p_c}^{\ln p_o} B(\nu, T_{[p]})\frac{\partial \tau}{\partial \ln p}\, d\ln p\right\}$$

$$+ (1-N)\left\{B(\nu, T_s)\,\tau(\nu, \theta, p_s) + \int_{\ln p_s}^{\ln p_o} B(\nu, T_{[p]})\frac{\partial \tau}{\partial \ln p}\, d\ln p\right\}$$

$$= N\,L_{\nu cld} + (1-N)\,L_{\nu cs} \quad . \qquad (2)$$

Two basic techniques using these equations to solve for cloud properties have been proposed. One is known as the radiance ratioing method.

It is described in Smith and Woolf (1976), McCleese and Wilson (1976), and Smith and Platt (1978). It is also used by Wielicki and Coakley (1980), who have described its applicability and limitations in detail. An outline of this method follows.

First rewrite Eq. (2) for grey clouds using the relationship $\alpha = \varepsilon_{\nu 1} N$ for a spectral radiance of wavenumber $\nu 1$.

$$L_{\nu 1} = \alpha L_{\nu 1 cld} + (1-\alpha) L_{\nu 1 cs} \tag{3}$$

where α and $L_{\nu 1 cld}$ are the unknowns and $L_{\nu 1 cld}$ depends only on p_c. Rearrange Eq. (3).

$$(L_{\nu 1} - L_{\nu 1 cs}) = \alpha (L_{\nu 1 cld} - L_{\nu 1 cs}). \tag{4}$$

To have one equation with one unknown (p_c), ratio Eq. (4) for two different wavenumber radiances and eliminate α assuming $N \varepsilon_{\nu 1} = N \varepsilon_{\nu 2}$.

$$\frac{(L_{\nu 1} - L_{\nu 1 cs})}{(L_{\nu 2} - L_{\nu 2 cs})} = \frac{(L_{\nu 1 cld} - L_{\nu 1 cs})}{(L_{\nu 2 cld} - L_{\nu 2 cs})} . \tag{5}$$

Iterate through different p_c's until the $L_{\nu 1}$ and $L_{\nu 2}$ that satisfy Eq. (5) are found. Finally take the $L_{\nu 1}$ just found and solve Eq. (4) for α.

A second method is described by Chahine (1974). It is based upon minimization of the RMS difference between the observed radiances and calculated radiances that are a function of cloud top pressure and effective cloud fraction. An iterative scheme is used to choose the cloud pressure and fraction used in the radiative transfer equation calculations. While the first technique is designed to use only two band radiances, the second method may use more than two bands. Requisite lengthy radiative transfer calculations are a disadvantage to operational use of this method.

Both of these techniques and the one developed in this paper assume the profile T(p) is known which implies the clear sky spectral radiance $L_{\nu cs}$ is known. All three methods assume spectral band emittances (ε_ν) are equal, thus the relationship $\alpha_1 = \alpha_2$ is assumed true. All three assume the clear sky spectral band weighting functions are known and are not identical to each other. All three methods assume the satellite radiance measured comes from a scene that contains only the representative grey body cloud top pressure. Measurements in either the 4.3 μm or 15 μm CO_2 band can be used. Sometimes the window channel (11 μm) is also used with the CO_2 bands even though they are widely separated in wavenumber (McCleese and Wilson, 1976). In this case, only as $\varepsilon_\nu \to 1$ does $\varepsilon_{\nu 1} = \varepsilon_{\nu 2}$ (Yamamoto et al. 1970). For this reason poor results can be expected using the window and CO_2 channels together to detect nonblack clouds. Notice that all terminology used in this paper is consistent with recommendations of the IAMAP Radiation Commission except that ν is used for wavenumber instead of κ (Raschke, 1978). The next chapter describes the third technique mentioned above.

III. SHAPE PARAMETER RETRIEVAL THEORY

As stated earlier, the basic approach used in this paper to determine the weighting function curve shape parameters is commonly called the infrared sounder cloud retrieval method for a single field of view. The commonly used procedures are described in detail by Chahine (1975) and by Smith and Platt (1978). Chapter II of this paper contains a brief review of their techniques. Because of the limited number of assumptions needed and the day-night capability, the CO_2 band approach is without question the most accurate for determining high and middle cloud information. Low cloud information in tropical atmospheres is limited primarily due to the high concentration and emittance of water vapor in the lower troposphere which masks the clouds' radiant signature. However, as will be shown this limitation is minimized by retrieving the atmospheres VIRES instead of clouds per se. A brief description of the radiative theory behind this method follows.

Equation 1 gives the IR integral form of the RTE for a plane-parallel clear sky atmosphere with no scatter under the assumption of local thermodynamic equilibrium. A plot of the variation of the transmittance with respect to pressure is called the weighting function. For radiation measured in the CO_2 absorption band or window band in the absence of clouds, the transmittance is a known function (with slight dependence on temperature and water vapor profiles) as is the weighting function.

Equation 2 represents the satellite-received spectral radiance $[L(\nu,\theta)]$ from a scene containing N fraction of radiatively black clouds. For nonblack clouds N takes on a different meaning and is replaced by

α, an effective cloud fraction (see Eq. 3). Because reflectance by black or nonblack clouds is assumed to be small compared to emittance in the IR bands of concern, effective emittance $\varepsilon(\nu)$ and transmittance $\tau(\nu)$ are related by $\varepsilon(\nu) + \tau(\nu) = 1$ for these wavenumber bands. Consequently, we may as stated above replace N with an equivalent fractional cloud cover value equal to the product $\varepsilon(\nu)\ N = \alpha$. Thus, true fractional cloud cover cannot be derived unless the cloud emittance is known.

Neglecting term $L_{\nu cs}$, which is usually calculated from assumed temperature and gas profiles, Eq. (2) has unknowns; p_c and N. If we assume $\varepsilon(\nu_1) = \varepsilon(\nu_2)\ldots$ for the wavebands of interest, then $\alpha = \varepsilon(\nu)\ N$ will be the same value in Eq. (3) written for each of the spectral radiances. We therefore, have a system of at least two equations with two unknowns, p_c and α. So far we have assumed knowledge of gaseous and temperature profiles which allow us to compute the appropriate clear sky spectral radiance $L_{\nu cs}$ and the many $L_\nu(p_c)$ values (using specified cloud radiative characteristics) used to find p_c and α. We also assume that the clouds in the scene all have approximately the same cloud top pressure level p_c. However, we do not need to assume the scene is overcast, nor is it necessary to make assumptions about adjacent scenes.

At this point the method used in this paper diverges from the so-called ratio method and minimization method described in Chapter II. Instead of using Eq. (3) that gives satellite measured radiance L_ν in terms of α, $L_{\nu cs}$, and $L_{\nu cld}$, an empirical equation with L_ν in terms of α, $L_{\nu cs}$ and p_c is derived. This step eliminates the need to solve the IR - RTE for the iteration value of $L_{\nu cld}$. The rationale is outlined

below using simulated satellite radiances. The spectral radiative transfer routine and specific wavenumber bands and cloud radiative characteristics used are described in Chapter IV.

The emphasis is on the relationship between specified effective clouds and the weighting function. With specified effective clouds present the weighting function is drastically changed. For example, Figure 2 shows the effect graphically using wavenumber 747.5 cm^{-1} (5 cm^{-1} band width) and different levels of overcast cloudiness for a typical tropical atmosphere. Cloud emittance is near 1 or is unity since thick clouds are specified using an emittance model (described later) related to specified cloud water content. Figure 3 shows the effect of effective clouds on the weighting function for different amounts of cloudiness for a tropical atmosphere. This is the same effect as changing cloud emittance to less than unity in an overcast case. In other words α is the important shape parameter ($\alpha = N\varepsilon_{\nu}$). Broadband weighting functions show the same general characteristic effects of clouds, except for low altitude effective clouds. Near the ground, water vapor (see Figure 4) acts much like a low effective cloud as far as the atmosphere's VIRES is concerned. This is particularly true in the tropics. Figures 3 and 5 show that small α's result in small changes in the weighting curve shape.

For each wavenumber interval in the CO_2 band there is a different shaped weighting function. Wavenumbers close to the center of the band show clear sky weighting function peaks near the tropopause due to stronger line absorption. Wavenumbers further from center such as 747.5 cm^{-1} show peaks at lower levels in the atmosphere. When there is an effective cloud present, primary or secondary peaks (p_{wf}) occur near

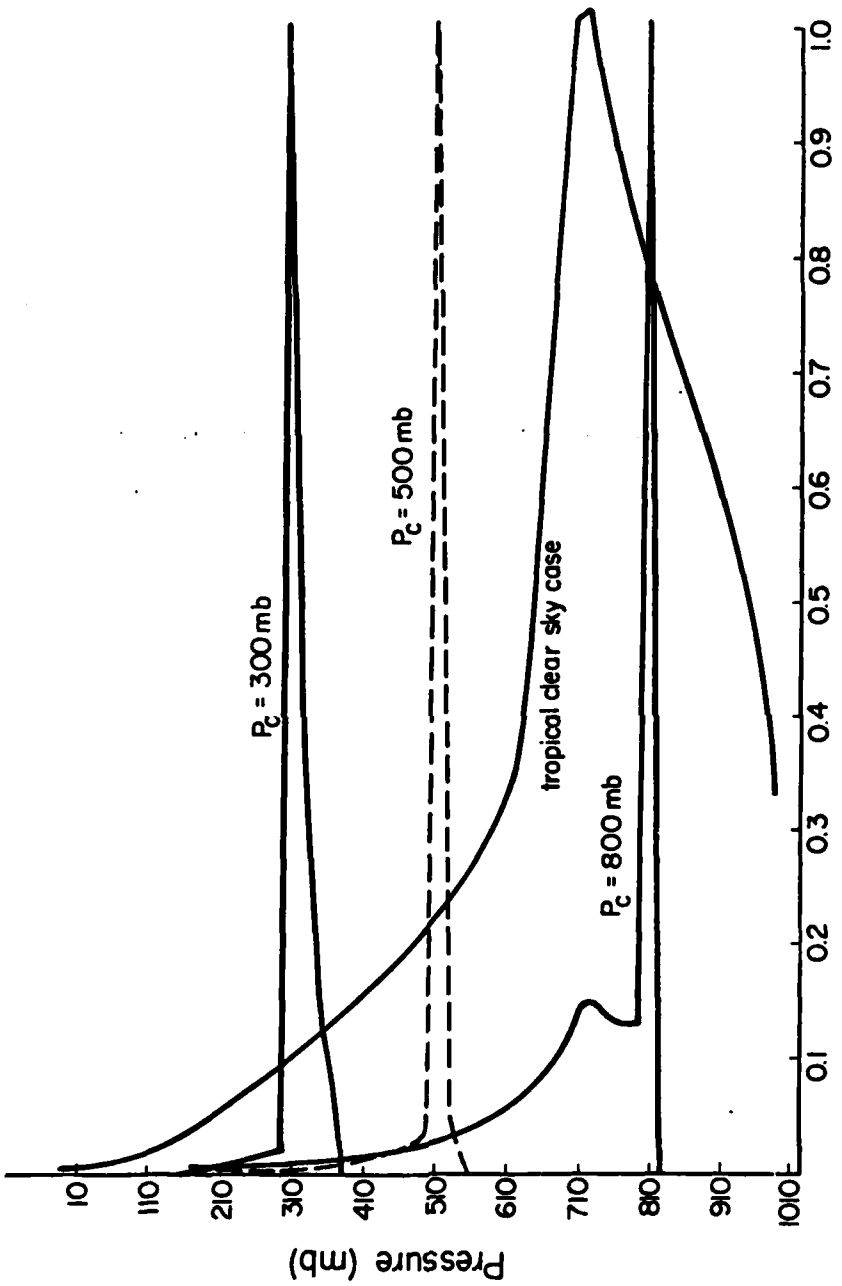

Figure 2. Weighting curves for given p_c and $\alpha = 1$ values, $\nu = 747.5\ cm^{-1}$, for a tropical atmosphere.

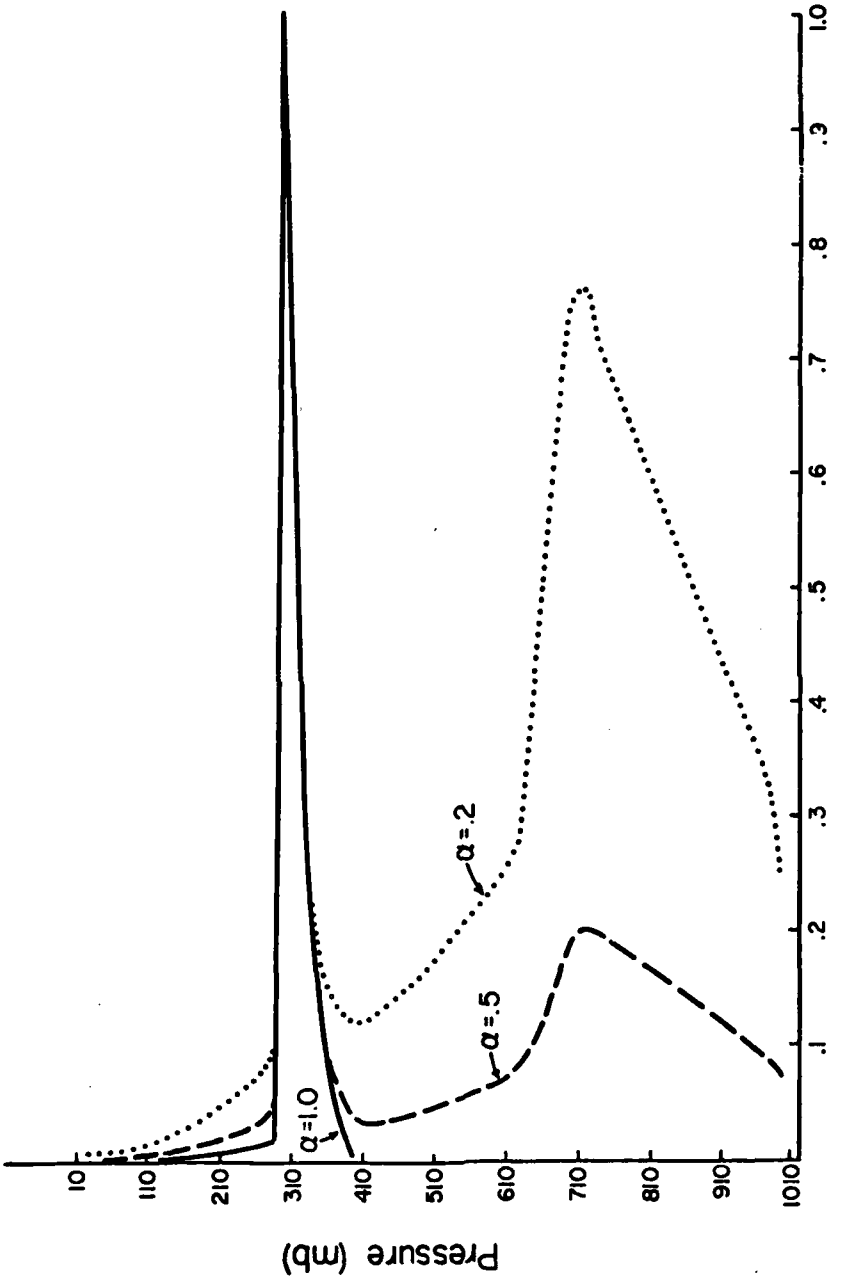

Figure 3. Weighting curves for given p_c = 300 mb and α values, ν = 747.5 cm^{-1}, for a tropical atmosphere.

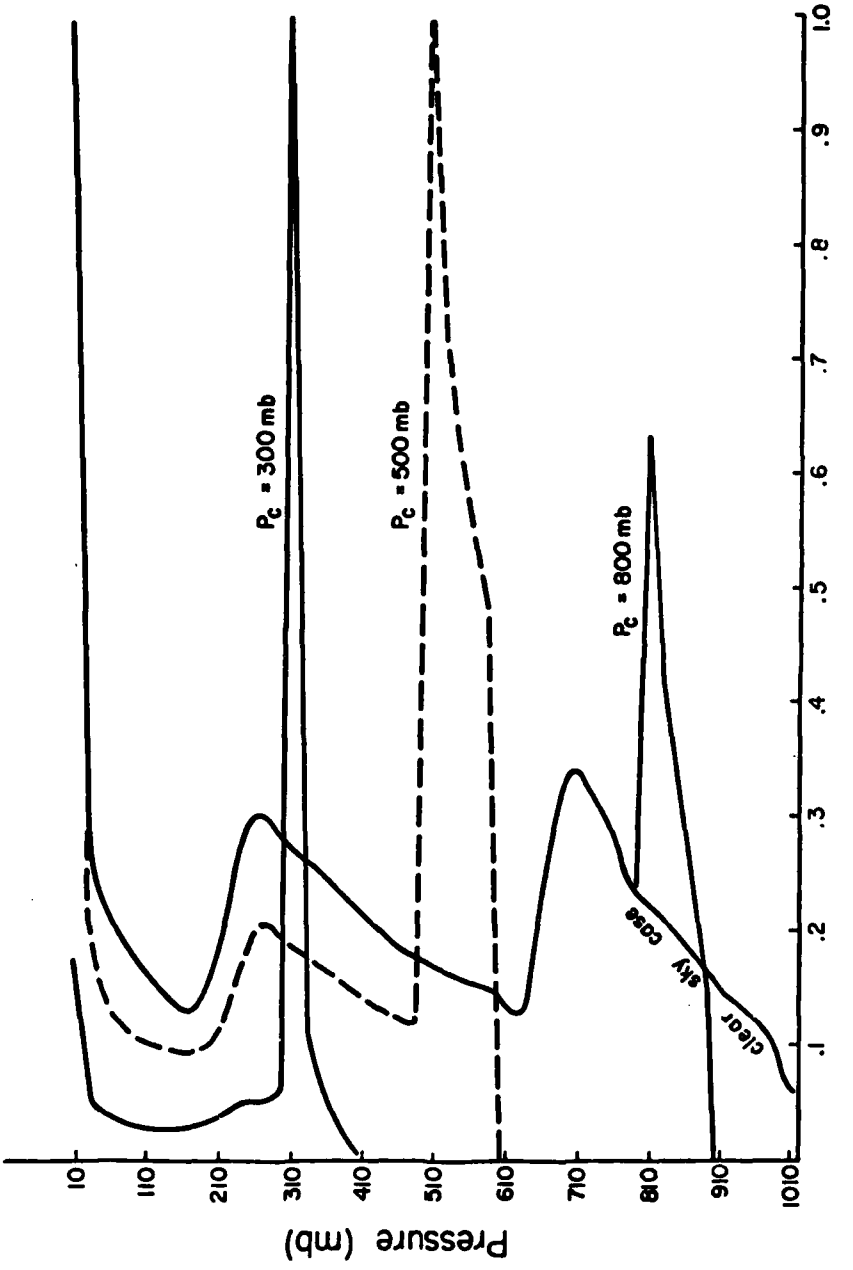

Figure 4. Broadband weighting curves for given p_c and $\alpha = 1$ values for a tropical atmosphere.

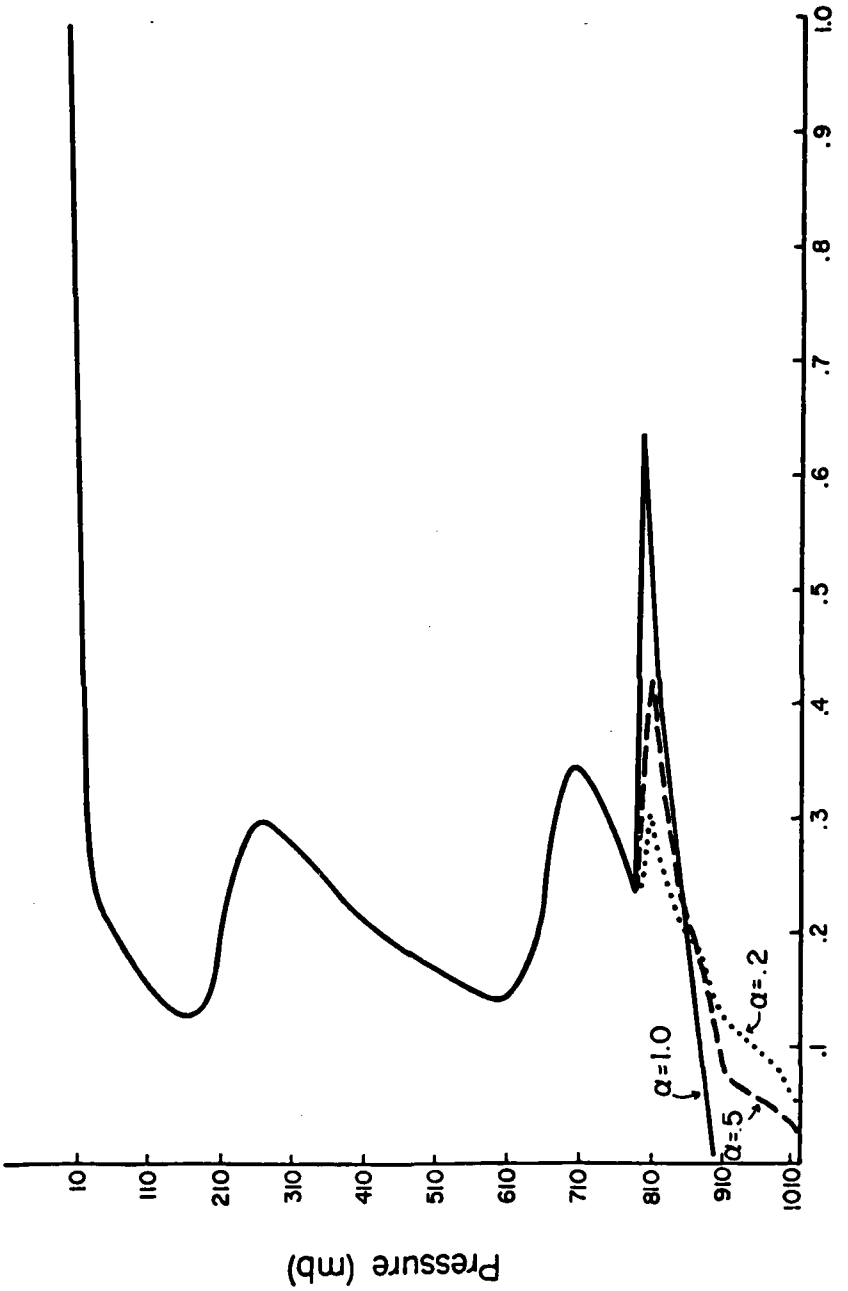

Figure 5. Broadband weighting curves for given p_c = 800 mb and α values for a tropical atmosphere.

the effective cloud top level as seen in Figures 2 and 3. The exact location of the peak is a function of model vertical resolution and in this 20 mb vertical resolution model it is found 10 mb below specified cloud top ($p_c = p_{wf} - 10$).

The most important radiative property in IR bands is cloud emittance as a function of depth into the cloud. Investigation shows that for a model vertical resolution of 20 mb, the level of the weighting function peak due to the cloud is not sensitive to cloud emittance specifications. Even for transluscent clouds the weighting function peak (p_{wf}) is 10 mb below specified effective cloud top (p_c).

To find an empirical relationship between $L_{\nu cs}$, p_{wf}, and α, values of weighting function peak heights (p_{wf}) due to specified effective clouds were plotted against the corresponding values of L (p_c, $\alpha = 1$) for a given temperature humidity profile. Figure 6 shows these plots for a mid-latitude summer profile. Figure 7a,b contains similar plots for a tropical atmosphere. The following relationship was found:

$$\left(\frac{\alpha}{C}\right) \ln \left(\frac{p_{wf}}{D}\right) = (L_\nu - L_{\nu cs}) \qquad (6)$$

The constants C and D depend on spectral wavenumber and atmospheric profile used although for small profile changes (1 to 2°C or 20-30% water vapor) they are nearly constant. The method used to derive and apply Eq. (6) is the topic of Chapter IV.

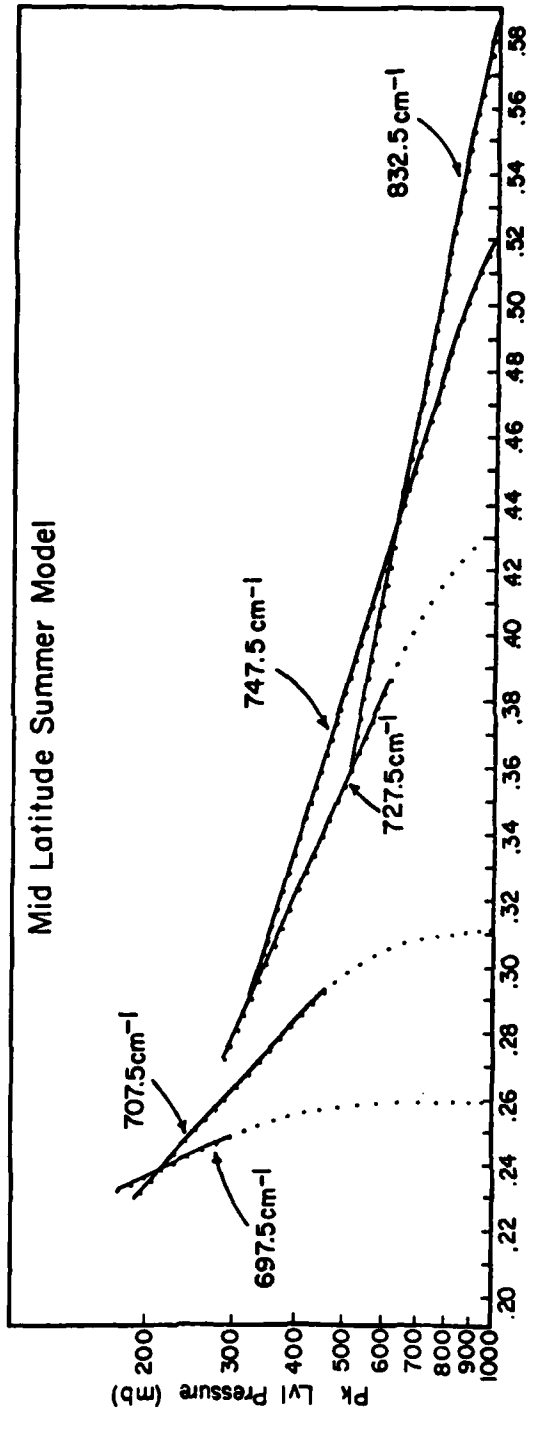

Figure 6. Empirical RTE curves for the mid-latitude summer model for $\alpha = 1$ case.

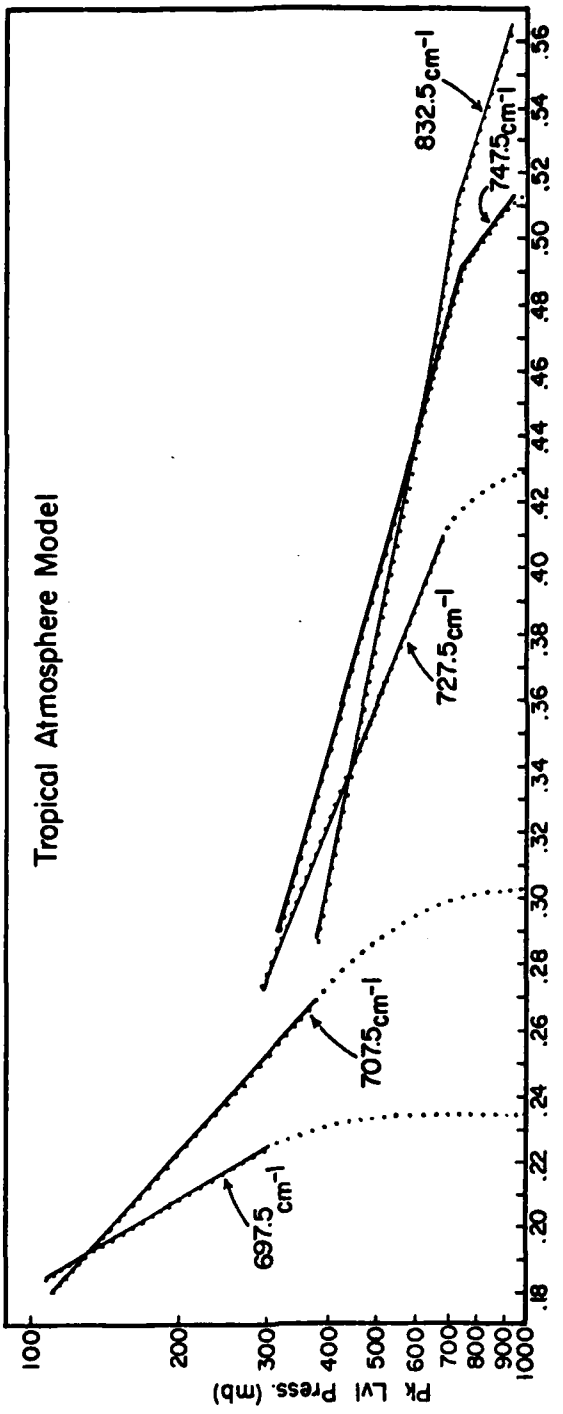

Figure 7a. Empirical RTE curves for the tropical model for $\alpha = 1$ case.

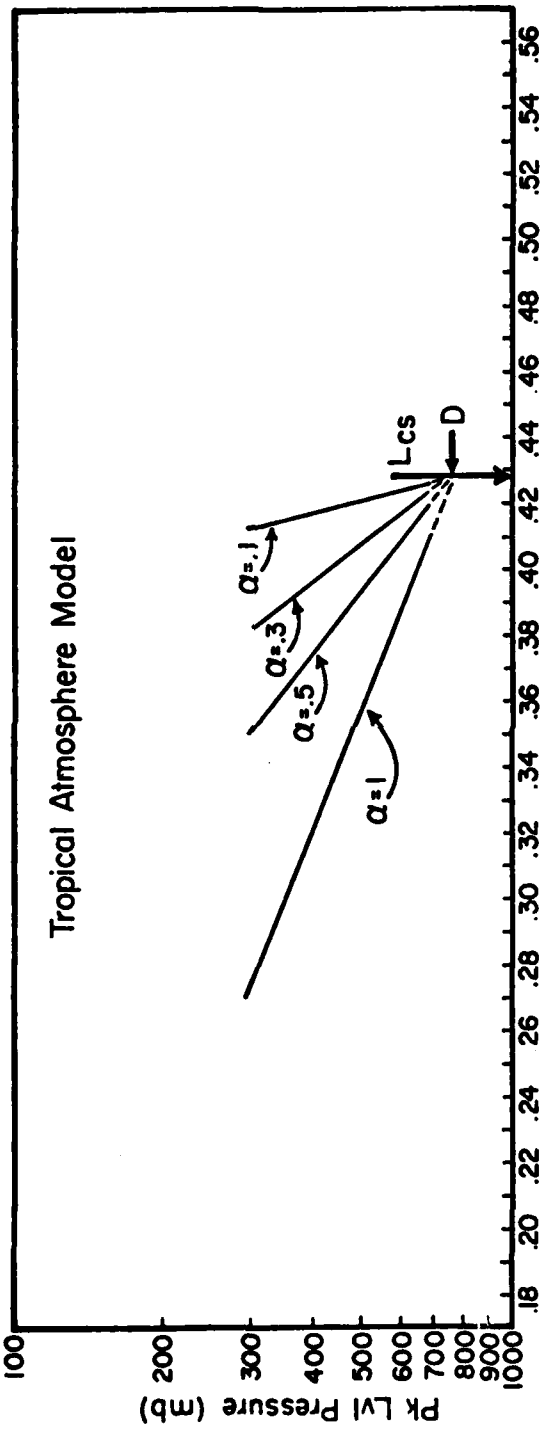

Figure 7b. Empirical RTE curves plotted for ν = 727.5 cm^{-1} and various cases of α, L_{cs} = .428 W/m^2 str 5 cm^{-1}, D = 752 mb.

IV. SHAPE PARAMETER RETRIEVAL PROCEDURE

Radiances received at satellite level are simulated using a spectral radiative transfer equation (RTE) for infrared radiation developed by Cox et al. (1976). Spectral absorption data are taken from Elasser and Culbertson (1960), Smith (1969) and Bignell (1970). For broadband infrared calculations a routine is used that is a broadband approximation to a rigorous line by line spectral radiative transfer equation, and which is described by Cox et al. (1976), and by Griffith and Cox (1977). Both sets of computer code were modified to produce the output requirements of this research. By design both radiative models are computationally fast with the consequence that approximations result in decreased accuracy. For example, N_2O and CH_4 absorption is ignored (Gupta et al. 1978). Nevertheless, the principals of the method described below are not dependent on the absolute accuracy of the radiative calculations.

Spectral bands chosen for use in this research are typical of those used on the satellite-borne radiometers called VTPR - Vertical Temperature Profile Radiometer (NOAA 2-5), HIRS - High Resolution Infrared Sounder (Nimbus 6, TIROS-N) and VAS-VISSR Atmospheric Sounder. Detailed descriptions of the instruments may be found in McMillin et al. (1973), Sissala (1975), and Schwalb (1978). Table 2 gives the central wavenumber of the bands used in this study. These represent typical values and are not necessarily the optimum ones. A 5 cm^{-1} band width is used. Table 2 also gives clear sky atmosphere weighting function properties of these channels.

Central WAVE Number cm^{-1}	Approximate VTPR Channel	Central WAVE Length μm	Clear Standard Atm. Wt. Fun. Pk.	Clear Tropical Atm. Wt. Fun. Pk.	Clear Mid Lat. Atm. Wt. Fun. Pk.
697.5	3	14.337	∿ 210 mb	210 mb	210
707.5	4	14.134	∿ 330 mb	330 mb	330
727.5	5	13.746	∿ 800 mb	710 mb	810
747.5	6	13.378	sfc	730 mb	sfc
832.5	8	12.012	sfc	950 mb	sfc

Table 2. Spectral band values used in the radiative transfer equation to simulate satellite data.

The tropical and mid-latitude atmospheric variables used in this study are given in Tables 3 and 4 respectively. These values were taken from the Handbook of Geophysics and Space Environments (1965) and from U.S. Standard Atmosphere 1976 (1976). As Tables 3 and 4 indicate, the radiative transfer routine is run with a 20 mb tropospheric resolution.

Besides gas and temperature profiles, cloud radiative properties must be specified. As stated earlier and as examined in more detail later, these specified cloud characteristics are not critical to obtaining the proper weighting function curve shape parameters (p_{wf} and α). Figure 8 describes the emittance model used in this research. Table 5 gives the specified cloud parameters. Notice that each of the 45 modeled effective clouds is 100 mb thick (where possible) and that below 300 mb the emittance is unity (black radiating surfaces). The effective cloud tops range from 100 mb to 980 mb at 20 mb intervals.

Since all parameters have been defined, radiance values can now be calculated for each of the six bands given in Table 2. Satellite received radiance values are simulated for each atmosphere and wave band for forty-five overcast cases and one clear sky case. From these 230 spectral radiance values, any simulated set of satellite values for a given atmospheric profile can be generated using Eq. (3). Figures 6 and 7a give plots of L_ν vs. p_{wf} for the overcast case (α values given in Table 5) simulated in this way. The procedure for obtaining the weighting curve shape parameters will be discussed next.

A standard least square linear regression model (Snedecor and Cochran, 1967) is applied to the data in Figures 6 and 7a using a log pressure transformation. The basic model is $y = b \exp(mx)$ and in its

PRESSURE mb	TEMPERATURE °K	W H2O G/KG	W 03 OG/G	W CO2 G/KG
1.6	265.0	.010	6.200	.486
20.0	225.6	.020	10.342	.486
40.0	215.3	.010	4.429	.486
60.0	205.6	.010	1.723	.486
80.0	198.7	.010	.623	.486
100.0	195.7	.010	.348	.486
120.0	200.0	.010	.227	.486
140.0	206.0	.010	.200	.486
160.0	211.0	.010	.175	.486
180.0	216.4	.010	.152	.486
200.0	221.0	.010	.138	.486
220.0	225.2	.020	.126	.486
240.0	228.7	.040	.114	.486
260.0	232.3	.070	.104	.486
280.0	235.9	.110	.096	.486
300.0	239.2	.160	.090	.486
320.0	242.5	.220	.085	.486
340.0	245.3	.300	.081	.486
360.0	247.8	.390	.077	.486
380.0	250.2	.480	.074	.486
400.0	252.8	.600	.072	.486
420.0	255.4	.730	.071	.486
440.0	257.9	.870	.069	.486
460.0	260.2	1.030	.068	.486
480.0	262.6	1.200	.067	.486
500.0	264.7	1.400	.066	.486
520.0	266.5	1.630	.065	.486
540.0	268.3	1.870	.064	.486
560.0	270.1	2.110	.063	.486
580.0	271.9	2.300	.062	.486
600.0	273.8	2.490	.061	.486
620.0	275.7	2.680	.060	.486
640.0	277.6	3.290	.059	.486
660.0	279.3	4.680	.059	.486
680.0	281.0	6.070	.058	.486
700.0	282.7	7.460	.058	.486
720.0	284.2	8.560	.058	.486
740.0	285.1	8.810	.057	.486
760.0	286.0	9.050	.057	.486
780.0	286.8	9.290	.057	.486
800.0	287.8	9.540	.056	.486
820.0	288.9	9.990	.056	.486
840.0	290.1	10.520	.055	.486
880.0	291.3	11.570	.054	.486
900.0	293.7	12.090	.053	.486
920.0	294.8	12.800	.052	.486
940.0	295.9	13.550	.051	.486

Table 3. (Page 1)

PRESSURE mb	TEMPERATURE °K	W H2O G/KG	W O3 OG/G	W CO2 G/KG
960.0	297.0	14.300	.050	.486
980.0	298.1	15.060	.050	.486
1000.0	299.2	15.810	.049	.486
1013.0	300.0	16.300	.048	.486

Table 3. Tropical atmospheric profile variables.

PRESSURE mb	TEMPERATURE °K	W H20 G/KG	W 03 UG/G	W CO2 G/KG
1.8	270.0	.003	8.600	.486
20.0	229.8	.003	9.775	.486
40.0	222.6	.003	6.597	.486
60.0	219.0	.003	4.260	.486
80.0	217.1	.003	2.782	.486
100.0	216.0	.003	1.813	.486
120.0	216.0	.003	1.258	.486
140.0	216.0	.003	.978	.486
160.0	216.0	.004	.782	.486
180.0	216.2	.006	.675	.486
200.0	220.2	.010	.568	.486
220.0	224.3	.014	.465	.486
240.0	228.4	.019	.365	.486
260.0	231.7	.030	.292	.486
280.0	234.8	.042	.223	.486
300.0	238.1	.064	.189	.486
320.0	241.3	.086	.157	.486
340.0	244.0	.133	.133	.486
360.0	246.5	.188	.112	.486
380.0	249.0	.239	.096	.486
400.0	251.6	.287	.089	.486
420.0	254.2	.336	.082	.486
440.0	256.4	.396	.077	.486
460.0	258.3	.462	.073	.486
480.0	260.3	.527	.069	.486
500.0	262.2	.599	.067	.486
520.0	264.0	.673	.065	.486
540.0	265.7	.748	.063	.486
560.0	267.5	.841	.062	.486
580.0	269.1	.976	.060	.486
600.0	270.7	1.111	.058	.486
620.0	272.4	1.246	.057	.486
640.0	273.9	1.373	.065	.486
660.0	275.3	1.495	.056	.486
680.0	276.8	1.617	.055	.486
700.0	278.3	1.739	.055	.486
720.0	279.7	1.909	.055	.486
740.0	281.0	2.126	.055	.486
760.0	282.3	2.344	.055	.486
780.0	283.6	2.561	.054	.486
800.0	284.9	2.778	.054	.486
820.0	285.9	2.962	.054	.486
860.0	287.9	3.322	.054	.486
880.0	288.9	3.502	.054	.486

Table 4. (Page 1.)

PRESSURE mb	TEMPERATURE °K	W H20 G/KG	W 03 UG/G	W CO2 G/KG
900.0	289.9	3.682	.054	.486
920.0	290.6	3.861	.054	.486
940.0	291.4	4.039	.054	.486
960.0	292.1	4.218	.054	.486
980.0	292.8	4.396	.054	.486
1000.0	293.5	4.575	.054	.486
1013.0	294.0	4.700	.054	.486

Table 4. Mid-latitude summer atmospheric profile variables.

$$\varepsilon_{CLOUD} = 1 - \exp(-K\ LWC\ \Delta z)$$

$$\varepsilon_{CLOUD} = 1 - \tau_{CLOUD} \qquad \Delta z = z_2 - z_1 = \frac{\bar{RT}}{g} \ln \frac{P_1}{P_2}$$

Cloud Top Pressure (mb)	Assumed average cloud ice or liquid water (LWC) content (gm^{-3})	Cloud penetration distance for satellite 11 μm radiance measurements (meters)
100	0.01	1660
200	0.02	830
300	0.05	332
400	0.10	166
500	0.20	83
600	0.33	50
700	0.50	33
800	1.00	20
900	1.00	20
1000	1.00	20

A mass absorption coefficient (K) of 0.045 $m^2 g^{-1}$ was used at all levels thereby allowing cloud emissivity to be determined by variations in cloud water content and cloud thickness. (After Cox and Griffith, 1978).

Figure 8. Description of cloud emittance model used in this paper.

CLOUD TOP	CLOUD BASE	LWC g/cm^3	COMP. τ	COMP. α,N=1	CLOUD TOP	CLOUD BASE	LWC g/cm^3	COMP. τ	COMP. α,N=1
100	200	.010	.15	.85	560	660	.248	.00	1.0
120	220	.011	.15	.85	580	680	.279	.00	1.0
140	240	.013	.13	.87	600	700	.313	.00	1.0
160	260	.016	.10	.90	620	720	.352	.00	1.0
200	300	.021	.08	.92	640	740	.395	.00	1.0
220	320	.025	.06	.94	660	760	.443	.00	1.0
240	340	.029	.04	.96	680	780	.498	.00	1.0
260	360	.034	.03	.97	700	800	.559	.00	1.0
280	380	.040	.02	.98	720	820	.628	.00	1.0
300	400	.047	.01	.99	740	840	.705	.00	1.0
320	420	.055	.01	.99	760	860	.792	.00	1.0
340	440	.064	.00	1.0	780	880	.890	.00	1.0
360	460	.075	.00	1.0	800	900	1.00	.00	1.0
380	480	.087	.00	1.0	820	920	1.00	.00	1.0
400	500	.100	.00	1.0	840	940	1.00	.00	1.0
420	520	.110	.00	1.0	860	960	1.00	.00	1.0
440	540	.124	.00	1.0	880	980	1.00	.00	1.0
460	560	.139	.00	1.0	900	1000	1.00	.00	1.0
480	580	.156	.00	1.0	920	1000	1.00	.00	1.0
500	600	.175	.00	1.0	940	1000	1.00	.00	1.0
520	620	.197	.00	1.0	960	1000	1.00	.00	1.0
540	640	.221	.00	1.0	980	1000	1.00	.00	1.0

Table 5. Specified Cloud Parameters.

linear form it is ln y = ln b + mx, where m = slope and ln b is the y intercept value. In this model the known independent variable x is given below:

$$x = L_\nu (p_{wf}, \alpha) = \alpha L_{\nu cld} + (1-\alpha) L_{\nu cs},$$

where L_ν is the satellite measured spectral radiance for a given spot, α is the effective cloud amount, $L_{\nu cld}$ is the radiance from the cloudy area of the spot, and $L_{\nu cs}$ is the radiance from the clear sky portion of the spot. The dependent variable y is equal to p_{wf}. Using the data represented in Figures 6 and 7a one can solve for the equation parameters m and b for $\alpha = 1$ for each wavenumber line.

One could solve for m and b values for a number of α value lines (Figures 6 and 7a represent an $\alpha = 1$ line) using the same procedure. However, an easier and faster approach is to rewrite the linear regression model in terms of α. First note Figure 7b which shows that regardless of the α value line plotted, as L_ν approaches $L_{\nu cs}$, p_{wf} approaches the constant value D. Furthermore, since x is a linear combination using $L_{\nu cs}$ and α, one might expect to be able to write the linear model in terms of $L_{\nu cs}$ and α which in effect gives an equation that represents a family of curves in p_{wf} and α. In other words consider the model

$$y = b \exp (Cx \div \alpha).$$

Analysis showed that for such a model

$$b = D \div \exp (CL_{\nu cs} \div \alpha).$$

This results in the following relationship

$$y = D \exp[\frac{C(L_\nu - L_{\nu cs})}{\alpha}] = p_{wf}. \quad (7)$$

In this equation p_{wf} is simply related to both L_ν and α. L_ν is measured and $L_{\nu cs}$ is known. For the $\alpha = 1$ case plotted in Figures 6 and 7a, constant C is simply the lines' slope m, and constant D = exp $(C\ L_{\nu cs} + \ln b)$.

Table 6 gives the respective values of C and D and $L_{\nu cs}$ for each wavenumber band. Computationally these values are used in Eq. (7), which is simply another form of Eq. (6) given in Chapter III. For each wavenumber there is a separate equation with two unknowns p_{wf} and α. One may solve a set of two equations with two unknowns. Two wavenumber equations are chosen. A simple iterative scheme that changes values of α in the two equations is used to solve simultaneously for the values of p_{wf} and α of Eq. (7). Computationally one looks for the best agreement between the two calculated values of p_{wf} as one iterates through the α values.

Each wavenumber family of curves (Eq. 7) represents information from a part of the atmosphere as given in Table 6. As stated in Table 2 and illustrated in Figures 9 and 10 for six spectral bands of interest, clear sky weighting functions peak at certain levels in the atmosphere. Most of the radiance information at a given wavelength comes from the part of the atmosphere above this peak. A relatively small

WAVE NUMBER cm^{-1}	WEIGHTING FUNCTION PEAK LEVEL RANGE (mb)	VARIABLES C*	D**	CCR***
MID LATITUDE SUMMER ATMOSPHERE				
832.5	500 - 690	3.09	1007	.587
832.5	690 - 890	2.87	971	.587
832.5	890 - 995	3.85	998	.587
747.5	320 - 790	4.55	920	.521
747.5	790 - 890	5.95	963	.521
747.5	890 - 995	9.11	996	.521
727.5	295 - 600	6.47	815	.433
707.5	190 - 455	14.0	581	.311
697.5	190 - 295	31.2	396	.259
TROPICAL ATMOSPHERE				
832.5	370 - 630	3.21	942	.578
832.5	630 - 730	2.62	856	.578
832.5	730 - 935	4.47	942	.578
747.5	320 - 730	4.12	795	.513
747.5	730 - 935	10.9	899	.513
727.5	295 - 660	6.00	744	.428
707.5	100 - 400	13.9	600	.302
697.5	100 - 295	26.2	381	.234

* units of $[W/m^2 \text{ str } 5 \text{ cm}^{-1}]^{-1}$

** modified intercept in units of mb, explained in text

*** clear column radiance (W/m^2 str 5 cm^{-1})

Table 6. Cloud retrieval empirical equation variables.

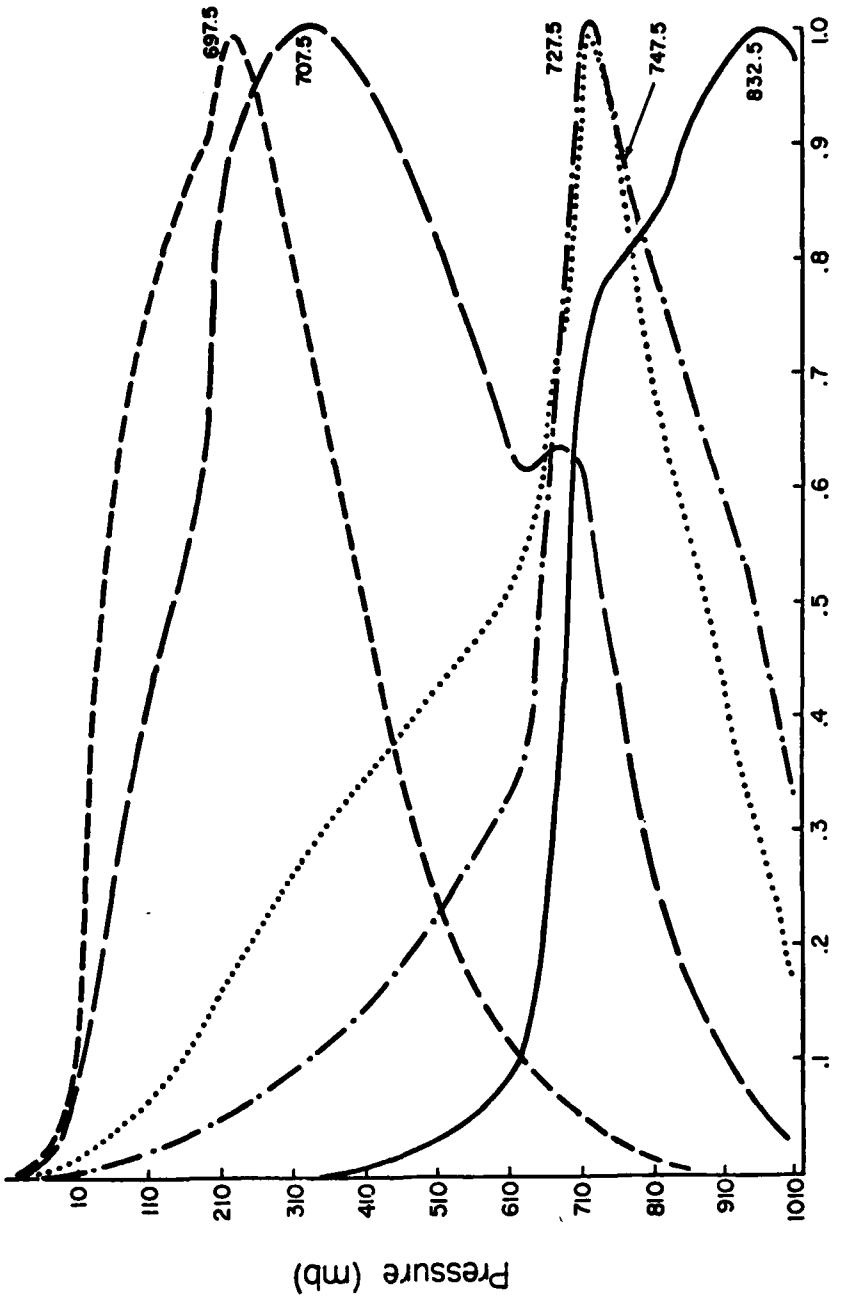

Figure 9. Tropical clear sky spectral weighting curves.

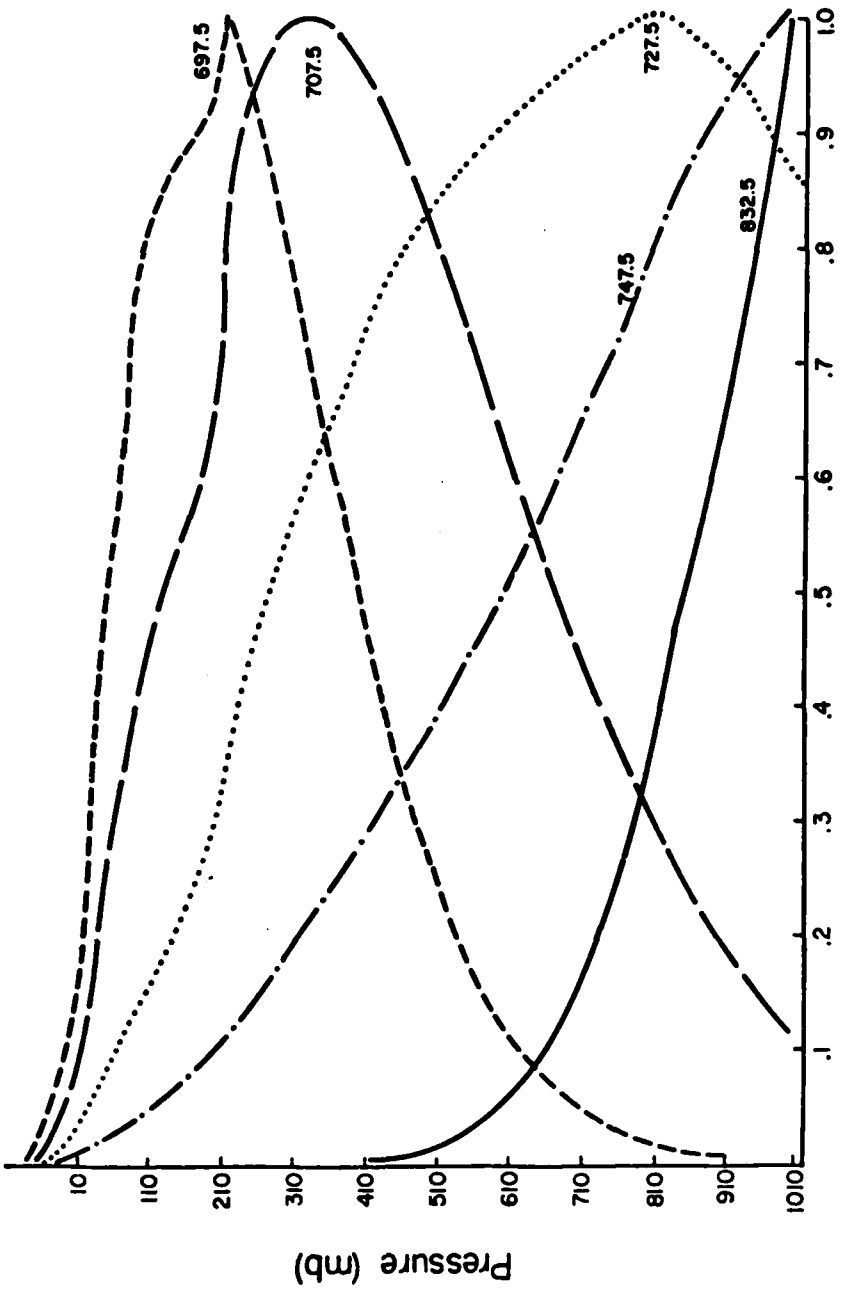

Figure 10. Mid-latitude summer clear sky spectral weighting curves.

portion of the total atmospheric spectral radiance received at satellite level originates below the clear sky weighting function peak level. Thus, any effective radiating surface below this clear sky peak level will not be strongly indicated in the satellite-received radiance value.

This effect can be seen in Figures 6 and 7a. Above the respective wave band natural clear sky weighting function peak, the relationship of ln p_{wf} to L_ν (satellite received spectral radiance) is nearly linear with a flat slope. However, below this point the slope steepens indicating very little change in L_ν for a change in p_{wf} (level of the effective radiating surface since $\alpha = 1$).

This effect is also evident in Figures 11 and 12 which plot wavelength dependent signal to noise ratio as a function of height for the tropical and mid-latitude atmospheres respectively. The signal $L_\nu - L_{\nu cs}$ (see Eq. 7) and the error values are given in Chapter V. In the figures, the solid lines indicate $\alpha = 1$ (overcast case) and the dashed lines are for α less than 1. For α values less than 1, the signal to noise ratio is reduced by a factor of α. For example, if $\alpha = .5$ the signal to noise ratio will be half the value it is for $\alpha = 1$. Note that as $\alpha \to 0$ and as p_{wf} (with constant $\alpha = 1$) $\to$ 1000 mb the signal to noise ratio decreases. In other words less information is available from which to make curve shape retrievals as these boundaries are approached. However, as illustrated in Figures 4 and 5 by the small curve shape change the VIRES of the atmosphere is least sensitive to errors near these boundaries. Figures 11 and 12 seem to indicate that the wavenumber band curves peaking near the surface should give the best results overall. However, the $\varepsilon_{\nu 1} = \varepsilon_{\nu 2}$ assumption limits the use of these widely spaced wavelength curves higher in the atmosphere where

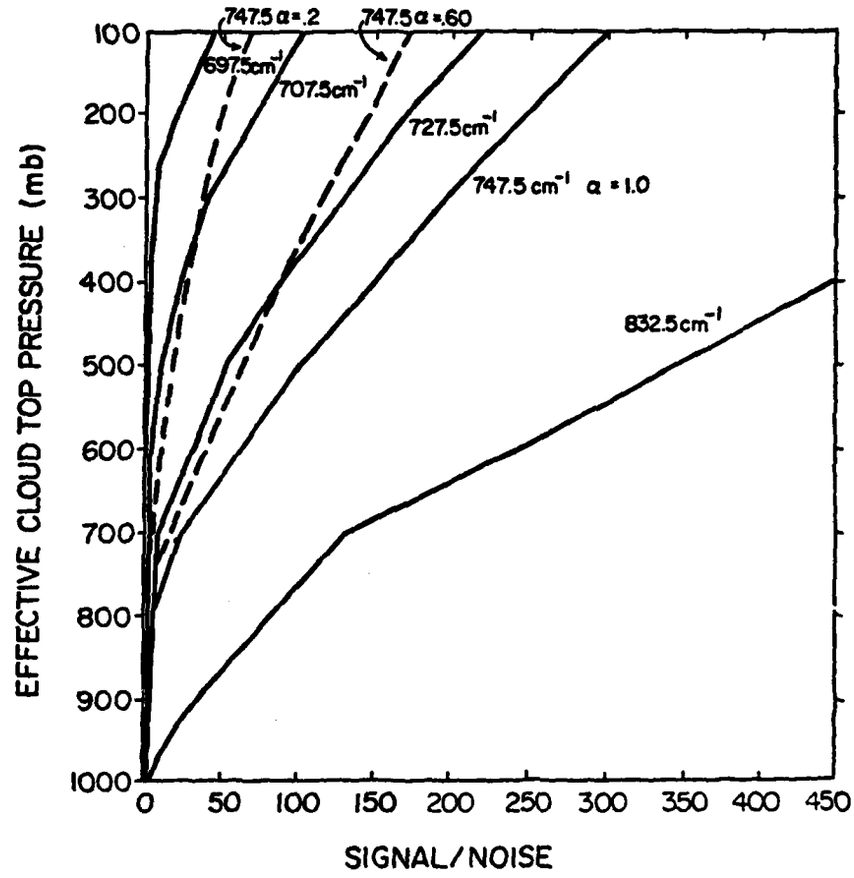

Figure 11. Signal to noise ratio vs. overcast effective cloud top pressure for tropical model. NOTE: Signal = $L_{\nu cs} - L_{\nu}$.

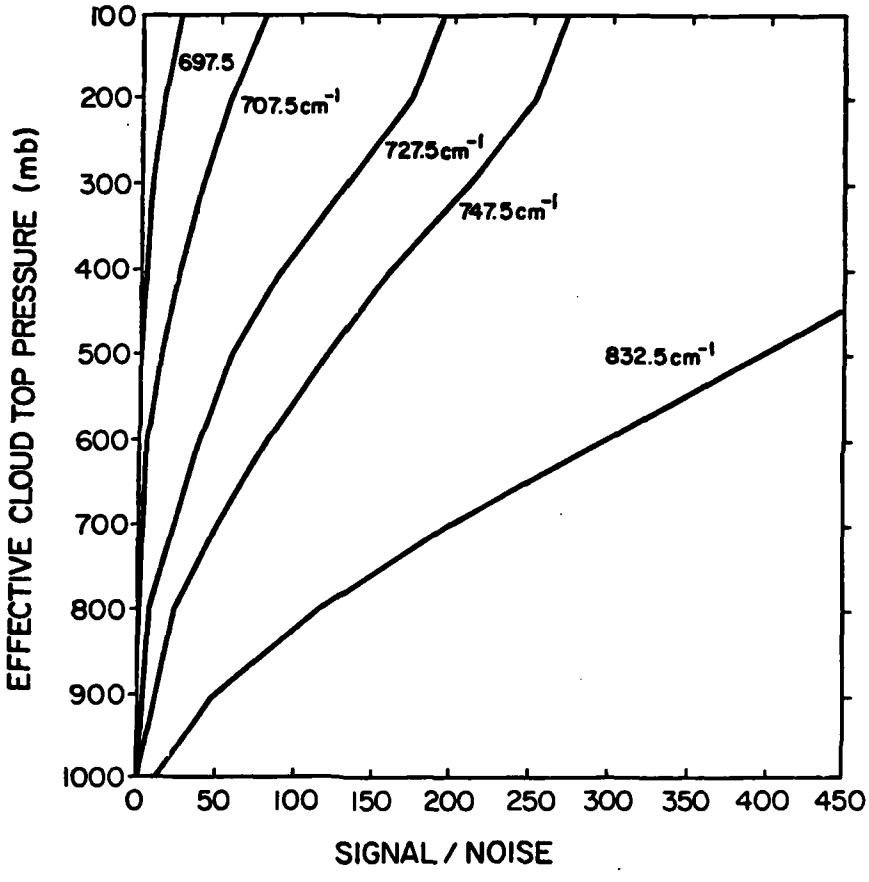

Figure 12. Signal to noise ratio vs. overcast effective cloud top pressure for the mid-latitude summer model.

nonblack clouds are common. Also, the slope and linearity of the curves in Figures 6 and 7a,b for these wavebands limit their use at upper tropospheric levels.

Therefore, since the curve shape parameter radiance signal is related to the clear sky weighting function peak level, only the areas of the atmosphere indicated by solid lines in Figures 6 and 7a,b for the respective wavebands are used in the retrieval calculations. This has the effect of maximizing the useful shape parameter information contained in the satellite radiance values.

Two further points can be made. First, the empirical RTE family of curves approach requires linearity in ln p which restricts the useful part of the curves in Figures 6 and 7a,b as indicated in Table 6. To obtain best results a few of the solid lines plotted in Figures 6 and 7a,b are actually broken down into two or three straight line segments. All lines calculated resulted in the coefficient of determination (r^2) exceeding 0.98. Secondly, for any given level of the atmosphere (100 - 980 mb) there must be at least two different waveband family of curves equations that can be compared to each other in order to determine the proper shape parameters p_{wf} and α. Table 6 indicates that this condition is met and that at times three curves overlap for comparison.

Neglecting input errors for now, it is useful to evaluate the statistical characteristics of the previously described empirical retrieval. Figures 13 and 14 show an evaluation of the bias and RMS error associated with retrieval of the two curve shape parameters p_{wf} and α. RMS error is the standard deviation of retrieval error. Bias error is the mean retrieved value minus the actual simulated value.

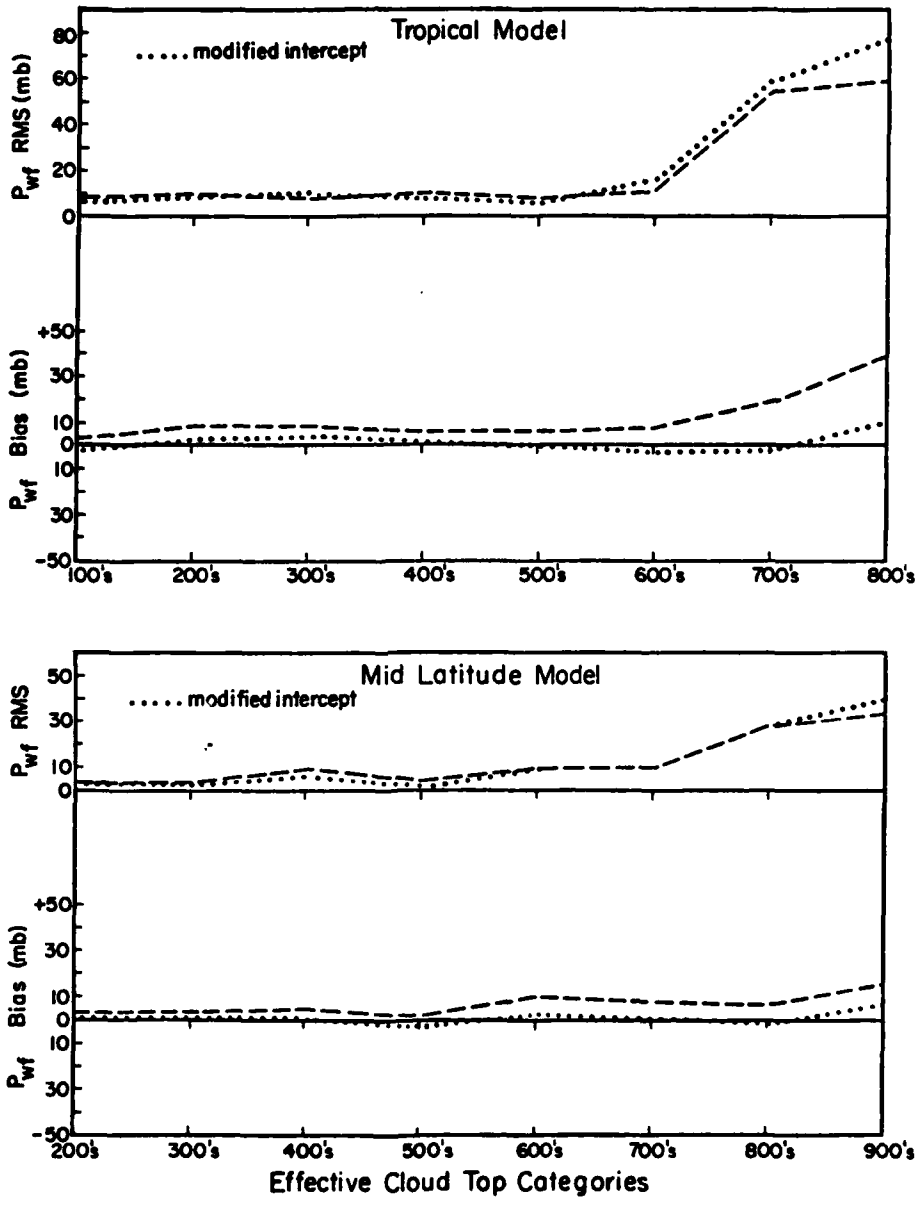

Figure 13. 'No error' empirical model statistical analysis of p_{wf}.

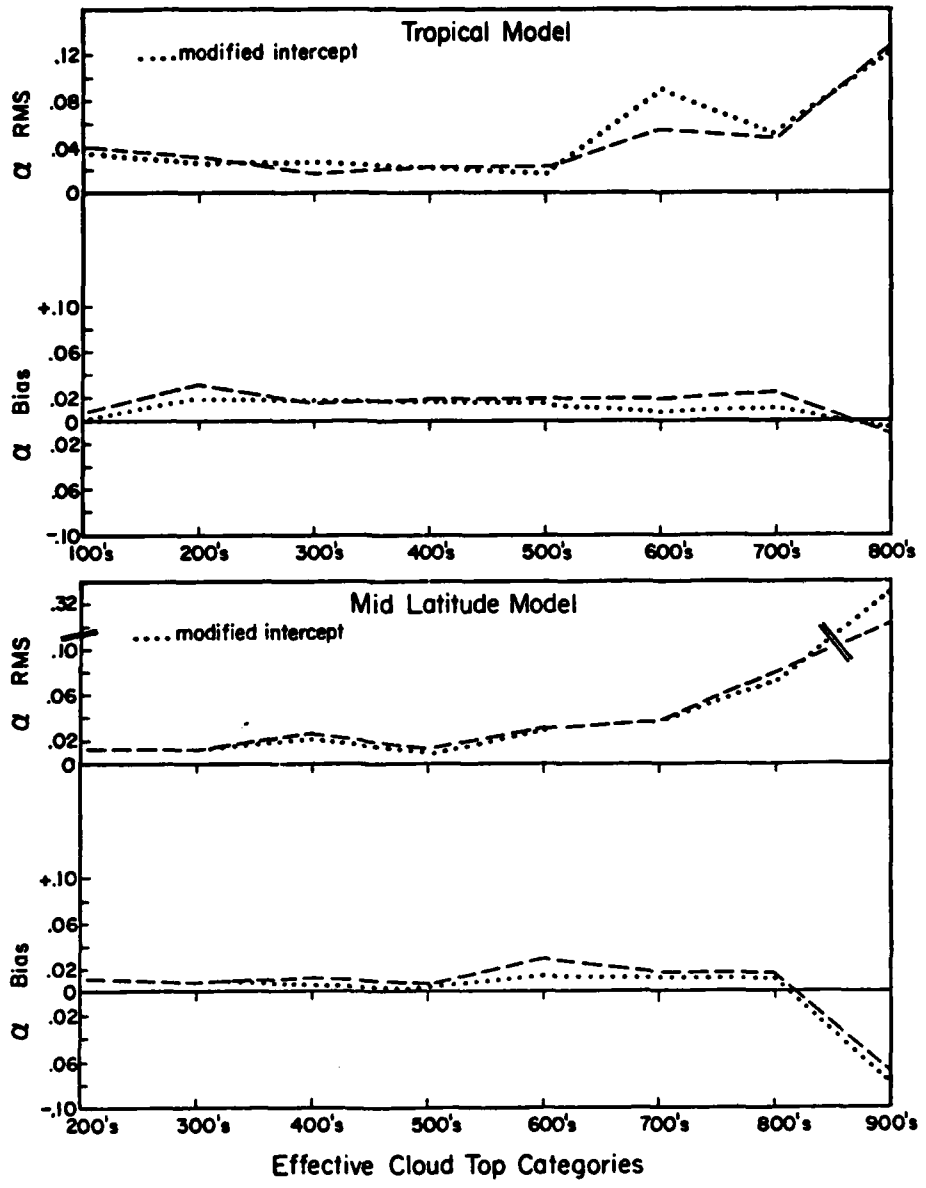

Figure 14. 'No error' empirical model statistical analysis of α.

Each point plotted is an evaluation of 50 values. The 50 values came from the 5 effective cloud top levels in a given 100's category (i.e. 300, 320, 340, 360 and 380 mb) evaluated at 10 clear versus cloudy fractional weightings (i.e. 1.0, 0.9, ..., 0.1). Values were calculated for the tropical atmosphere between 100 and 880 mb and between 200 and 980 mb for the mid-latitude summer atmosphere. Values above the tropopause were not considered because isothermal conditions give no indication of p_{wf} changes in the satellite radiance values (i.e. $\frac{\partial T}{\partial z} \neq 0$). Values at 900 mb and below in the tropical atmosphere were not considered because the high concentration of water vapor at these levels essentially has the same effect on the atmosphere VIRES whether an effective cloud is there or not.

From Figures 13 and 14 it can be seen that the RMS curves are influenced by the signal to noise ratio values discussed previously. As pointed out before, the errors occurring in the retrieval low in the atmosphere have the least effect on the shape of the broadband weighting function curve. However, the error shown by the bias curves is only due to the failure of the empirical RTE to exactly duplicate calculation of the RTE for every combination of p_c and α. The dotted line shows an adjustment made to the empirical method to remove a small consistently high bias. Variable D (an intercept value) of Eq. (7) is slightly reduced to nearly eliminate this bias. Apparently solving for C and D by the method described earlier using $\alpha = 1$ which is at a boundary, results in this $\simeq$ 5 mb bias.

As stated previously and as outlined in Figure 1a the shape parameter p_{wf} and α are used in the broadband computer routine referred to earlier in this chapter. The program is run using the same atmospheric

profile used to compute the C and D values of Eq. (7) and listed in Table 6. One may run the program with many pairs of shape parameters to produce a composite VIRES curve. Chapter VI gives examples of this procedure and explains how the VIRES broadband curves are used to yield the proposed VIRES index. The next chapter evaluates the retrieval errors under realistic system error conditions. Note also that at the end of Chapter V it is shown that one may produce useful composite curves by combining the simulated spectral radiances before curve shape parameter retrieval is performed.

V. SENSITIVITY ANALYSIS

To help assess the feasibility of using the atmospheric VIRES as a climate index in the form of broadband infrared weighting functions, it is useful to know the characteristic errors of inferring these profiles from satellite spectral radiances. First, the uncertainties both random and bias associated with the empirical RTE technique used to retrieve the weighting curve shape parameters p_{wf} and α are examined. Secondly, the sensitivity of the final weighting curve product to reasonable errors is examined. All error sources evaluated are associated with implicit or explicit assumptions.

A. Shape parameter retrieval errors

Error sources examined in this section include system-instrument errors, errors associated with temperature, humidity, and CO_2 profile unknowns, and errors due to specified cloud properties assumptions. The sensitivity of the weighting curve shape parameters to these likely error sources is investigated. The chosen approach and specific error magnitudes are discussed below.

The calculation of the statistics used in this analysis is straightforward. The p_{wf} and α RMS errors are variations of the retrieved values about the retrieval mean p_{wf} and α values. Thus the RMS is a measure of the retrieved values standard deviation about the mean. However, because the RMS is large compared to the mean, the described RMS value is nearly equal to the RMS calculated the standard way. Bias error is the difference between the actual and retrieved mean value.

Important to the calculation of the statistics is the empirical-RTE technique boundary conditions. Naturally the values of α are found between 1.0 and 0. For clear sky conditions α is given the value 0 and p_{wf} = 1000 mb. Clear sky conditions are assigned when $L_\nu \geq L_{\nu cs} - 2\sigma_\nu$, where ν = 747.5 and 832.5 cm^{-1}, and σ_ν is the standard deviation of instrument error at a given wavenumber. Retrieval calculations giving radiating surfaces above the tropopause are taken to indicate the radiating surface location at the tropopause level (100 mb for tropical atmosphere, and 180 mb for mid-latitude atmosphere). Because of the strong influence of water vapor in the tropical model, radiating surfaces calculated to be below 935 mb are taken to indicate clear sky conditions. Specifics of the error analysis are given in the Appendix. A summary of these results including error assumptions follows.

Instrument system noise is assumed to be Gaussian with a mean of zero and a standard deviation of 0.22 mW $m^{-2}sr^{-1}cm$ for the CO_2 channels and 0.11 mW $m^{-2}sr^{-1}cm$ for the window channel. These values represent the state of the art precision of the HIRS instrument on TIROS-N (Schwalb, 1978). It is also assumed that channel errors for a specific spot measurement are correlated. Thus each simulated spectral radiance value was modified in a like manner by an error value distributed as described above and chosen randomly for each set of radiance values. The effect of this approach, compared to random assignment of individual errors to the spectral radiances in a set, is to give $\approx$ 30% smaller overall bias errors and $\approx$ 20% smaller RMS errors to the retrieved curve shape parameters. The bias and RMS errors are smaller because the retrieval routine is better able to find a unique solution when errors are in the same direction and of similar magnitude. Real

characteristic sensor noise of course, lies somewhere between the two descriptions given above. Although example comparisons of the results from the two approaches showed the trend described above, the noise correlation approach was chosen for the overall sensitivity analysis.

Temperature and water vapor profile errors are also assumed to be Gaussian with zero mean. Errors vary randomly from one 20 mb layer to another and temperature errors are assumed not to be correlated with humidity errors. Reasonable temperature and humidity errors are assumed to be $\leq$ 5°C RMS for temperature and an RMS $\leq$ 100% of the correct mixing ratio (Wielicki and Coakley, 1980). Although analysis was done for a number of reasonable values, the results reported on in the Appendix are for a 2°C RMS and an RMS water vapor noise of 50% (Susskind and Rosenfield, 1980; Weinreb and Crosby, 1977).

CO_2 profile maximum errors are assumed to be of magnitude 1%. This represents a value that is $\frac{2}{3}$ of the seasonal change in CO_2 concentration (Bolin and Bischof, 1970; Miller, 1978). CO_2 is assumed to be well mixed in the troposphere and, therefore, the 1% error is applied equally from layer to layer.

For all profile errors a simple correction technique is sometimes useful. Using additional radiative information in the form of a clear column radiance correction (CCRC) decreases error values. Application of CCRC is explained in the Appendix.

Cloud radiative properties must be specified or assumed to be of a certain nature. For emitted radiation the most important property (and only one examined here) is cloud effective emittance. As Platt and Stephens (1980) have recently pointed out, there are scattering and reflection components of effective cloud emittance, especially for ice

clouds. However, for the cloud model used in this research, two properties determine the cloud effective emittance; cloud thickness and cloud liquid water content (LWC). Two errors that are most likely to occur are examined. First a 100 mb thick cloud is specified when in reality a 20 mb thin cloud is present. In other words, cloud emittance is specified too large. Second, a cloud of higher LWC than specified is present. This is the case of cumulonimbus cloud at cirrus level. In this situation cloud emittance is specified too small. This occurs only above 300 mb since below thin level cloud emittance is specified at the maximum value of 1. As stated previously and as shown by this analysis, the retrieval process is essentially independent of cloud radiative properties specified.

Table 7 gives a summary of the error sources and the corresponding bias and RMS order of magnitude error for the two curve shape parameters retrieved. The combination error source includes a random 2°C RMS and 50% RMS water mixing ratio error. It also includes instrument noise as described above. Cloud depth is allowed to randomly vary from 20 to 180 mb and cloud LWC varies randomly from $\pm$ 50% of the specified value. This table shows results that testify to the capability of this retrieval method.

B. Error effects on the weighting curves

The next source of error evaluated is the assumption that the satellite sensor views only one effective cloud layer in non-clear situations. Direct sensitivity of the weighting curve to this error is investigated. The error is examined by means of a sensor resolution argument. We compare two models. In the first model the sensor

Error Sources*	p_{wf} bias (mb)	p_{wf} RMS (mb)	α bias	α RMS
Empirical RTE	0	5	± .01	.03
Sensor noise	± 15	80	± .04	.15
Temperature + humidity	± 30	160	± .06	.30
Temperature + humidity with CCRC*	± 15	20	± .06	.05
CO_2 profile	± 30	40	± .02	.02
CO_2 profile with CCRC	± 2	10	± .01	.02
Specified emittance	± 2	8	± .01**	.03**
Combination	± 15	160	± .05	.35
Combination with CCRC	± 15	90	± .05	.20

* defined in text

** not plotted in the Figures

Table 7. List of representative errors in shape parameter retrieval due to given error sources.

detects, for example, 200 sets of radiances, representing single layer effective clouds. This model is compared to the second model which senses 100 sets of radiance values for the same area of effective cloud. The second set of radiances are simply averages of the first set of radiances taken by pairs. For both cases curve shape parameters are retrieved assuming single layer effective clouds and composite weighting function curves which represent the same 200 spot (high resolution) area are computed. The two curves are statistically compared to test the one layer error assumption. In the 200 spot specified model the assumption is totally true, while in the 100 pair model the assumption is completely false.

In this analysis the 200 spot area represents a sample from an effective cloud layer distribution. Three different distributions of effective cloud top heights are specified to provide a more complete test. The test in general as well as the distributions are described in detail in the Appendix. The statistical test used is described in Chapter VI.

Table 8 shows the results of the single effective cloud layer assumption analysis. The statistical test values indicate that for the situations of curve compositing the errors associated with the single layer assumption are minimized. For the test cases presented, the retrieved composite weighting function curves are extraordinarily similar to the true (specified) curves. Although the statistical test is designed to indicate curve differences, small T values imply likeness. In other words, if the calculated T values are as large or larger than the critical T value then H_0 (the curves are the same) can be rejected

	DISTRIBUTIONS	SIGN COUNTS FOR SIGN TEST 100 - 380 mb Pos.	100 - 380 mb Neg.	400 - 680 mb Pos.	400 - 680 mb Neg.	700 - 980 mb Pos.	700 - 980 mb Neg.	T Statistic
	FLATS vs FLATR	9	6	9	6	7	8	1.96
(Cut off correction)	FLATS vs FLATR	6	5	1	1	0	0	0
	FLATS vs FLATR*	7	8	9	6	7	8	0.98
(Cut off correction)	FLATS vs FLATR*	7	6	0	2	0	0	1.39
	BIMOS vs BIMOR	7	8	9	6	7	8	0.98
(Cut off correction)	BIMOS vs BIMOR	4	5	1	1	0	0	0
	1PK3S vs 1PK3R	8	7	8	7	4	11	4.17
(Cut off correction)	1PK3S vs 1PK3R	5	7	4	1	0	0	1.45

P values	Critical T values (see text)
.01	16.8
.05	12.6
.10	10.6
.25	7.8
.50	5.4

Table 8. Statistical test of the differences between the curves in Figures 40-42.

at the given P value significance level. Otherwise, H_0 is accepted as true, the differences in the curves being explained by chance happenings.

This last section looks at the sensitivity of the final product broadband weighting curve to the factors that are most important to curve parameter retrieval, temperature and humidity. The two climatological profiles (Tables 3 and 4) are assumed to be correct when using the retrieval method, i.e. when determining C and D values and when calculating the broadband curves from the retrieved curve shape parameters. However, each of these profiles are modified to produce 'actual' cases. Temperature and humidity at each level in the climatological profiles are increased or decreased by a specified percentage to produce these 'actual' cases. From these 'actual' profiles the simulated satellite radiances are calculated. Finally, the broadband weighting curve retrieved assuming a climatological atmosphere (without using CCRC) when an 'actual' profile exists is compared to the weighting curve produced directly from the true atmospheric profile and 'true' specified cloud distribution. The specified cloud profile used is called 1N24 and it represents the actual 24 hour average cloud conditions for the B array north section during Phase III of GATE (see Cox and Griffith, 1978). This cloud distribution as well as those used in Chapter VI and the Appendix are given in Table 9.

Changing the profiles has the following general effects. Increasing the temperature or decreasing the humidity in the profiles gives radiance values higher than those calculated using a climatological profile. Likewise given specified p_{wf} and α values the radiances from a climatological profile will be higher than those

Eff. Cld. Top Pres.	225 Spot Flat 1	215 Spot BIM01	185 Spot 1PK2	190 Spot 1PK4	190 Spot 1PK6	185 Spot 1PK8	240 Spot Flats	230 Spot BIM05	200 Spot 1PK3S
100	5	2	5	1	1	1	4	2	2
120	5	2	5	1	1	1	4	2	2
140	5	2	5	1	1	1	4	2	2
160	5	2	5	1	1	1	4	2	2
180	5	2	5	1	1	1	4	2	2
200	5	16	20	2	1	1	6	4	5
220	5	16	20	2	1	1	6	4	5
240	5	16	20	2	1	1	5	4	5
260	5	16	20	2	1	1	6	4	5
280	5	16	20	2	1	1	6	4	5
300	5	2	5	5	1	1	6	12	15
320	5	2	5	5	1	1	7	12	15
350	5	2	5	5	1	1	6	12	15
360	5	2	5	5	1	1	7	12	15
380	5	2	5	5	1	1	6	12	15
400	5	1	2	20	2	1	6	4	6
420	5	1	2	20	2	1	5	4	6
440	5	1	2	20	2	1	5	4	6
460	5	1	2	20	2	1	5	4	6
480	5	1	2	20	2	1	5	4	6
500	5	1	1	5	5	1	5	2	4
520	5	1	1	5	5	1	5	2	4
540	5	1	1	5	5	1	5	2	4
560	5	1	1	5	5	1	6	2	4
580	5	1	1	5	5	1	5	2	4
600	5	2	1	2	20	2	4	2	2
620	5	2	1	2	20	2	5	2	2
640	5	2	1	2	20	2	5	2	2
660	5	2	1	2	20	2	4	2	2
680	5	2	1	2	20	2	5	2	2
700	5	16	1	1	5	5	5	4	2
720	5	16	1	1	5	5	6	4	2
740	5	16	1	1	5	5	6	4	2
760	5	16	1	1	5	5	5	4	2
780	5	16	1	1	5	5	6	4	2
800	5	2	1	1	2	20	5	12	2
820	5	2	1	1	2	20	5	12	2
840	5	2	1	1	2	20	5	12	2
860	5	2	1	1	2	20	5	12	2
880	5	2	1	1	2	20	5	12	2
900	5	1	1	1	1	5	7	4	2
920	5	1	1	1	1	5	6	4	2
940	5	1	1	1	1	5	6	4	2
960	5	1	1	1	1	5	6	4	2
980	5	1	1	1	1	5	6	4	2

Table 9. (Page 1)

Eff. Cld. Top Pres. (mb)	215 Spot BIM02	210 Spot BIM03	190 Spot 1PK3	190 Spot 1PK5	190 Spot 1PK7	165 Spot 1PK9	215 Spot 1PK3M	250 Spot 1N24
100	1	1	2	1	1	1	1	1
120	1	1	2	1	1	1	1	1
140	1	1	2	1	1	1	1	1
160	1	1	2	1	1	1	1	1
180	1	1	2	1	1	1	1	1
200	2	2	5	1	1	1	1	4
220	2	2	5	1	1	1	1	4
240	2	2	5	1	1	1	1	4
260	2	2	5	1	1	1	1	4
280	2	2	5	1	1	1	1	4
300	16	16	20	2	1	1	35	4
320	16	16	20	2	1	1	35	4
340	16	16	20	2	1	1	35	5
360	16	16	20	2	1	1	35	5
380	16	16	20	2	1	1	35	5
400	2	2	5	5	1	1	1	5
420	2	2	5	5	1	1	1	5
440	2	2	5	5	1	1	1	6
460	2	2	5	5	1	1	1	5
480	2	2	5	5	1	1	1	5
500	2	16	2	20	2	1	1	5
520	2	16	2	20	2	1	1	4
540	2	16	2	20	2	1	1	4
560	2	16	2	20	2	1	1	4
580	2	16	2	20	2	1	1	4
600	16	2	1	5	5	1	1	4
620	16	2	1	5	5	1	1	4
640	16	2	1	5	5	1	1	5
660	16	2	1	5	5	1	1	5
680	16	2	1	5	5	1	1	5
700	2	1	1	2	20	2	1	5
720	2	1	1	2	20	2	1	5
740	2	1	1	2	20	2	1	5
760	2	1	1	2	20	2	1	4
780	2	1	1	2	20	2	1	4
800	1	1	1	1	5	5	1	4
820	1	1	1	1	5	5	1	4
840	1	1	1	1	5	5	1	4
860	1	1	1	1	5	5	1	5
880	1	1	1	1	5	5	1	5
900	1	1	1	1	2	20	1	5
920	1	1	1	1	2	20	1	5
940	1	1	1	1	2	20	1	5
960	1	1	1	1	2	20	1	4
980	1	1	1	1	2	20	1	4
								64 Clear

Table 9. Model effective cloud distributions (frequency of occurrences).

calculated using cooler or moister profiles. In general then, the p_{wf} values retrieved using radiances from a warmer or drier atmosphere will be a few millibars (20 - 40 mb given the conditions in the next paragraphs) larger (lower in the atmosphere) than the specified value. Just the opposite is true for the cooler or moister case. Typically, retrieved α values remain equal or slightly smaller than the specified α value.

To illustrate the findings, Table 10 gives the results of this analysis for the case of increasing the temperature of the climatological profile by 1% at each level and for the case of increasing the water mixing ratio at each level by 20%. Results for both tropical and mid-latitude cases are given.

It is clear that for these cases the VIRES index (described in the next chapter) is not sensitive to these reasonable assumption errors. The small T statistic values also indicate that the broadband weighting curves are little effected. Looking at the specified and retrieved effective cloud distributions one notices good agreement for the high, middle and combined low and clear categories but poor agreement for the low and clear categories taken separately. This simply supports what has already been said concerning poor retrieval capabilities in the low troposphere. It also shows the advantage of retrieving the VIRES index.

A qualifying statement is in order. A more severe test of this retrieval method would be to not only shift the temperature and humidity profiles but to also change their shape. This was done of course, for the tests in Section A. Also, a rather flat distribution of clouds with some clear sky is a reasonable test, but poorer results would be expected from a sharper (more peaked) distribution. Different shaped

Profile Case	Atmosphere	Mean T 100-1013 mb °K	Precip. H_2O cm	VIRES Index	T Statistic
Actual (+ 20% H_2O)	Tropical	263.2	5.30	270-460-680-0	0
Assume Climatology	Tropical	263.2	4.42	280-480-680-0	
Actual (+ 20% H_2O)	Mid. Lat.	261.7	1.60	280-500-780-.10	2.48
Assume Climatology	Mid. Lat.	261.7	1.34	290-500-780-.15	
Actual (+ 1% Temp)	Tropical	265.8	4.42	280-480-700-0	0
Assume Climatology	Tropical	263.2	4.42	290-490-700-0	
Actual (+ 1% Temp)	Mid. Lat.	264.3	1.34	290-500-800-.11	4.73
Assume Climatology	Mid. Lat.	261.7	1.34	300-520-810-.16	

	SPECIFIED CLOUD DISTRIBUTION IN %				
	High 100-390 mb	Middle 400-690 mb	Low and Clear Combined 700-surface	Low 700-surface	Clear
Actual/Given Trop. and Mid. Lat.	19.2	28.0	52.8	27.2	25.6
Retrieved with + 20% H_2O Trop.	19.2	31.9	48.9	13.5	35.4
Retrieved with + 20% H_2O Mid. Lat.	19.2	28.0	52.8	19.1	33.7
Actual/Given Trop. and Mid. Lat.	19.2	28.0	52.8	27.2	25.6
Retrieved with + 1% T Tropical	16.3	26.0	56.7	10.0	46.7
Retrieved with + 1% T Mid. Lat.	15.2	28.0	56.8	18.0	38.8

Table 10. Example of sensitivity analysis for VIRES index and specified cloud distribution retrievals.

effective cloud distributions and their respective VIRES indexes are examined in the next chapter.

The Appendix has a detailed description of the error investigation as well as a discussion on minimizing the errors. For example, the use of CCRC improves the accuracy of the retrieval over using pre-selected climatological profiles (Crutcher and Mesere, 1970; Jenne et al. 1974; Smith et al. 1972). Nevertheless, the true strength of this climate index approach is that radiation information is used to produce an index directly from radiation theory. Thus, the error prone process of inferring standard physical meteorological variables is avoided.

VI. WEIGHTING CURVES AS A CLIMATE INDEX

A first step in developing a climate index from composite weighting curves is to find an objective way to infer from the curves when there are different types of VIRES (indicators of climatological cloudiness). Section A of this chapter describes a statistical technique and shows that it is a powerful test for objectively determining when two weighting function curves and thus two effective cloud top distributions are different. The remainder of the chapter deals with developing and using a climate index based on the retrieved broadband weighting function curves.

A. Sign Test with Fisher's Method

Utilizing the broadband infrared RTE described earlier, the weighting function curves are computed using a finite differencing scheme which provides one curve value every 20 mb between 100 and 1000 mb. These 45 point values describe the weighting function in the part of the atmosphere influenced by effective clouds. These curves quite obviously represent no standard statistical distribution. Therefore, when comparing two broadband weighting function curves one must use non-parametric statistics.

Because the continuous curve is computed using discrete points, it is easy to compare two curves by pairing their respective point values. A non-parametric statistical test may then be used to test the likeness or difference of the paired values. Although the Wilcoxon Matched Pair Signed Rank Test and the Kolomogorov - Smirnov Test are sometimes useful in such cases, the simple Sign Test gives the best

results in this case. The following is a description of the Sign Test (Beyer, 1971).

In this test, observations from sample x and sample y are paired and the differences are calculated. The null hypothesis (H_0) is that the difference d_i has a distribution with median zero, i.e. the true proportion of positive (negative) signs is equal to $P = \frac{1}{2}$. The probability of positive (negative) signs is given by the binomial probability function f(x) such that

$$f(x) = f(x;\ n,\ P = \tfrac{1}{2}) = \binom{n}{x} \left(\tfrac{1}{2}\right)^n,$$

where x is either the number of positive signs or negative signs, and n is the sum of positive and negative signs. The probability P_i of the samples being the same (true H_0) given x positive (negative) signs is given by the expression

$$P_i\ (x \leq k) = 2\ [\sum_{x=0}^{k} \binom{n}{x}]\ \left(\tfrac{1}{2}\right)^n,$$

where $P_i(x)$ is the Sign Test Probability Function for the two-tailed case. The test is two-tailed because there is no reason to expect more positive signs than negative signs. For example, if k = 3 and n = 15, the probability of x being three or less (either of positive or negative sign) if H_0 is true is given by the following calculation.

$$P_i\ (x \leq 3) = 2\ [\binom{15}{0}\ \binom{15}{1}\ \binom{15}{2}\ \binom{15}{3}]\ \left(\tfrac{1}{2}\right)^{15} = .035156.$$

In other words, 1 - .035156 = .964844 is the probability that H_0 is false. In this case H_0 would be rejected at the 5% level. When they occur, zero differences are excluded because they contribute no information for deciding whether positive or negative differences are more likely.

To evaluate the usefulness of the Sign Test sixteen effective cloud top distributions are specified. Figure 15 and Table 9 describe these distributions in detail. Note that three of these distributions are used for the error analysis in the last chapter and detailed in the Appendix. The specified distributions are intended to represent the type of observed effective cloud top distributions illustrated in Figure 16. The corresponding infrared broadband weighting function curves for these sixteen distributions are given in Figures 17-23 for the tropical atmosphere. These are the curves we wish to discriminate between.

The characteristic shape of the curves in Figures 17-23 result in two problems when using the Sign Test. First, the curves exhibit a characteristic known as crossover. When comparing two curves such as FLATS and BIMOS, or FLATS and 1PK3S in Figure 17, one notices the curves crossover each other many times in the first case and at least once in the second case. Because the curves indicate vertical weighting and total weighting changes little from case to case, the curve that shows large weighting at one vertical position must show small compensating weighting at another point in the vertical. This constraint is the primary cause of curve crossovers. The crossover effect reduces the ability of the Sign Test to discriminate between two obviously different curves. This is clearly seen in Figure 19. 1PK2

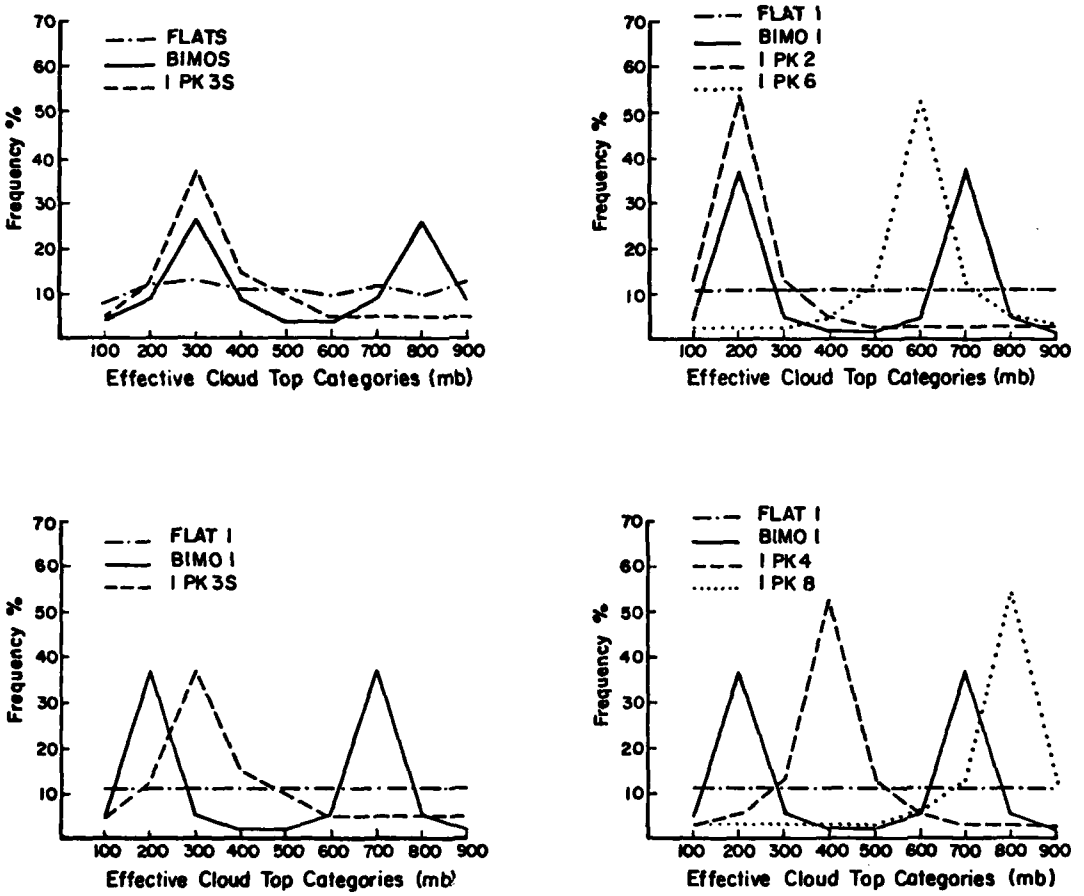

Figure 15. Plots of effective cloud top model distributions.

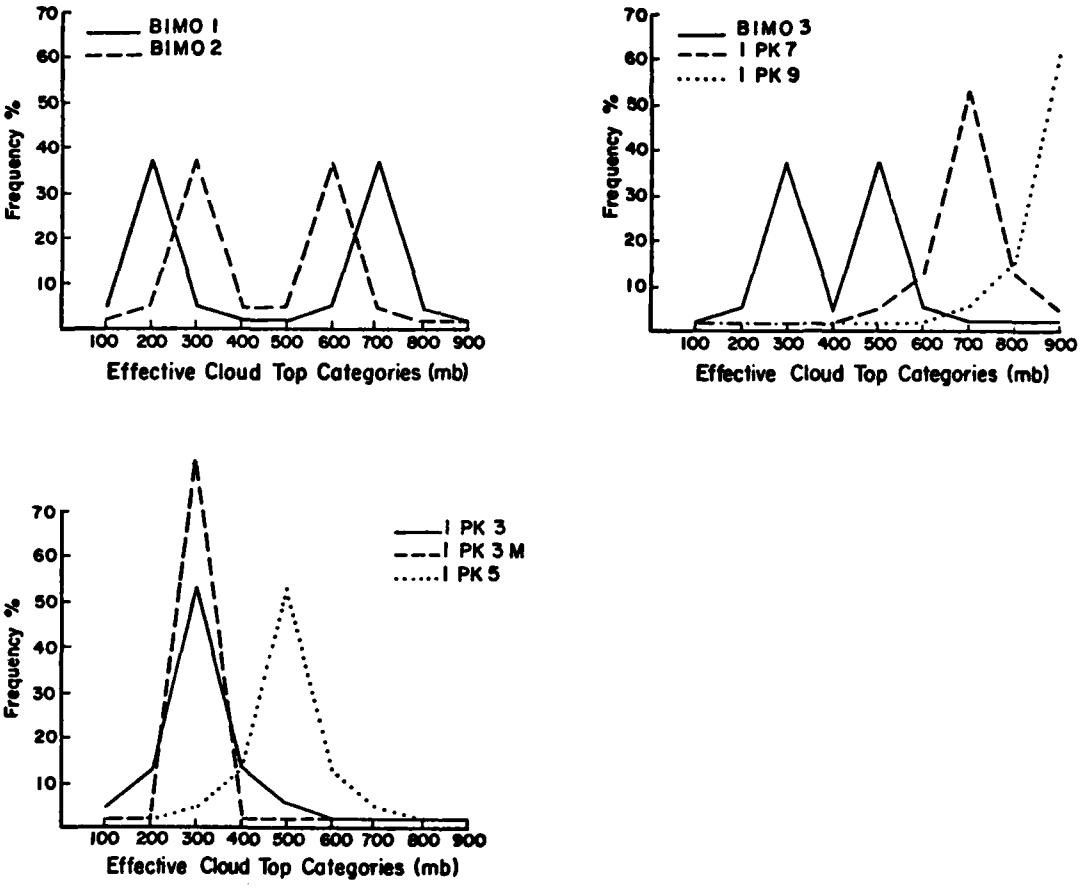

Figure 15 (Continued). Plots of effective cloud top model distributions.

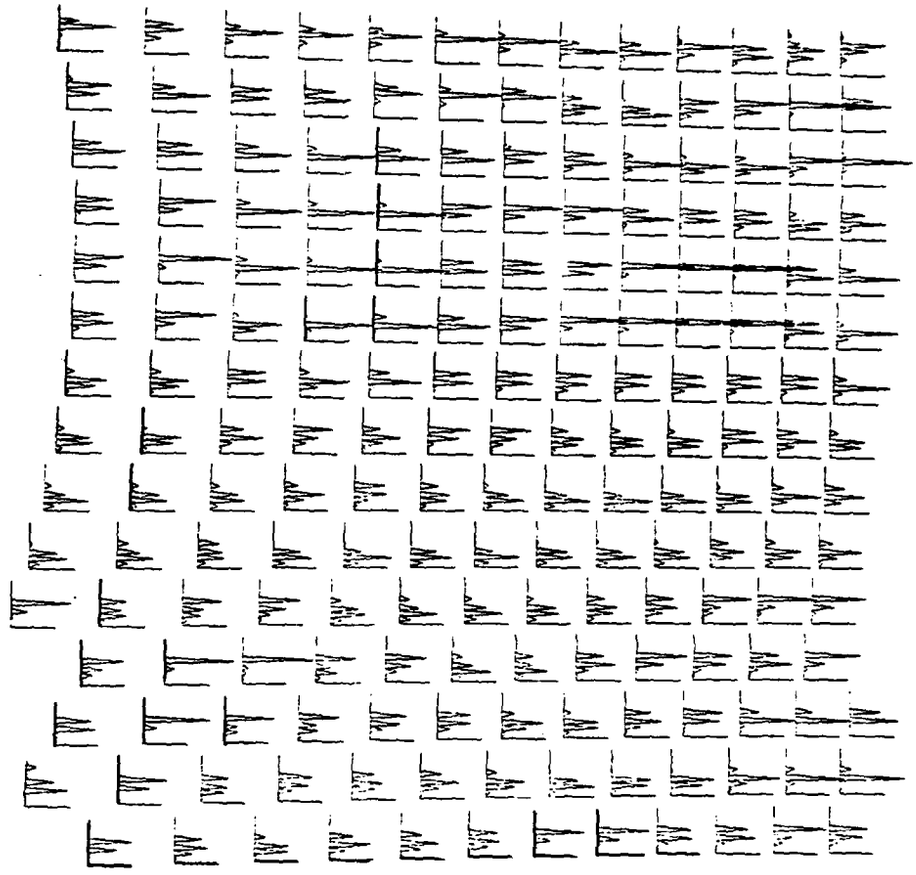

Figure 16. Unpublished figure by G. G. Campbell showing histograms (5°K resolution, 16 cat.) of geosynchronous satellite IR window radiance temperatures that approximate the cloud top distribution. Each histogram represents 200 x 200 km area. The total figure represents data taken on 16 Nov. 1978 at 1500 L for the Pacific Ocean region 10°N - 20°S latitude and 235°E - 265°E longitude.

NOTE: The length of the x-axis represents a 50% frequency and the y-axis has temperature decreasing up the axis.

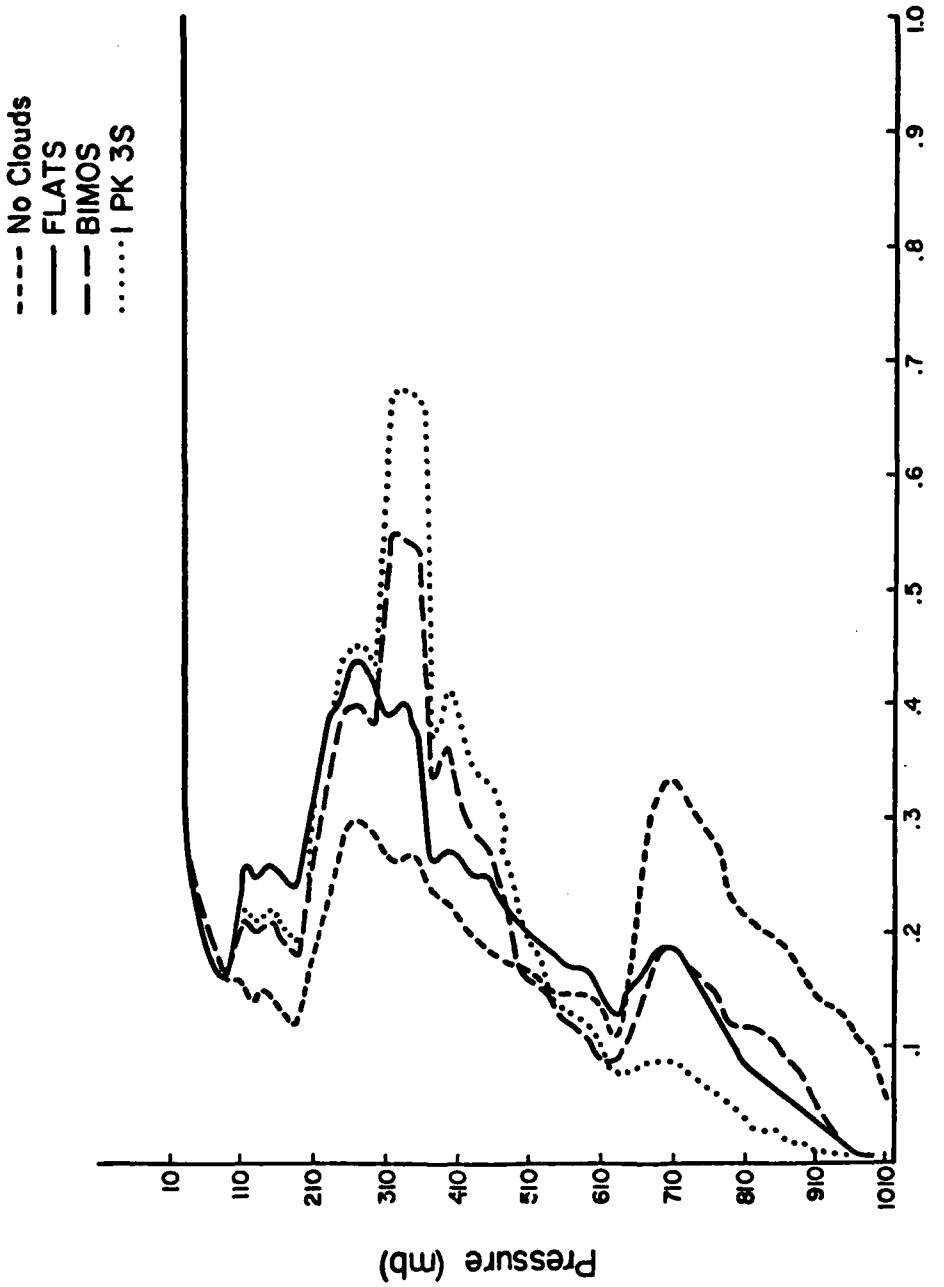

Figure 17. Broadband weighting curves for given specified distributions.

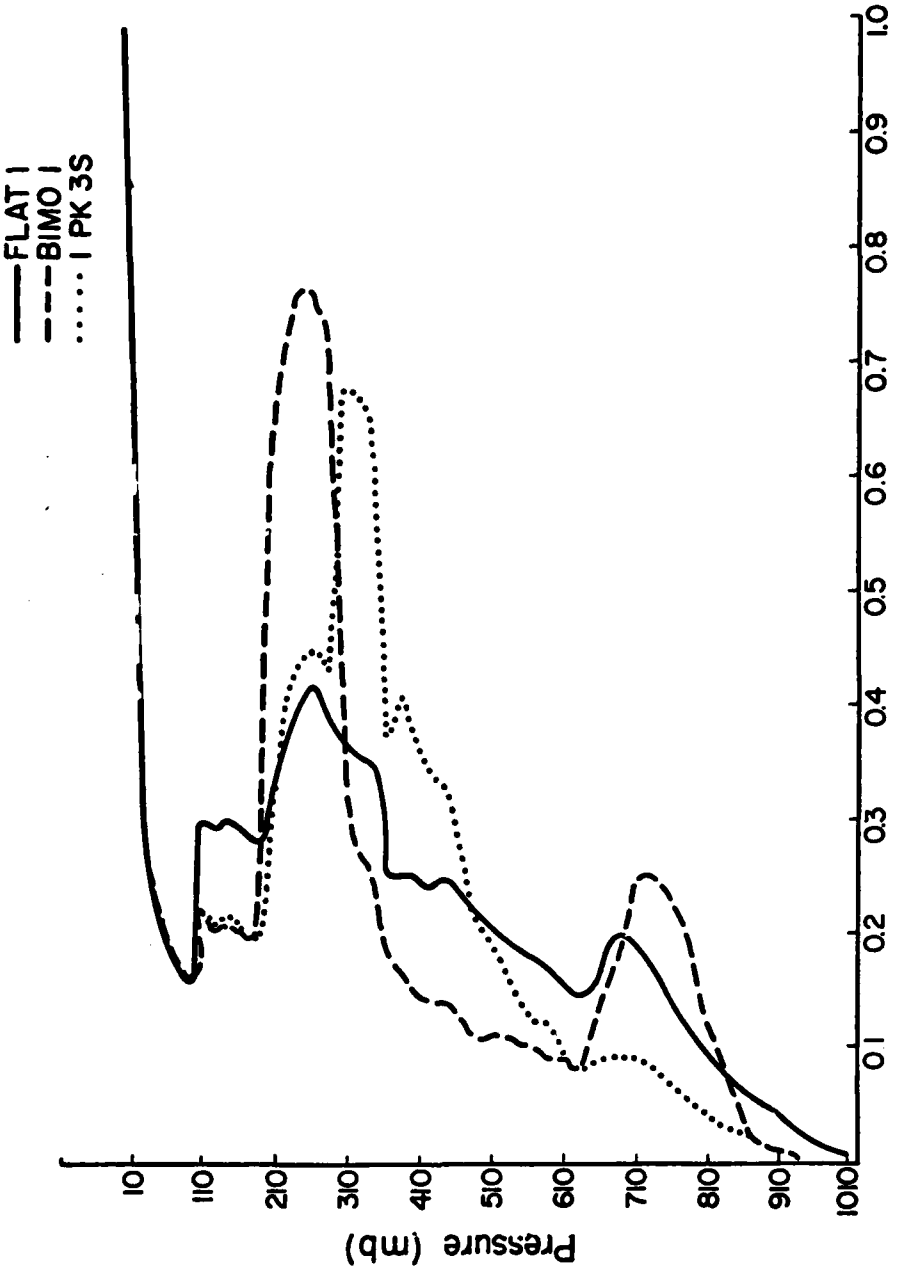

Figure 18. Broadband weighting curves for given specified distributions.

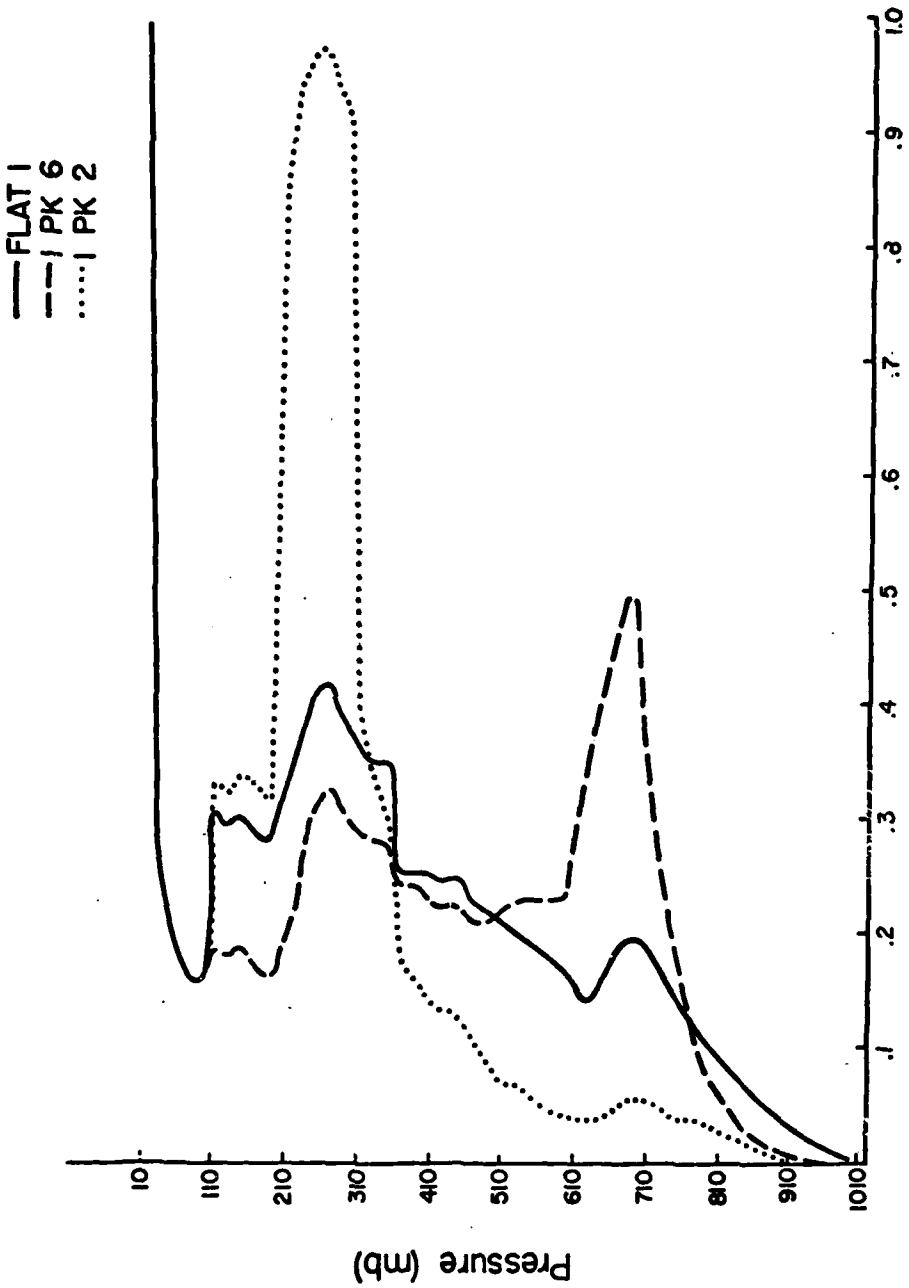

Figure 19. Broadband weighting curves for given specified distributions.

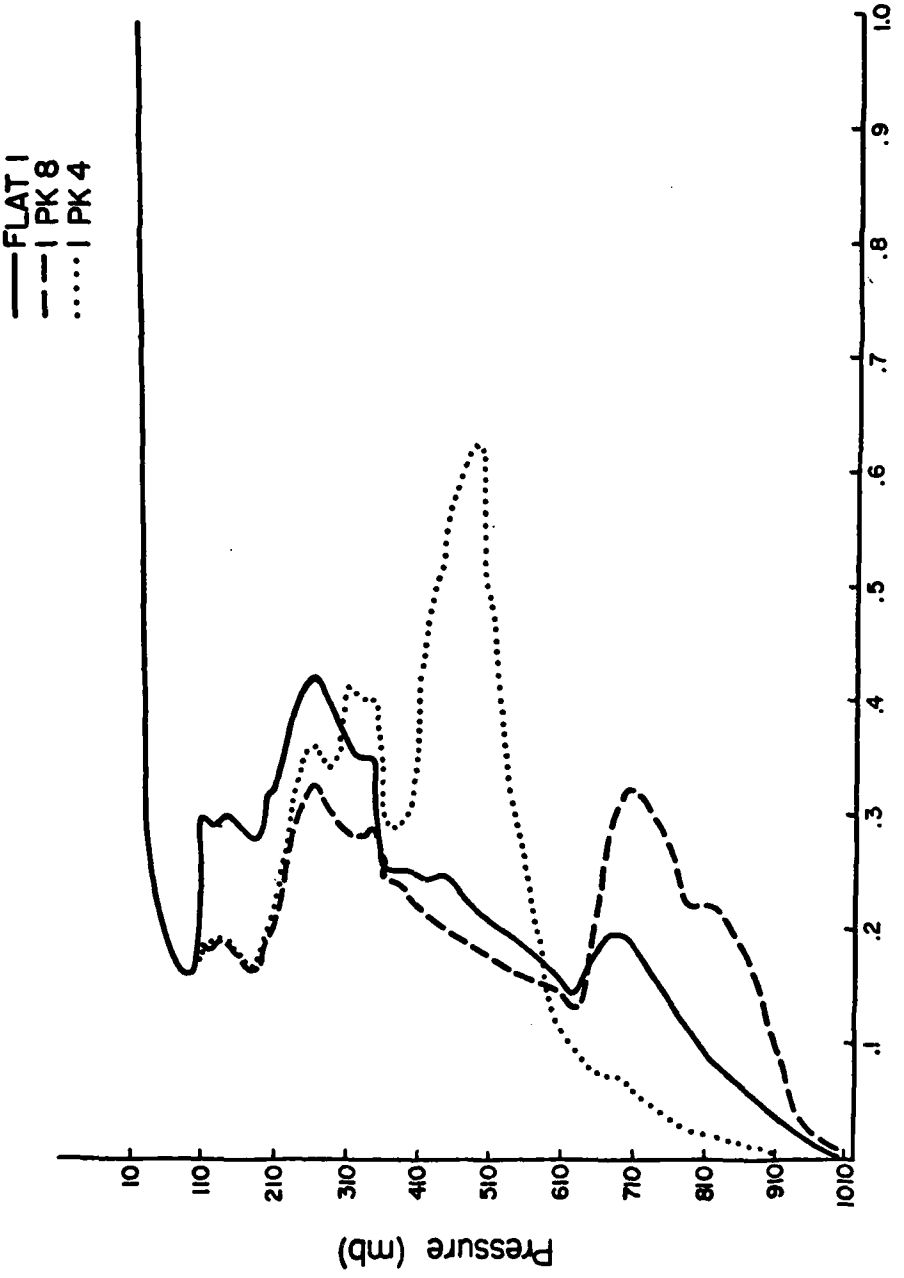

Figure 20. Broadband weighting curves for given specified distributions.

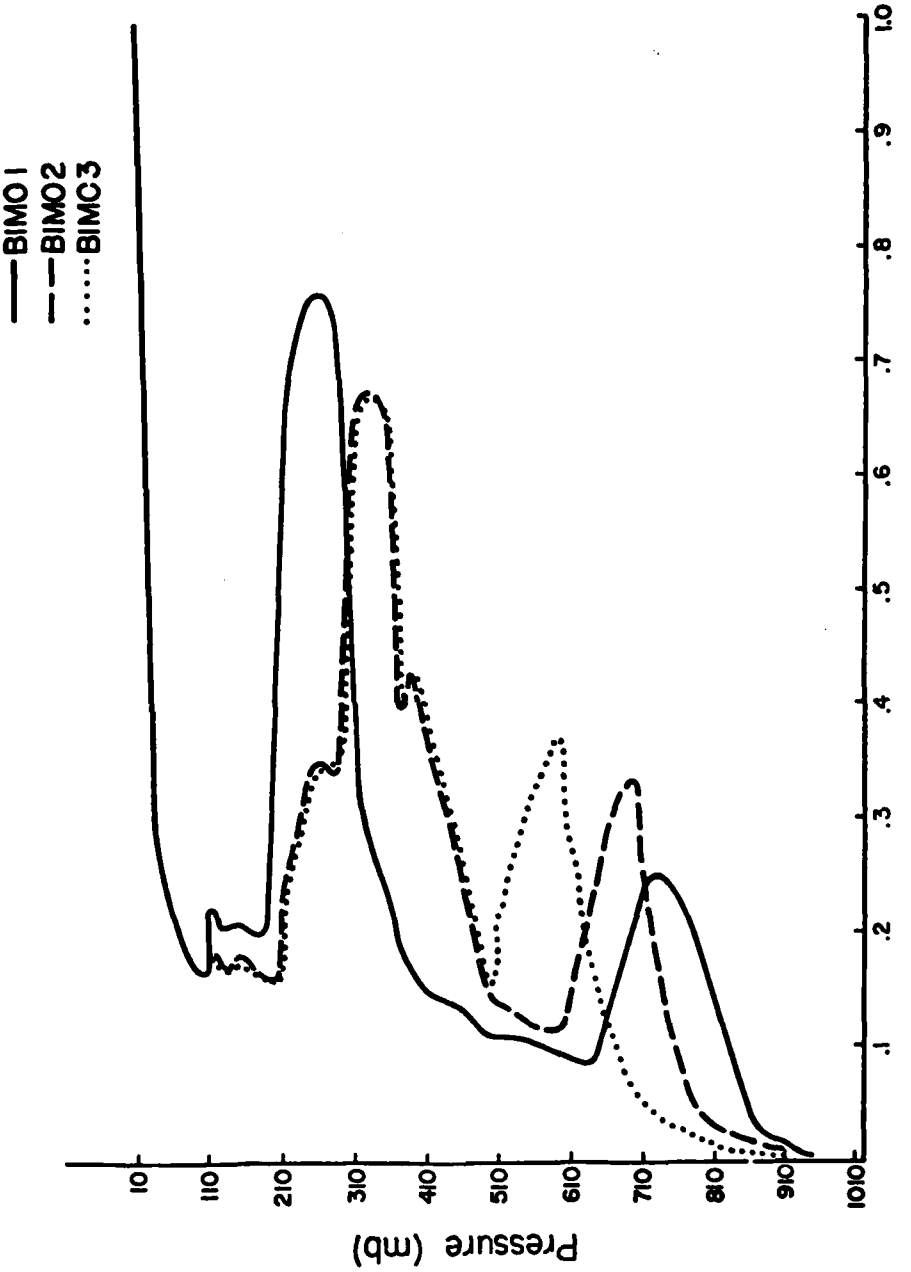

Figure 21. Broadband weighting curves for given specified distributions.

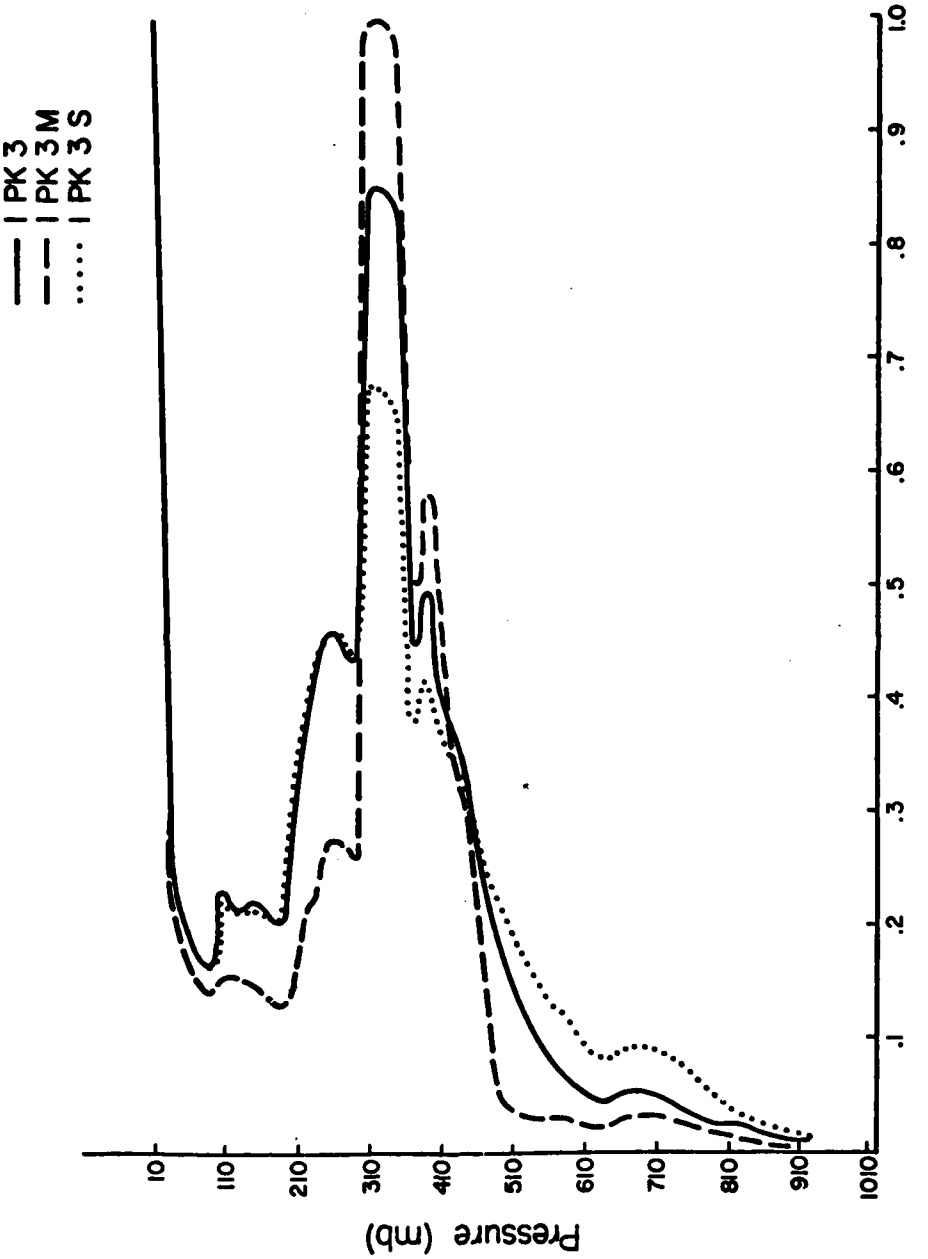

Figure 22. Broadband weighting curves for given specified distributions.

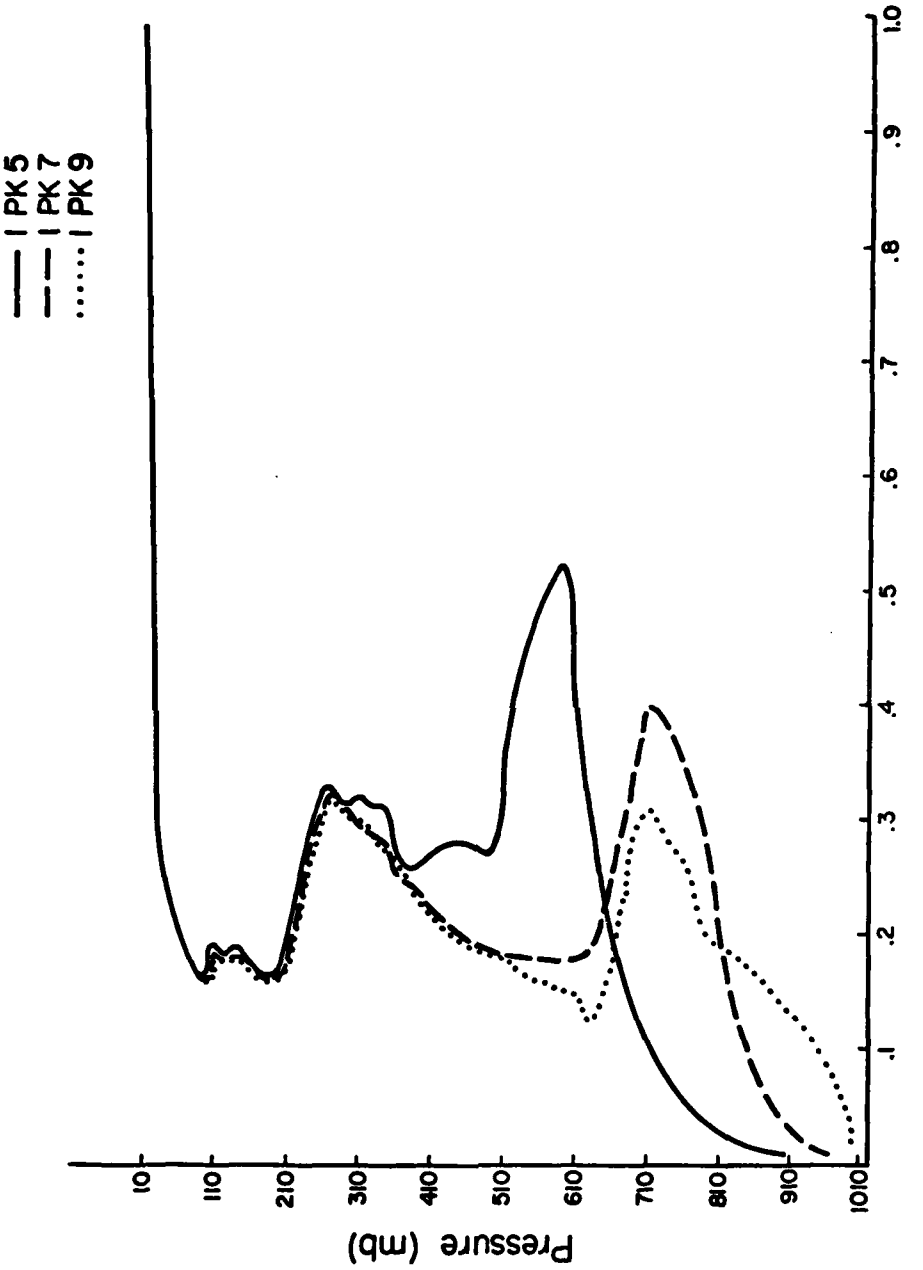

Figure 23. Broadband weighting curves for given specified distributions.

and 1PK6 are compared. For this case n = 45 and x = 19. The Sign Test cannot reject H_0 even at the 25% level. The test shows that there is greater than 1 chance in 4 that these two curves are the same. The crossover effect is to be blamed for this test deficiency.

The crossover effect may be greatly reduced by considering the curves in three equal parts of 15 pairs each instead of taken as a whole (45 pairs). The curves may be divided into three physically distinct parts. This division parallels the well known high, middle and low cloud categories. The part between 980 and 700 mb represents the lower tropospheric area of high water vapor content (approximately 85% of the total). In this area water vapor represents an important source of infrared emission as illustrated by the low level weighting function peak for clear sky in Figure 17. From 380 to 100 mb another naturally occurring clear sky weighting function peak is seen. This is also the area of cirrus cloud formation. Since ice clouds are somewhat different emittors than water clouds it is not unreasonable to examine their respective influence on the weighting curves separately. Finally, the 680 to 400 mb layer is found between the two layers described above. It lacks the consistent large amount of water vapor and the clear sky weighting function peaks. It is also true that the emitting structure within these three divisions are for the most part determined using different pairs of spectral radiative values.

Fisher's Method of Combining Three P Values is used with the Sign Test when comparing corresponding pairs from two curves in three parts (Fisher, 1958). Fisher found that the probability function distribution of - 2 times the sum of the logarithms of m independent P values is Chi-Squared with 2m degrees of freedom. Thus, the three P statistic

values are distributed as Chi-Squared with 6 degrees of freedom. The calculation of the T statistic is done using the values in Table 11 computed from the following equation,

$$T = (-2)\,[\ln P_1 + \ln P_2 + \ln P_3] \approx X^2_{d.f. = 6}.$$

For example, if $\ln P_1 = -4.9$, $\ln P_2 = -6.3$, and $\ln P_3 = -2.1$ (see Table 11), the T statistic is calculated as 26.6. Since for P = .01, $X^2_6 = 16.8$, one would reject H_0 at the 1% level (i.e. less than 1 chance in 100 that the two samples are the same and H_0 is true). The critical T values for a specified P level are given in Table 11.

Table 12 gives the T statistic for the different curve comparisons. By considering a critical value of T = 10.6 (P = 0.10), Table 12 shows that the test indicates curve differences in all cases except one (BIM01 vs. 1PK3S). Notice also that the test says FLAT1 vs. FLATS are different curves when in fact they are nearly identical. These two cases point up the second drawback of this test. Although the test allows for zero differences, the 45 curve point pairs never give an absolute difference value of zero primarily because values are computed beyond reasonable significant figures. Therefore, at times their difference is very small, but as computed for Table 12 there are always 3 sets of 15 sign values calculated with no zeros. Notice that above 100 mb (Figures 17-20) curve points are identical but they are not used in the Sign Test.

To correct this deficiency, when the difference between curve points is smaller than a specified significance level, it is set to

n = 15	
x	lnP
0	-9.7040605
1	-6.99601
2	-4.90827
3	-3.34795
4	-2.13310
5	-1.198131
6	- .49883
7	0

n = 14	
x	lnP
0	-9.010913
1	-6.302863
2	-4.35695
3	-2.8603106
4	-1.717896
5	- .85843
6	- .23521
7	0

n = 13	
x	lnP
0	-8.31777
1	-5.67871
2	-3.79598
3	-2.38287
4	-1.32108
5	- .5429104
6	0

n = 12	
0	-7.62462
1	-5.05967
2	-3.255171
3	-1.92418
4	- .947536
5	- .255649
6	0

n = 11	
0	-6.93147
1	-4.4466
2	-2.72678
3	-1.4847
4	- .59997
5	0

n = 10	
0	-6.2383
1	-3.84043
2	-2.2197
3	-1.06784
4	- .28248
5	0

n = 9	
0	-5.54518
1	-3.2426
2	-1.71654
3	- .67764
4	0

n = 8	
0	-4.8520
1	-2.6548
2	-1.2411
3	- .31943

n = 7	
0	-4.1589
1	-2.0794
2	- .79159
3	0

n = 6	
0	-3.46574
1	-1.5198
2	- .3747
3	0

n = 5	
0	-2.7726
1	- .9808
2	0

n = 4	
0	-2.07944
1	- .4700
2	0

n = 3	
0	-1.3863
1	0

n = 2	
0	- .6931
	0

n = 1	
0	0

Table 11. The logarithm of Sign Test probabilities for given n and x values.

DISTRIBUTIONS	SIGN TEST 100 - 380 mb Pos.	Neg.	400 - 680 mb Pos.	Neg.	700 - 980 mb Pos.	Neg.	T-statistic
FLATS vs. BIMOS	10	5	12	3	4	11	13.4
FLATS vs. BIMO1	10	5	15	0	8	7	21.8
FLATS vs. 1PK3S	6	9	10	5	15	0	22.8
FLAT1 vs. FLATS	6	9	12	3	1	14	21.7 +
FLAT1 vs. BIMOS	10	5	12	3	4	11	13.4
FLAT1 vs. BIMO1	10	5	15	0	8	7	21.8
FLAT1 vs. 1PK2	4	11	15	0	15	0	43.1
FLAT1 vs. 1PK3S	5	10	11	4	15	0	26.1
FLAT1 vs. 1PK4	10	5	6	9	15	0	22.8
FLAT1 vs. 1PK6	15	0	5	10	12	3	28.5
FLAT1 vs. 1PK8	15	0	12	3	14	1	40.1
BIMO1 vs. BIMOS	5	10	13	2	9	6	13.2
BIMO1 vs. 1PK2	2	13	15	0	10	5	31.6
BIMO1 vs. 1PK3S	5	10	4	11	9	6	7.7 +
BIMO1 vs. 1PK4	10	5	3	12	15	0	28.5
BIMO1 vs. 1PK6	11	4	0	15	13	2	33.5
BIMO1 vs. 1PK8	11	4	0	15	0	15	43.1
1PK2 vs. 1PK3S	10	5	0	15	3	12	28.5
1PK2 vs. 1PK4	11	4	0	15	14	1	37.7
1PK2 vs. 1PK6	13	2	0	15	6	9	30.2
1PK2 vs. 1PK8	13	2	0	15	0	15	48.6
1PK3S vs. 1PK4	15	0	3	12	15	0	45.5
1PK3S vs. 1PK6	15	0	5	10	7	8	21.8
1PK3S vs. 1PK8	15	0	6	9	0	15	40.1
1PK4 vs. 1PK6	10	5	8	7	14	1	16.4
1PK4 vs. 1PK8	10	5	9	6	0	15	22.8
1PK6 vs. 1PK8	0	15	15	0	1	14	52.8

+ referred to in the text

Table 12. Sign Test results without zero cutoff correction.

zero. Figure 18 illustrates the small differences between curves BIM01 and 1PK3 below 850 mb. These differences are set to zero. We refer to this procedure as zero cutoff correction. Table 13 which includes more curve comparisons than Table 12 gives the T values with this correction applied. Notice that most of the change occurs in the 700-980 mb group. Also notice that BIM01 and 1PK3S now pass the test for being different while FLATS and FLAT1 as well as 1PK8 and 1PK9 have small T values that indicate likeness. It is also instructive to note that the test does not catch the difference between FLAT1 and BIM0S at the P = 5% level but it does at the P = 10% level. As Figure 15 illustrates, BIM0S represents a flatter bimodal effective cloud top distribution than BIM01 which explains why FLAT1 and BIM01 are judged to be different.

From the P values given in Table 8 it is clear that T values greater than about 10 represent rejection of the null hypothesis. Curves with smaller T values indicate acceptance of H_0: the curves are the same. Referring to Table 13, values of T greater than 10 indicate unlike curves. Of the 48 combinations of curve pairings only 6 cases resulted in T values where H_0 cannot be rejected at the 5% level (two cases are mentioned above). In two of these cases (BIM02 vs. BIM03 and 1PK3 vs. 1PK3M) the effective cloud top distributions are nearly the same, explaining the statistical results. In the other two cases (BIM01 vs. 1PK3 and 1PK8 vs. 1PK7) the large amount of water vapor in the lower troposphere effectively acts as a radiating surface resulting in broadband weighting curve pairs that are quite similar, yet represent different effective cloud top distributions.

Two other points can be made from Table 13. The test is able to distinguish between two slightly different distributions peaking at

AD-A106 733 AIR FORCE INST OF TECH WRIGHT-PATTERSON AFB OH F/G 4/1
A CLIMATE INDEX DERIVED FROM SATELLITE MEASURED SPECTRAL INFRAR--ETC(U)
APR 81 M D ABEL
UNCLASSIFIED AFIT-CI-81-46D NL

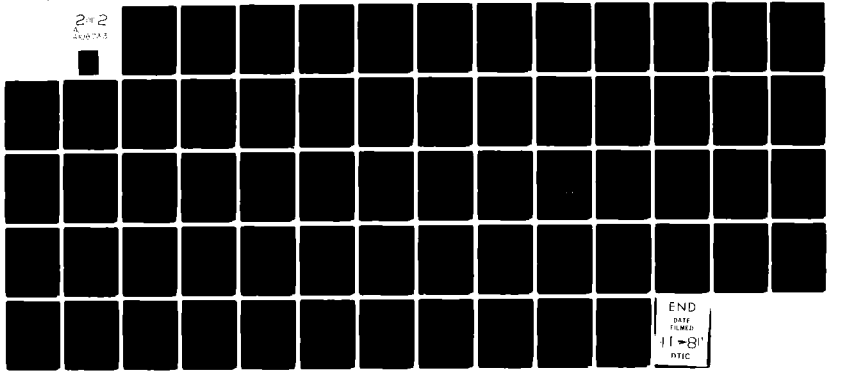

END
DATE FILMED
11-81
DTIC

DISTRIBUTIONS	SIGN TEST 100 - 380 mb Pos.	Neg.	400 - 680 mb Pos.	Neg.	700 - 980 mb Pos.	Neg.	T-statistic
FLATS vs. BIMOS	9	5	10	2	0	5	13.8
FLATS vs. 1PK3S	5	6	8	4	11	0	15.8
FLATS vs. BIMO1	10	5	13	0	3	6	20.4
FLAT1 vs. FLATS	5	3	0	0	0	0	0.6 +
FLAT1 vs. BIMOS	7	5	11	3	0	5	11.3 +
FLAT1 vs. 1PK3S	5	8	9	4	10	0	16.2
FLAT1 vs. 1PK2	3	11	15	0	11	0	39.0
FLAT1 vs. 1PK3	5	9	11	3	12	0	22.7
FLAT1 vs. 1PK4	10	5	6	9	12	0	18.6
FLAT1 vs. 1PK5	13	0	1	12	12	0	43.2
FLAT1 vs. 1PK6	13	0	2	9	7	3	24.2
FLAT1 vs. 1PK8	13	0	8	2	12	0	36.3
FLAT1 vs. BIMO1	10	5	14	0	3	6	20.4 +
FLAT1 vs. BIMO2	10	5	7	7	10	1	11.3
BIMO1 vs. BIMOS	5	5	9	0	6	5	11.1
BIMO1 vs. BIMO2	10	5	0	10	7	0	23.2
BIMO1 vs. BIMO3	10	5	2	12	8	0	20.8
BIMO2 vs. BIMO3	0	0	3	6	4	0	5.5 +
BIMO1 vs. 1PK2	0	13	11	0	8	0	40.2
BIMO1 vs. 1PK3	5	5	6	6	8	0	9.7 +
BIMO1 vs. 1PK4	10	5	3	10	8	0	16.9
BIMO1 vs. 1PK5	10	4	1	14	8	0	27.1
BIMO1 vs. 1PK6	11	3	0	15	6	2	27.6
BIMO1 vs. 1PK8	11	3	0	15	0	13	41.8
1PK2 vs. 1PK3	10	5	0	9	0	0	13.5
1PK2 vs. 1PK4	10	4	0	14	0	0	21.5
1PK2 vs. 1PK5	12	2	0	15	0	2	29.5
1PK2 vs. 1PK6	12	2	0	15	0	6	35.1
1PK2 vs. 1PK8	12	2	0	15	0	13	44.8

Table 13. (Page 1)

DISTRIBUTIONS	SIGN TEST 100 - 380 mb Pos.	Neg.	400 - 680 mb Pos.	Neg.	700 - 980 mb Pos.	Neg.	T-statistic
1PK3 vs. 1PK4	15	0	0	13	0	0	36.0
1PK3 vs. 1PK5	15	0	3	12	0	3	28.9
1PK3 vs. 1PK6	15	0	4	11	0	7	32.0
1PK3 vs. 1PK8	15	0	4	10	0	13	39.5
1PK4 vs. 1PK5	10	0	6	9	0	3	16.2
1PK4 vs. 1PK6	10	0	8	6	0	7	21.3
1PK4 vs. 1PK8	10	0	9	5	0	13	30.8
1PK5 vs. 1PK6	3	0	11	4	0	7	15.4
1PK5 vs. 1PK8	3	0	13	2	0	13	29.2
1PK6 vs. 1PK7	0	0	11	0	0	10	26.3
1PK6 vs. 1PK8	0	0	11	0	1	12	25.2
1PK8 vs. 1PK7	0	0	0	5	8	5	6.6 +
1PK8 vs. 1PK9	0	0	0	0	4	5	0.0 +
1PK3 vs. 1PK3S	5	0	2	11	0	4	17.3 +
1PK3 vs. 1PK3M	10	5	8	2	0	0	6.8 +
1PK3S vs. 1PK3M	10	5	12	2	6	0	18.0 +
BIMO1 vs. 1PK3S	5	5	3	10	8	0	14.5 +
1PK3 vs. 1/2PK3	15	0	4	9	0	15	41.5 +
1PK5 vs. 1/2PK5	3	0	13	2	0	15	32.0 +

+ Referred to in text

Table 13. Sign Test with zero cutoff correction.

the same level. For example, consider the cases 1PK3 vs. 1PK3S and 1PK3S vs. 1PK3M. Table 9 gives the cloud frequency distribution for these two similar cases of a single peak within the 300 mb category. The 1PK3 vs. 1PK3S case represents only a 15% cloud amount difference in the 300 mb category. It is also clear that the test is most sensitive when total 300 mb category cloud amounts are less than 50%. Secondly, the test can distinguish between two cases where the effective cloud top distribution is the same but the proportion of clear versus cloudy varies. For example, 1PK3 represents an overcast case whereas $\frac{1}{2}$ PK3 represents $\frac{1}{2}$ clear sky. The test is also done using 1PK5 and $\frac{1}{2}$ PK5. In summary these results show that the statistical test is capable of distinguishing between VIRES curves representing either cloud distribution shifts in the vertical or in total amount. It is successful in about 90% or more of all cases at the 95% confidence level.

The zero cutoff correction requires further explanation. The small difference value is considered zero when the difference is less than a specified constant. This constant is 5% of the average maximum point value of all points between 100 and 980 mb for all the weighting curves plotted. In reference to Figures 40-43, this is approximately a distance of .02 on the X-axis.

B. Form of the proposed climate index

Because the climate index proposed in this paper is an indicator of climatological cloudiness, it is instructive to review the status and nature of current global cloud climatologies. As mentioned earlier good cloud climatologies are especially needed for climate modeling and

climate monitoring. The VIRES climate index would be in direct competition with standard cloud climatologies to fill certain of these requirements. Therefore, a short review of the standard approach follows. A more detailed synopsis of the currently available cloud climatologies is given in two reports, one by Suomi et al. (1977) and another by Smith (1978).

The most widely used surface based observational data set seems to be that of Telegados and London (1954). Three dimensional distribution of clouds are given for the Northern Hemisphere. However, the spatial resolution of cloudiness is poor and as a consequence even the mean zonal cloudiness values given are of questionable accuracy.

Climatologies of clouds from a combination of ground and satellite sources are given by Sherr et al. (1968) and by Fye (1978). The latter reference describes the U.S. Air Force's three dimensional nephanalysis model. Both sets of climatologies suffer from the lack of spatial and temporal homogeneity in the quality of the compiled data. Nevertheless both climatologies represent global coverage and have three dimensional cloud fields. Furthermore, the Air Force's data base is continually being added to.

The longest uniform time-series of cloud satellite data are in the form of visible wavelength brightness values. From brightness values total cloud amount is inferred. Such climatologies are given by Sadler (1969), Sadler et al. (1976), Miller and Feddes (1971), and Environmental Satellite Imagery (1975-1976). Steiner (1978) summarized the Sadler et al. data, and Avaste et al. (1979) attempted to compare and combine all the brightness derived cloud climatologies given above. Avaste found that the main limitation of this data is its

non-comparability and lack of accuracy. There is also no cloud height information. This last drawback almost eliminates climate and cloud modeling applications.

Inferences of clouds from satellite data using other methods (see Chapter II) have been limited to brief periods and usually less than global coverage. Although most methods strive for three dimensional information, they suffer from a lack of accuracy mainly due to errors in retrieval technique assumptions. As mentioned earlier, all the approaches use standard cloud classification. Some reduce the classification to 3 heights (low, middle and high) and 5 fractional categories, while others use more elaborate classifications in an attempt to be more descriptive. Against this background the proposed VIRES climate index will be discussed.

Figures 17-23 show the final composite form of the infrared broadband weighting functions for 16 different distributions of cloudiness for the typical tropical atmosphere. Because it is too awkward to use the whole curve for purposes of an index, a simpler approach is needed. Of course the two curve shape parameters define the curve for a single case situation, but they will not define the curve for the composite case. Besides being simple, the index should be unique or nearly so for a given cloud distribution.

After much searching an index containing four parameters was found to be suitable. The first parameter of the index represents the level of the atmosphere above which 25% of the energy emitted to space originates. Likewise the next two parameters represent the 50% and 75% levels. The fourth number represents the percentage energy escaping to space from the surface. The approach described above can be

illustrated using the following equation:

$$\frac{\int_{p_i}^{0} \sigma T^4 \frac{\partial \bar{\tau}}{\partial \ln p} \, d \ln p}{\bar{L}_{sat}\uparrow} = i,$$

where $\bar{L}_{sat}\uparrow$ is the broadband infrared radiance measured at satellite level, p_i is one of the first three VIRES index numbers, and i is .25, .50 and .75. Of course other i values may be chosen to define another index.

Table 14 gives the calculated index values for 25 atmospheric VIRES using a tropical and mid-latitude profile atmosphere. The atmospheric levels specified in the index are in mb. For reference purposes Table 15 gives the conversion from mb to meters. The RTE model used produced index values to the nearest 10 mb. Table 14 shows no surface emission from the surface in the tropical case due to water vapor diameter absorption and approximations used in the RTE model. However, ideally a small amount of surface emission would be expected.

Index values given in Table 14 show that weighting curves that are nearly identical give identical indexes (i.e. FLATS and FLATR, BIMOS and BIMOR, 1PK3S and 1PK3R). Specified cloud distributions in the two different atmospheres give the same index at high levels (i.e. 1PK3) but a somewhat different index at lower atmospheric levels (i.e. 1PK8) due primarily to the fact that low level water vapor contributes to the atmospheric VIRES. Notice that low clouds (1PK7, 1PK8, 1PK9) have nearly the same index in the tropical case where low level water vapor

Effective Cloud Top Distribution	TROPCIAL ATMOSPHERE				MID-LAT. SUMMER ATM.			
	25%	50%	75%	Sfc %	25%	50%	75%	Sfc %
FLATS	250	430	650	0	250	450	690	1
FLATR	250	430	650	0	250	450	690	5
FLATR*	250	430	650	0	250	450	690	6
FLAT1	250	430	650	0	250	450	690	1
BIMOS	270	410	670	0	270	430	750	0
BIMOR	270	410	670	0	270	430	750	6
BIMO1	230	370	690	0	230	370	730	1
BIMO2	290	390	630	0	290	390	630	0
BIMO3	270	390	550	0	270	390	550	0
1PK3S	250	350	510	0	250	350	510	0
LPK3R	250	350	510	0	250	350	510	4
1PK2	190	270	390	0	190	270	390	3
1PK3	230	330	430	0	230	330	430	0 +
1PK4	270	430	510	0	270	430	510	0
1PK5	290	490	590	0	310	510	590	0
1PK6	310	550	670	0	310	570	690	0
1PK7	310	570	730	0	330	610	770	0 +
1PK8	310	590	750	0	330	630	850	0 +
1PK9	310	590	750	0	330	650	910	0 +
CLEAR	350	650	790	0	370	790	-	37
½ CLEAR FLAT1	290	530	730	0	310	570	950	21
½ CLEAR BIMO1	270	530	730	0	270	590	930	21
½ CLEAR 1PK3	290	430	710	0	290	450	930	12 +
½ CLEAR 1PK5	310	530	710	0	330	550	890	20
½ CLEAR 1PK7	330	610	750	0	330	670	890	19

+ Referred to in the text

Table 14. Proposed VIRES climate index.

Table 15. Pressure to Height Conversion.

Pressure mb	Mid. Lat. Atm. (m)	Tropical Atm. (m)
110	16280	16330
130	15150	15200
150	14150	14230
170	13330	13430
190	12600	12710
210	11930	12050
230	11340	11450
250	10780	10880
270	10260	10360
290	9760	9860
310	9290	9390
330	8850	8940
350	8430	8510
370	8030	8120
390	7640	7720
410	7270	7351
430	6920	6990
450	6570	6650
470	6240	6320
490	5930	6000
510	5620	5690
530	5320	5390
550	5030	5090
570	4750	4810
590	4480	4540
610	4210	4270
630	3960	4010
650	3710	3750
670	3460	3510
690	3220	3260
710	3000	3030
730	2760	2800
750	2540	2570
770	2320	2350
790	2110	2130
810	1900	1920
830	1690	1720
850	1490	1520
870	1300	1320
890	1110	1120
910	917	933
930	732	745
950	550	561
970	372	379
990	197	201
1007	55	56

emits like a cloud. This is not true for the mid-latitude case where low level water vapor does not contribute much to the atmospheric VIRES. Also notice that similar distributions of clouds but with a different percentage of clear sky have different indexes (i.e. $\frac{1}{2}$ clear 1PK3 vs. 1PK3).

In general the VIRES climate index outlined above may be considered an appropriate and accurate atmospheric descriptor. The parameters in the index indicate the vertical source of emitted earth-atmospheric energy. The index is especially compatible with the original satellite data resulting in minimal anticipated errors. The analysis shows the index has the desired uniqueness characteristic while at the same time remaining straightforwardly simple.

Of course one could consider it a drawback that the index is not compatible with standard measures of cloudiness. However, the index is meant to be closely related to the radiative measurements. Clouds are thought of as simply one constituent (albeit the most important) of the atmospheric VIRES. Furthermore real physical clouds are never considered at all. Only the equivalent radiative effects of specified clouds are taken into account. This approach avoids many difficulties while at the same time providing information that may be used for climate monitoring and for calibration and parameterization of radiative calculations in climate models (the topic of Chapter VII). The next section discusses possible specifications for index use.

C. Climate index specifications

The climate index described in this paper will be used similar to a cloud climatology. It should, therefore, have some of the same

characteristics. Smith (1978) suggests that for purposes of parameterization of cloudiness and radiation in climate models, cloud climatologies should have global coverage with a space resolution of 250 km (≈ 2½° Lat. by 2½° Long.) and a time resolution of 4 hours. Research by Avaste et al. (1979) suggests that for climate monitoring purposes the space resolution be 500 km (≈ 5° Lat. by 5° Long.) and time resolution be monthly. A weekly specified time resolution has been suggested by the U.S. Committee for GARP (1975). Before specifying time and space resolution for the proposed climate index let us consider satellite data collection limitations.

Present operational and experimental sun-synchronous weather satellites carry infrared radiometers that have nadir resolutions of at least 30 km. Similar radiometers for geosynchronous satellites will have comparable resolution. Therefore, compiling a VIRES index climatology with useful space resolution seems feasible. However, the global coverage requirement is harder to meet when combined with the time resolution demand.

Satellites such as NIMBUS and TIROS are in sun-synchronous orbits and only make observations over any single earth location twice a day at the same times everyday although the whole globe is covered. Because of diurnal cloudiness variations, twice a day observations give biased results (Harrison et al. 1978, 1980). On the other hand, geosynchronous satellites make observations at all hours but in general can effectively view only between 60°N and 60°S latitude and about 120° of longitude. More complete coverage can be achieved by observing nearly all the low and middle latitudes at each hour by adding a satellite with a mid-inclined orbit which precesses (Harrison et al. 1978).

A good discussion concerning optimizing satellite observations is given by Campbell and Vonder Haar (1978). Nevertheless, it is clear that no one type of satellite offers both the ideal spatial coverage and ideal temporal resolution.

Remembering this limitation, one should consider the importance of cloud classification. Sherr et al. (1968) proposed 29 different cloud climatological regions globally. These regions were based primarily on seasonal distributions of mean monthly cloud cover. Also considered were annual cloud distributions, area precipitation distributions, and different climate classification schemes. Most regions were repeated two or more times throughout the world. Some of Sherr's typical region descriptions are; tropical cloudy, desert marine, mid-latitude clear summer, high latitude clear winter, mediterranean and polar. A similar cloud classification scheme is given by Winston (1969).

By considering cloudiness regions instead of strictly global measurements one might for instance actually have a more sensitive measure for the purpose of climate monitoring. Applications of the climate modeling type might also be stronger on a regional basis. Consequently, global coverage seems to be of secondary importance. Thus, one would expect a climate index derived from geosynchronous satellite data to be the basis of a good climatology except where total global coverage is required. Sun-synchronous satellites could provide additional information if the time bias problem is avoided.

From this discussion one may conclude that the best approach is to take the geostationary satellite information available and average it to a 250 km space resolution and 4 hour time resolution. From these values longer time and larger space scale values can be obtained

with emphasis on weekly regional averages. Of course there should be an attempt to use sun-synchronous satellite data to complete the global picture.

Related to the time resolution problem is the problem of instrument continunity through time. In other words, how do we keep the satellite instrument absolutely calibrated? Without the absolute calibration it becomes necessary to intercompare instruments from different satellites for the purpose of obtaining a homogeneous data set. It is also necessary to detect and correct changes in a specific instrument over time. Of course intercomparisons would be useful as a second check even with absolute calibration. The proposed Space Shuttle may offer the means of intercomparing instruments, although for now such a process is impossible (COSPAR, 1978b). Also, a common ground base laboratory test facility for all satellite instruments would provide a chance to uncover systematic differences.

Calibrating radiation instruments in any absolute sense is very difficult if not impossible (COSPAR, 1978b) especially for SW sensors. Calibration targets such as black bodies are sometimes used successfully for IR instruments. One may also use a transfer technique; observe the same target at the same time with two different instruments whose output can be compared. If one of the instruments has a trusted calibration then the other one may be calibrated. Another approach is to convert radiant energy into heat energy using a known, stable process. The advantage here is that the efficiency of this conversion as a function of temperature can be determined independently and therefore 'known' calibration sources are not needed. Lastly, it can be said that the nature of radiation (e.g. its amplitude, wavelength,

interference and diffraction effects, and polarization) makes calibration of radiometers a complex operation with many uncertainties, especially for SW instruments. Fortunately, the more easily calibrated IR sensitive radiometers are used to derive the VIRŁS index.

VII. POSSIBLE APPLICATIONS OF A SATELLITE DERIVED CLOUDINESS INDEX

Most of the cloud retrieval methods mentioned in Chapter II have been developed with the idea that deducing global cloud climatology information from satellite data is desirable. Most have tried to conform with classical ground observational definitions of clouds. The present research suggests that a more realistic and progressive point of view is to consider clouds in light of their radiative properties. After all, counting and typing individual clouds on a global climatological basis is probably an impossible task, and the results of such a census may not provide the best information for the application. Therefore, a climatic index that represents cloudiness by means of the infrared broadband weighting function is proposed. How might such an index be used? Perhaps the two most important applications for such a climatological index are in the areas of climate modelling and climate monitoring (Smith, 1978).

A quote from GARP Publication 16 (Stockholm, 1974) relates the importance between climatic processes of clouds and their radiative effects: "... proper treatment of radiative effects of clouds is the single most important factor in the overall parameterization of radiation in a climate model". However, proper treatment of clouds is difficult even for the most advanced climate models. For example, most clouds are sub-grid scale for the typical general circulation model (GCM). Thus, clouds will undoubtedly be parameterized in future models much as they are now. Furthermore, these cloud parameterizations are one of the weakest aspects of the present GCM's. Climate models now lack the ability to meaningfully calculate radiative forcing due to the

failure of cloud-dynamic parameterizations (Webster, 1978). Nevertheless, as newer and better cloud models are developed they must be verified and tuned against actual measurements of global cloudiness (Cox, 1978).

Because climate models necessarily have many assumptions, approximations and parameterizations, verification of their results is quite important. Furthermore, computation of one parameter may be successful because the model contains compensating errors in, for example, the treatment of physical processes. One can have more confidence in the validity of ones model by checking calculated against measured parameters that are both a direct measure of a physical process and available in time and space scale detail. The climatic cloudiness index outlined in this paper is a particularly useful parameter because it is a radiative index that can be compiled for weekly or seasonal worldwide vertical profile values. In other words, the 4-dimensional characteristic of this observable variable would make it a particularly good verification tool for the parameterization of clouds in the GCM radiative calculations.

The values of the proposed index may also be useful in GCM cloud parameterization studies. Instead of dealing directly with clouds in a model, one might go directly from dynamic-thermodynamic considerations to radiative effects (COSPAR, 1978a). Another approach is to relate model derived cloudiness directly to radiative divergence profiles without any model cloud radiative calculations (Cox and Vonder Haar, 1973). Such "direct" parameterization studies will need to use observational data like the cloudiness and radiative information contained in the index.

The second area of potential index application is in climate monitoring. The earth's climate is a function of the earth-atmosphere system reacting to the equator-to-pole gradient of net energy; this net energy budget may be quantified and divided into components by the net radiation budget studies using satellite data (Vonder Haar and Oort, 1973; Campbell and Vonder Haar, 1980a,b). Clouds are the principal modulators of the radiation for they strongly influence the earth's solar albedo and infra-red absorption. To extend and improve the climate monitoring aspect of these radiation budget studies there is a need to determine cloudiness independent of the satellite radiation budget measurements (Vonder Haar, 1979). The index described in this paper would be useful for this purpose.

Because we feel that cloudiness is an important climate variable, and since the VIRES index is strongly a function of cloudiness, it follows that the index itself represents a physical characteristic of the climate system. The temporal and spatial variations of this index can be detected using the statistical method described earlier. This could be done on a global or regional scale in an attempt to detect climatic trends. Regional changes which can be concealed in global averages may provide a more sensitive measure of climatic change. Moreover, climatic anomalies in one area are often correlated with variations in another area. Occassionally there is also a time lag. In such cases climatic forecasts can be made. These teleconnections might be identified and observed easier by processing satellite data into meteorological indexes like the one described in this paper.

The index described in this paper has both information about cloudiness and outgoing longwave radiation. In this respect it would

be especially valuable to the National Climatic Research Program (NCRP). The NCRP Committee proposes satellite observations in the form of a Climatic Index Monitoring Program in addition to conventional meteorological observations (U.S. Committee for GARP, 1975). This VIRES index would represent two indexes in one. Furthermore, it can be computed for the global coverage and weekly frequency required.

There are other possible uses for a radiatively defined cloudiness index. When combined with radiation budget studies a better assessment of atmospheric energetics may be possible (COSPAR WG 6, 1978a). Climatic change may be viewed as an adjustment among compensating feedback processes. Using this index one may be able to identify and quantify coupling between cloudiness and other atmospheric variables. Perhaps by using the index more specific relationships between the cloudiness and the earth-atmosphere energy balance (Hartman and Short, 1980; Herman et al. 1980; Ohring and Clapp, 1980) can be found. Conceivably this index could help determine whether or not a change in cloudiness necessarily results in a change in the climate (Cess, 1976; Ellis, 1978; Coakley, 1979; Van Den Dool, 1980). In this regard the index could shed some much needed light on the role of cloud vertical structure as it applies to the cooling to space portion of the earth-atmosphere radiation budget. The VIRES index would also be useful in understanding more clearly the consequence of tropospheric water vapor emission as it relates to the earth-atmosphere radiative loss.

VIII. CONCLUSIONS

This paper introduces and describes a climate index called the VIRES index. VIRES is the acronym for Vertical Infrared Radiative Emitting Structure and quite by chance it is also the plural form of the Latin word vis, meaning forces or powers. Thus, the acronym seems especially appropriate since the atmosphere's VIRES is one of the major forcing factors behind the earth's climate. The VIRES index is related to the earth's climate through the earth's radiation budget and therefore can be considered a climate index. The logic behind this claim may be stated as follows. The climate system is determined by the energy input to the system and the distribution, transformation and storage of energy in various forms within the system. These processes are mirrored in the components of the earth's radiation budget, one of which is the outgoing emitted thermal radiation (COSPAR Report to ICSU and JOC, 1978b). This cooling to space is described by the VIRES which is primarily a function of the cloud distribution.

This index is an attempt to optimize the use of satellite data for climate purposes by directly utilizing the radiative aspects of the atmosphere while avoiding some of the difficulties of inferring standard meteorological variables from satellite radiances. The VIRES index is based on broadband infrared weighting curves retrieved from operationally measured spectral, earth-emitted radiation in the CO_2 absorption band. These curves describe the vertical structure of infrared radiative emission and are a function of the cloud, temperature and moisture distributions. The most important findings of this research are summarized below.

A. Cloud - VIRES relationship

This paper demonstrates under both tropical and mid-latitude atmospheric conditions the predominate influence of the three dimensional cloud distribution on the atmosphere's Vertical Infrared Radiative Emitting Structure (VIRES). Therefore, the VIRES index can be considered an indicator of cloudiness with the caution that low cloud or high water vapor content can both result in the same VIRES. Also illustrated is the fact that the atmospheric VIRES is responsive to the three dimensional distributions of water vapor and temperature.

B. VIRES retrieval technique

VIRES curves may be inferred directly from satellite measured radiances. A retrieval technique utilizing CO_2 band spectral radiances is described which determines two weighting curve shape parameters (p_{wf} and α). The empirical RTE method was found to be both computationally fast and accurate. The two parameters inferred using the empirical RTE method define a single scene VIRES. The single scene retrievals are composited to give a temporal and spatial average VIRES curve. A sensitivity study and error analysis using simulated satellite data that included the effect of sampling inadequacies quantified the abilities of the empirical RTE retrieval approach.

C. VIRES uniqueness

The VIRES curves calculated for diverse cloud (climate) regimes have been shown to be statistically different in all cases with the following two exceptions. In the moist atmosphere case the high concentrations of low level water vapor radiatively emit to space almost identically like the case with low level cloud. The second exception

occurs for comparisons between two similar cloud shape distributions. The simple non-parametric statistical test compares the points from two VIRES curves every 20 mb. As might be expected, the VIRES index values show (qualitative) uniqueness. Thus, climate change can be effectively monitored using the VIRES index which conveniently and quantitatively expresses the vertical structure of terrestrial emission to space.

D. VIRES index

Although the VIRES curves contain the maximum vertical information, they are cumbersome to work with. Therefore, a useful descriptor of the VIRES curve called the VIRES index was developed. As stated above, the index is able to protray differences in the atmosphere's vertical emitting structure. The first three number parameters in the index represent pressure levels in the atmosphere above which a specified fraction (.25, .50, .75) of the infrared energy lost to space originates. The last parameter represents the fraction of energy lost to space which originated at the earth's surface. The index is especially useful since it represents the VIRES curve information in a shortened, interpretable, and flexible form. The four parameter index prposed in this work may be easily modified to maximize its usefulness for different applications.

E. Suggested applications and sampling strategies

A number of specific applications have been proposed and in general they are related to climate monitoring and climate modeling. For example, to monitor the climate, regional VIRES index averages can be compiled. These values would probably be very sensitive to climate

variations. It is recommended that this basic index, calculated from geostationary satellite radiance measurements, be averaged to a spatial resolution of 250 km (2 1/2° latitude by 2 1/2° longitude) with the smallest time resolution being 4 hours. Of course sun synchronous satellite data may be used to supplement coverage. From these data coarser spatial and temporal averages can be calculated for other specific applications such as regional or global climate modeling. The VIRES index can be used for climate model baselining and verification of radiative calculations. Index values may also be useful to research efforts in the area of cloud parameterizations.

LITERATURE CITED

Avaste, O. G., G. Campbell, E. Smith, S. Cox and T. Vonder Haar, 1979: Determination and analysis of total cloud cover over the oceans 1975-1978. Dept. of Atmospheric Science Report No. 300, Colo. State Univ., Ft. Collins, CO., 73 pp.

Beyer, W. H. ed., 1971: CRC Basic Statistical Tables. The Chemical Rubber Co., Cleveland, Ohio, 310 pp.

Bignell, K. J., 1970: The water vapor infrared continuum. Quart. J. Roy. Meteor. Soc., 96, 390-403.

Bolin, B., and W. Bischof, 1970: Variations of the carbon dioxide content of the atmosphere in the northern hemisphere. Tellus, XXII, 431-442.

Campbell, G. G., and T. H. Vonder Haar, 1978: Optimum satellite orbits for accurate measurement of the earth's radiation budget. Atmos. Sci. Paper No. 289, Colo. State Univ., Ft. Collins, CO., 61 pp.

_____, E. A. Smith and T. H. Vonder Haar, 1980: Cloud amount estimation from geosynchronous satellites: a demonstration of diurnal variation. Proceedings of the 1980 International Radiation Symposium, Ft. Collins, CO., Aug. 11-16, 312-314.

_____, and T. H. Vonder Haar, 1980a: An analysis of two years of Nimbus 6 earth radiation budget observations: July 1975 to June 1977. Atmos. Sci. Paper No. 320, Colo. State Univ., Ft. Collins, CO., 83 pp.

_____, and _____, 1980b: Climatology of radiation budget measurements from satellites. Atmos. Sci. Paper #323, Colo. State Univ., Ft. Collins, CO., 74 pp.

Cess, R. D., 1976: Climate change: an appraisal of atmospheric feedback mechanisms employing zonal climatology. J. Atmos. Sci., 33, 1831-1843.

Chahine, M. T., 1974: Remote sounding of cloudy atmospheres, I. The single cloud layer. J. Atmos. Sci., 31, 233-243.

_____, 1975: An analytical transformation for remote sensing of clear-column atmospheric temperature profiles. J. Atmos. Sci., 32, 1946-1952.

Chen, T. S., L. L. Stowe, V. R. Taylor and P. F. Clapp, 1980: Classification of clouds using THIR data from Nimbus 7 satellite. Proceedings of the 1980 International Radiation Symposium, Ft. Collins, CO., Aug. 11-16, 315-317.

LITERATURE CITED (Continued)

Clapp, P. F., 1964: Global cloud cover for seasons using TIROS nephanalysis. Mon. Wea. Rev., 92, 495-507.

Coakley, J. A. Jr., 1979: A study of climate sensitivity using a simple energy balance model. J. Atmos. Sci., 36, 260-269.

COSPAR Report to ICSU and JOC, 1978a: Status of satellite observing possibilities for study of climate physical processes. NCAR, Boulder, CO., 111 pp.

_____, 1978b: Toward an internationally coordinated earth radiation budget satellite observing system: scientific uses and system considerations. NCAR, Boulder, CO., 76 pp.

Cox, S. K., and T. H. Vonder Haar, 1973: Measurements of solar energy for the study of time dependent meteorological systems. Proceedings of Symposium on Solar Radiation, Smithsonian Institution Radiation Biology Laboratory, Nov. 13-15, 32-35.

_____, M. C. Polifka, K. Griffith, A. Rockwood and D. Starr, 1976: Radiative transfer computational routines for atmospheric science applications. Dept. Atmos. Sci., Colo. State Univ., Ft. Collins, CO., 75 pp.

_____, 1978: Review of parameterizations of radiation and extended cloudiness. JOC Study Conference on Parameterization of Extended Cloudiness and Radiation for Climate Models. Oxford, U.K., 27 Sept. - 4 Oct., 21 pp.

_____, and K. T. Griffith, 1978: Tropospheric radiative divergence during Phase III of the GARP Atlantic Tropical Experiment (GATE). Atmos. Sci. Paper #291, Colo. State Univ., Ft. Collins, CO., 166 pp.

Crutcher, H. L., and J. M. Meserve, 1970: Selected level heights, temperatures and dewpoints for the Northern Hemisphere, NAVAIR 50-1C-52.

Dalton, J. T., M. L. Desjarding, A. F. Hasler and R. A. Minzner, 1979: Digital cloud stereography from geostationary orbit. Proceedings of the 13th International Symposium on Remote Sensing of the Environment (Ann Arbor, Michigan, April 23-27), 1479-1488.

Elasser, W. M., and M. F. Culbertson, 1960: Atmospheric Radiation Tables. Meteorological Monographs, 4, No. 23.

Ellis, J. S., 1978: Cloudiness, the planetary radiation budget, and climate. Ph.D. thesis, Dept. of Atmos. Sci., Colo. State Univ., 129 pp.

LITERATURE CITED (Continued)

Environmental Satellite Imagery, March 1975 - February 1976: NOAA Environmental Data Service, KMRD No. 5.4g, Washington, D.C.

Fisher, R. A., 1958: Statistical Methods for Research Workers. 13th Edition, Hafner Pub. Co. Inc., N.Y., 356 pp.

Fye, F. K., 1978: The AFGWC automated cloud analysis model. AFGWC Tech. Memo. 78-002, HQ AFGWC, Offutt AFB, Nebraska, 97 pp.

Griffith, K. T., and S. K. Cox, 1977: Radiative properties of clouds inferred from broadband measurements. Atmos. Sci. Paper #269, Colo. State Univ., Ft. Collins, CO., 102 pp.

Gupta, S. K., S. N. Tiwari, and J. T. Suttles, 1978: Longwave radiation transfer in the atmosphere. Proceedings of the 3rd Conference on Atmospheric Radiation, Davis, CA., June 28-30, 40-43.

Handbook of Geophysics and Space Environments, 1965: Air Force Cambridge Research Laboratories, Office of Aerospace Research, U.S. Air Force, 649 pp.

Harrison, E. F., G. G. Gibson and P. Minnis, 1978: Sampling analysis for the earth radiation budget satellite system mission based on orbital coverage and cloud variability. 3rd Conf. on Atmospheric Radiation, Davis, CA., 28-30 June.

_____, P. Minnis and G. G. Gibson, 1980: Temporal and spatial variability of cloud cover from GOES data for radiation budget studies. Proceedings of the 1980 International Radiation Symposium, Ft. Collins, CO., Aug. 11-16, 361-363.

Hartman, D. L., and D. A. Short, 1980: On the use of earth radiation budget statistics for studies of clouds and climate. J. Atmos. Sci., 37, 1233-1250.

Heath, D., 1973: Space observations of the variability of solar irradiance in the near and far infrared. J. Geophys. Res., 78, 2779-2792.

Herman, G. F., M. C. Wu, and W. T. Johnson, 1980: The effect of clouds on the earth's solar and infrared radiation budgets. J. Atmos. Sci., 37, 1251-1261.

Houghton, J. T., 1979: The future role of observations from meteorological satellites. Quart. J. Roy. Met. Soc., 105, 1-23.

International Cloud Atlas, Vol. 1, WMO 1956, Geneva, Switzerland.

Jenne, R. L., H. L. Crutcher, H. Van Loon, and J. J. Taljaard, 1974: A selected climatology of the southern hemisphere: computer methods and data availability. NCAR-TN/STR-92, 91 pp., Boulder, CO.

LITERATURE CITED (Continued)

Koffler, R. A., A. G. DeCotiis, and P. Krishna Rao, 1973: A procedure for estimating cloud amount and height from satellite infrared radiation data. Mon. Wea. Rev., 101, 240-243.

McCleese, D. J., and H. M. Wilson, 1976: Cloud top heights from temperature sounding instruments. Quart. J. Roy. Met. Soc., 102, 781-790.

McMillin, L. M., D. Q. Wark, J. M. Siomakajlo, P. G. Abel, A. Werbowetzki, L. A. Lauritson, J. A. Pritchard, D. S. Crosby, H. M. Woolf, R. C. Luebbe, M. P. Weinreb, H. E. Fleming, F. E. Bittner and C. M. Hayden, 1973: Satellite infrared soundings from NOAA spacecraft. NOAA Technical Report NESS 65, National Environmental Satellite Service, Washington, D.C., 112 pp.

Mendola, C., and S. K. Cox, 1978: Cloud analysis from bi-spectral satellite data. Atmos. Sci. Paper #295, Colo. State Univ., Ft. Collins, CO., 75 pp.

Miller, D. B., and R. G. Feddes, 1971: Global atlas of relative cloud cover 1967-1970. U. S. Nat. Envir. Sat. Ser. and USAF ETAC, AD 739434-Rpt. No. 1, 237 pp.

Miller, J., Ed., 1978: Maunalon Observatory, a 20th anniversary report. NOAA Special Report, Air Resources Laboratories, Silver Spring, MD., 158 pp.

Ohring G., and P. Clapp, 1980: The effect of changes in cloud amount on the net radiation at the top of the atmosphere. J. Atmos. Sci., 37, 447-454.

Platt, C. M. R., 1979: Remote sounding of high clouds: I. Calculation of visible and infrared optical properties from lidar and radiometer measurements. J. Appl. Met., 18, 1130-1143.

_____, and G. L. Stephens, 1980: The interpretation of remotely sensed high cloud emittances. J. Atmos. Sci., 37, 2314-2322.

Rao, P. K., 1970: Estimating cloud amount and height from satellite infra-red radiation data. ESSA Technical Report, N.E.S.C. 54, Washington, D. C., 11 pp.

Raschke, E., Ed., 1978: Terminology and units of radiation quantities and measurements. NCAR, Boulder, CO., 17 pp.

LITERATURE CITED (Continued)

Remsberg, E. E., J. M. Russell III, L. L. Gordly, M. Paglia, J. C. Gille, and P. L. Bailey, 1980: Measurement of the radiance signature and distribution of clouds by the LIMB infrared monitor of the stratosphere experiment (LIMS) on Nimbus 7. Proc. of the 1980 International Radiation Symposium, Aug. 11-16, Ft. Collins, CO., 21-22.

Reynolds, D. W., and T. H. Vonder Haar, 1977: A bi-spectral method for cloud parameter determination. Mon. Wea. Rev., 105, 446-457.

_____, M. L. Brown, E. A. Smith and T. H. Vonder Haar, 1978: Cloud type separation by spectral differencing of image pairs. Mon. Wea. Rev., 106, 1214-1218.

Sadler, J. C., 1969: Average cloudiness in the tropics from satellite observations. Internatl. Indian Ocean Expedition Meteorol. Monogr. No. 2, East - West Center Press, Honolulu, 22 pp and 12 plates.

_____, L. Oda and B. J. Kilonsky, 1976: Pacific Ocean cloudiness from satellite observations. Rept. Meteorol. Univ. Hawaii, 137 pp.

Schwalb, A., 1978: The TIROS-N/NOAA A-G Satellite Series. NOAA Tech. Mem., NESS 95, 75 pp.

Shenk, W. E., and R. J. Curran, 1973: A multi-spectral method for estimating cirrus cloud top heights. J. Appl. Meteor., 12, 1213-1216.

Sherr, P. F., A. H. Glaser, J. C. Barnes and H. I. Willand, 1968: World-wide cloud cover distributions for use in computer simulations. NASA CR-61226, Huntsville, Al.

Sissala, J. E., Ed., 1975: The Nimbus 6 user's guide. Goddard Space Flight Center, NASA, Beltsville, MD., 58 pp.

Smith, W. L., 1969: A polynomial representation of carbon dioxide and water vapor transmission. Tech. Report, NESC 47, 20 pp.

_____, H. M. Woolf and W. C. Jacob, 1970: A regression method for obtaining real-time temperature and geopotential height profiles from satellite spectrometer measurements and its application to Nimbus III SIRS observations. Mon. Wea. Rev., 98, 582-603.

_____, H. M. Woolf and H. R. Fleming, 1972: Retrieval of atmospheric temperature profiles from satellite measurements for dynamical forecasting. J. Appl. Meteor., 11, 113-122.

LITERATURE CITED (Continued)

Smith. W. L., and H. M. Woolf, 1976: The use of eigenvectors of statistical convariance matrices for interpreting satellite sounding radiometer observations. J. Atmos. Sci., 33, 1127-1140.

_____, J. Hickey, H. B. Howell, H. Jacobowitz, D. T. Hilleary, and A. J. Drummond, 1977: Nimbus-6 earth radiation budget experiment. Appl. Opt., 16, 306-318.

_____, 1978: Status and plans for cloud climatology programme. JOC Study Conference on Parameterizations of Extended Cloudiness and Radiation for Climate Models (Oxford, 27 Sept. - 4 Oct), 16 pp.

_____, and C. M. R. Platt, 1978: Comparison of satellite-deduced cloud heights with indications from radiosonde and ground-based laser measurements. J. Appl. Meteor., 17, 1796-1802.

Snedecor, G. W., and W. G. Cochran, 1967: Statistical Methods. Sixth Edition, Iowa State Univ. Press, Ames, Iowa, 593 pp.

Steiner, E. J., 1978: A comparison of surface wind parameters, cloud amount, and sea surface temperature in tropical Pacific, 3rd NOAA Climate Conference, Miami, FL., 10-78.

Stockholm, 1974: JOC Study Conference on the Physical Basis of Climate and Climate Modeling, GARP Publications Series No. 16.

Suomi, V. E., F. R. Mosher and D. P. Wylie, 1977: Development of satellite imaging processing techniques from the First GARP Global Experiment. Final Report prepared for NASA, Goddard Space Flight Center under contract NAS 5-23462.

Susskind, J., and J. Rossenfield, 1980: Temperature soundings from TIROS-N. Proceedings of 1980 International Radiation Symposium, Ft. Collins, CO., Aug. 11-16, 90-93.

Taylor, F. W., 1974: Remote temperature sounding in the presence of cloud by zenith scanning. Appl. Opt., 13, 1559-1566.

Telegados, K., and J. London, 1954: A physical model of the northern hemisphere troposphere for winter and summer. New York Univ., Sci. Rept. No. 1, Contract AF 19(122)-165, 55 pp.

U. S. Committee for GARP, 1975: Understanding Climate Change...A program for action. National Academy of Sciences, Washington, D.C.

U.S. Standard Atmosphere 1976, 1976: NOAA, NASA and U.S. Air Force Pub. NOAA-SIT 76-1562, 227 pp.

Van Den Dool, H. M., 1980: On the role of cloud amount in an energy balance model of the earth's climate. J. Atmos. Sci., 37, 939-946.

LITERATURE CITED (Continued)

Vonder Haar, T. H., and A. H. Oort, 1973: New estimate of annual poleward energy transport by Northern Hemisphere Oceans. Phys. Ocean., 3, 169-172.

_____, 1979: Climatic indicators from space. Proceedings of the 13th International Symposium on Remote Sensing of the Environment (Ann Arbor, MI., April 23-27) 327-335.

Webster, P. J., 1978: Sensitivity of climate to variations in cloudiness and the treatment of cloudiness in climate models. JOC Study Conf. on Parameterization of Extended Cloudiness and Radiation for Cliamte Models. Oxford, 27 Sept. - 4 Oct., 417 pp.

Weinreb, M. P., and D. S. Crosby, 1977: A technique for estimating atmospheric moisture profiles from satellite measurements. J. Appl. Met., 16, 1214-1218.

Wielicki, B. A., and J. A. Coakley Jr., 1980: The retrieval of cloud amount and cloud top pressure from infrared sounder data: an error analysis. Proceedings of the 1980 International Radiation Symposium, Ft. Collins, CO., Aug. 11-16, 137-139.

Winston, J. S., 1969: Global distribution of cloudiness and radiation as measured from weather satellites. I: Climate of the free atmosphere, Ed. by D. F. Rex, Amsterdam, Elsevier, 247-280.

Yamamoto, G., M. Tanaka, and S. Asano, 1970: Radiative transfer in water clouds in the infrared region. J. Atmos. Sci., 27, 282-292.

Yeh, H., and K. Liou, 1980: Infrared and microwave sounding of the cloud liquid water content and temperature profile in cloudy atmospheres. Proc. of the 1980 International Radiation Symposium, Ft. Collins, CO., Aug. 11-16, 128-130.

APPENDIX

Retrieval Error Analysis

Chapter V is an introduction and summary of the analysis presented below. For an explanation of the boundary conditions and assumed error values refer to Chapter V. This Appendix contains the following detailed error analysis. Errors due to system-instrument errors are investigated first, followed by errors due to temperature and humidity profile unknowns. The magnitude of errors due to CO_2 profile variations are also examined. Errors due to specified cloud properties are reviewed, followed by a brief analysis of combined error sources. The last source of error examined is the assumption that a single representative radiating surface is in the radiometer field of view. The following sections detail the error findings.

A. Random sensor error effects

Figures 24-31 give the bias and RMS retrieval errors due to random sensor errors for both a mid-latitude and tropical atmosphere. Instrument system noise is assumed Gaussian with a mean of zero and a standard deviation of 0.22 mW $m^{-2}sr^{-1}cm$ for the 15 μm channels, and 0.11 mW $m^{-2}sr^{-1}cm$ for the window channel. These values represent the state of the art precision of the HIRS instrument on TIROS-N (Schwalb, 1978). For calculation purposes the set of spectral values representing a particular atmosphere are modified with random noise errors that are distributed as described above. These modified spectral radiance values are then used in the empirical RTE curve shape parameter retrieval algorithm to solve for the calculated p_{wf} and α values, which are then compared to the known correct values. Statistics are

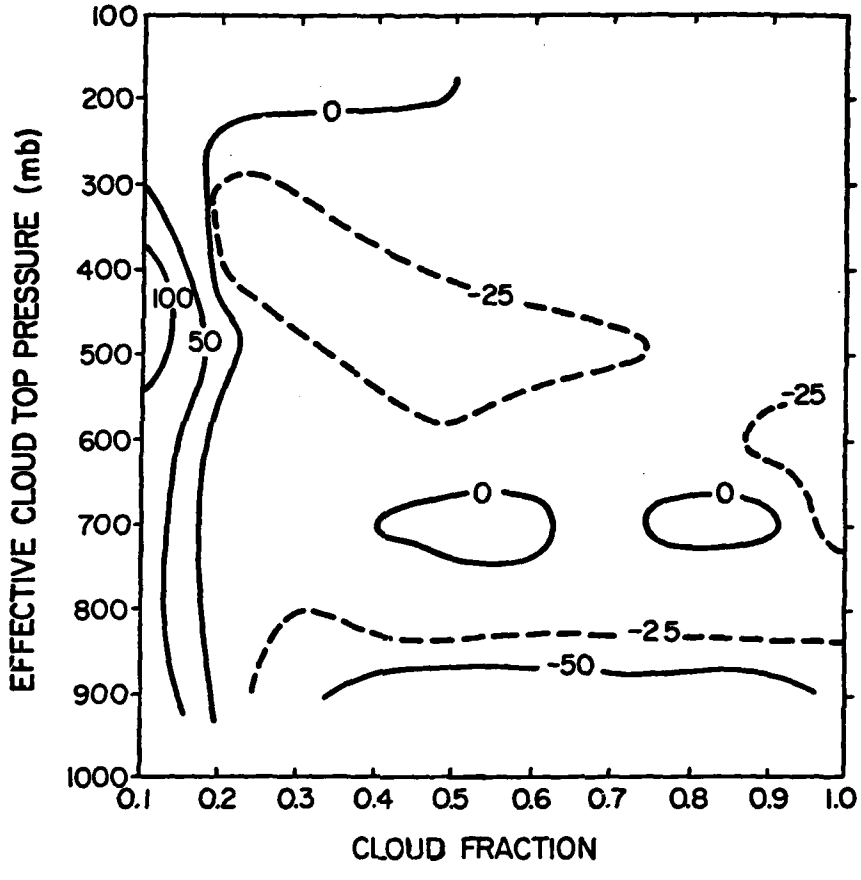

Figure 24. p_{wf} pressure level bias: random sensor errors for mid-latitude summer model.

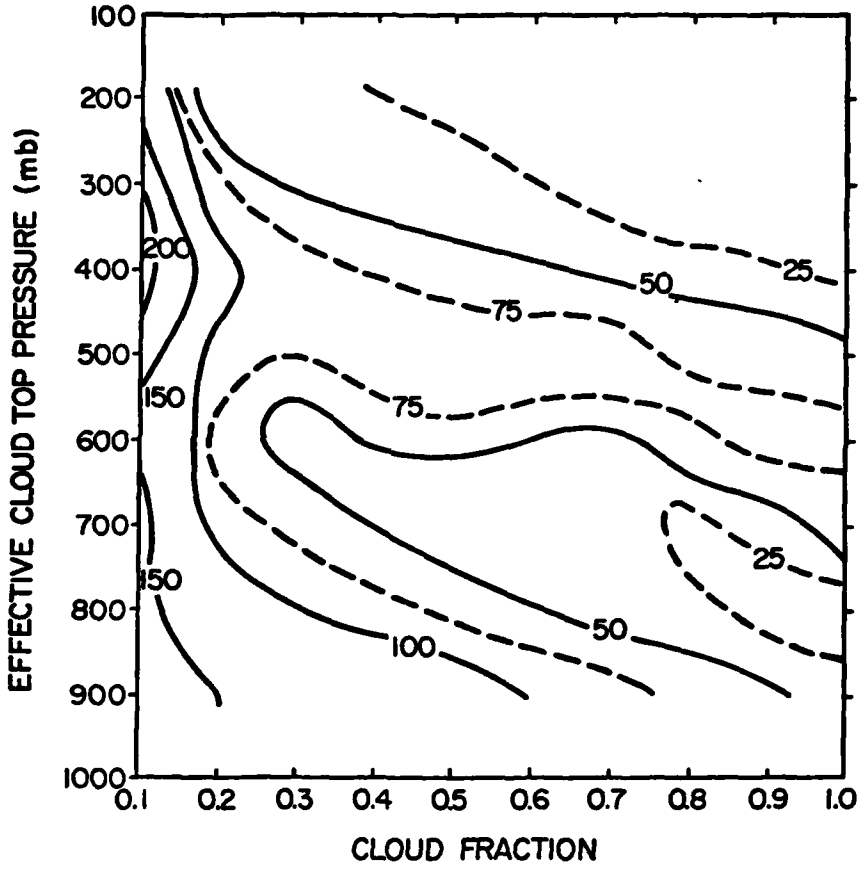

Figure 25. p_{wf} pressure level RMS: Random sensor errors for mid-latitude summer model.

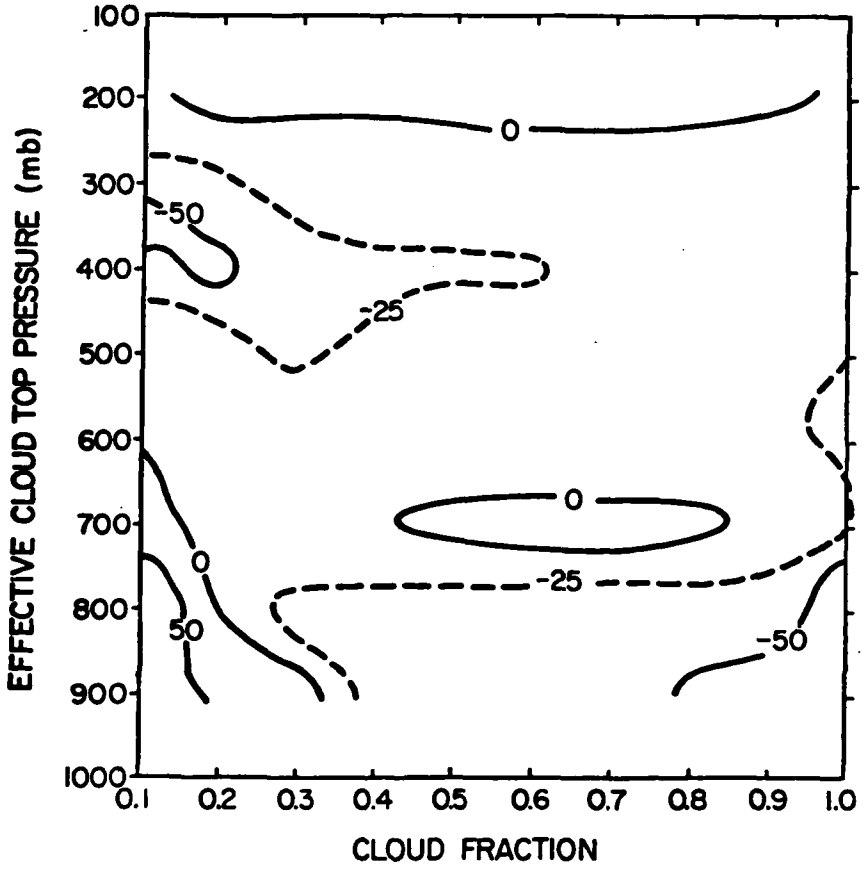

Figure 26. p_{wf} pressure level bias: Random sensor errors for tropical model.

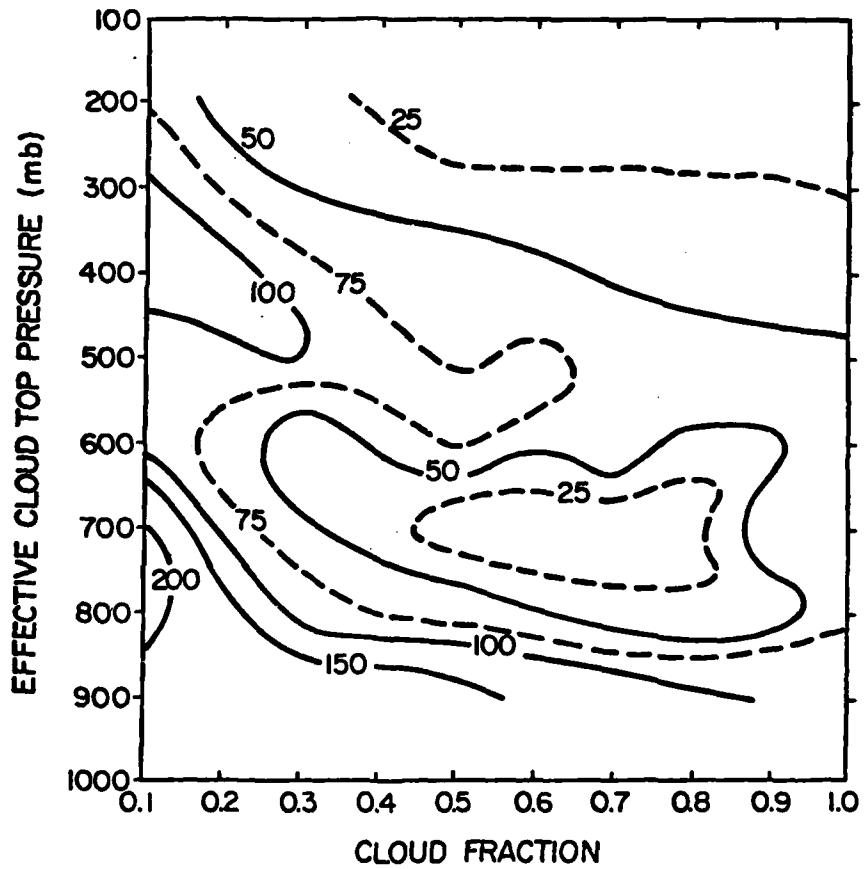

Figure 27. p_{wf} pressure level RMS: Random sensor errors for tropical atmosphere model.

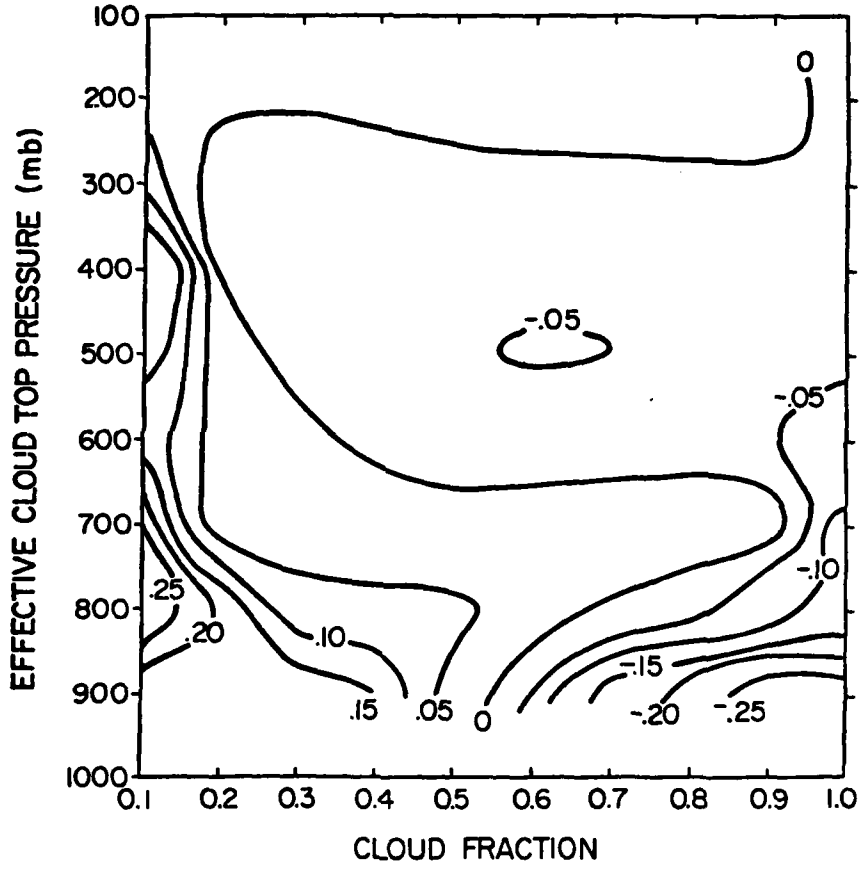

Figure 28. α bias: Random sensor error for mid-latitude summer model.

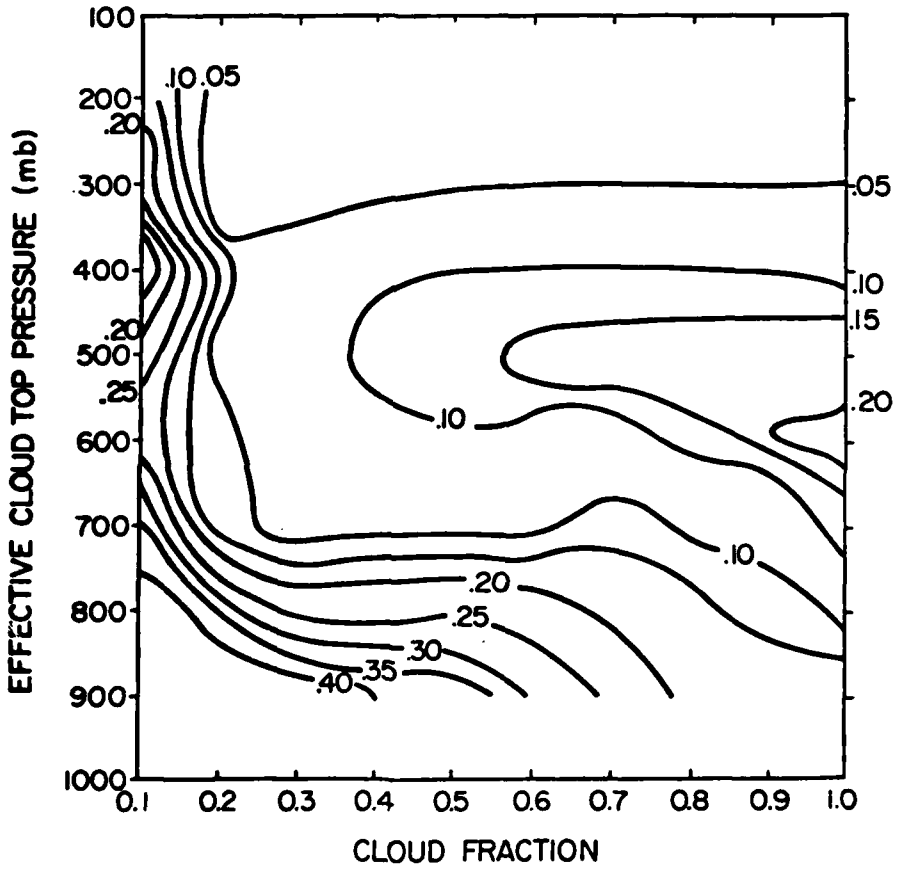

Figure 29. α RMS: Random sensor error for mid-latitude summer model.

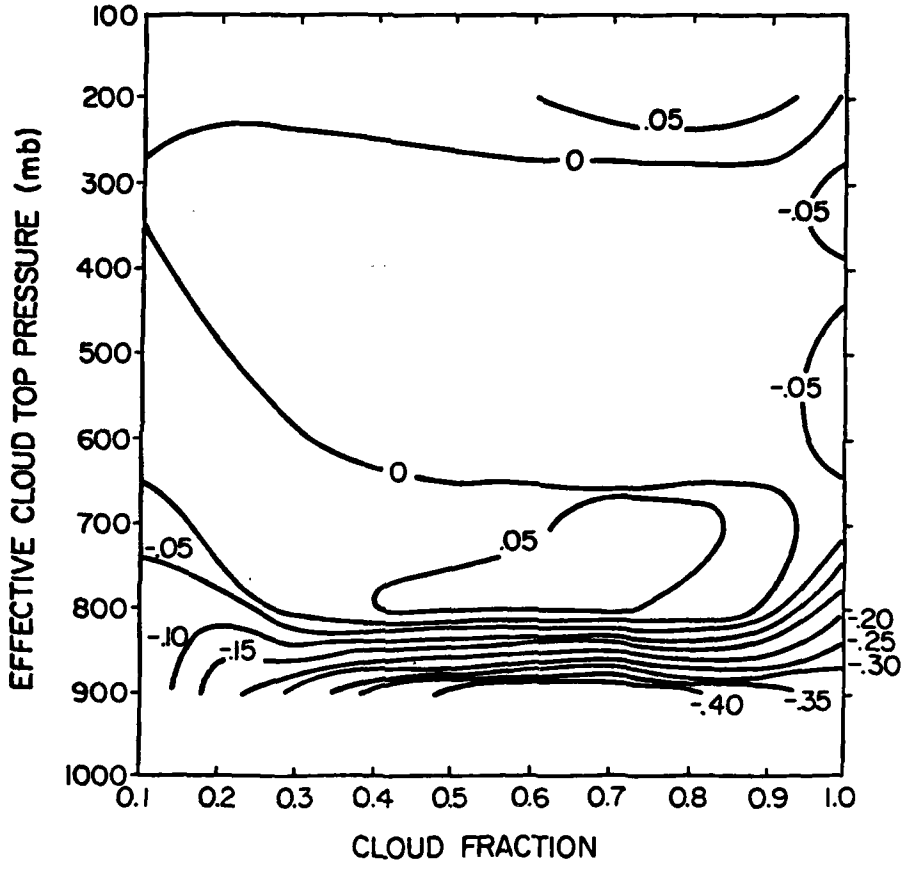

Figure 30. α bias: Random sensor error for tropical model.

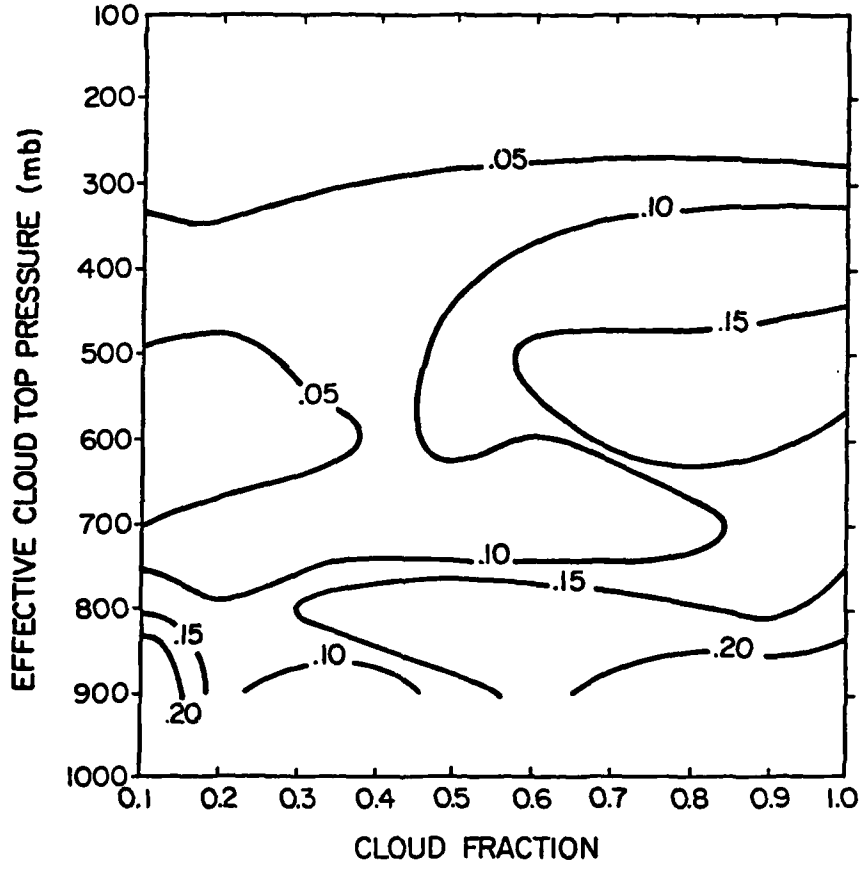

Figure 31. α RMS: Random sensor error for tropical model.

calculated using 60 sets of calculated versus given values for each particular atmospheric condition. As seen in Figures 24-31, one hundred statistics per figure are calculated using combinations of 10 effective cloud top pressures and 10 effective cloud fraction values.

Understanding the bias statistic in Figures 24, 26, 28 and 30 is simplified if one realizes that there is a correlation between the retrieved values of p_{wf} and α. For example, a single spectral radiance may be the result of small p_{wf} and α values or the result of large p_{wf} and α values. For the single spectral radiance there is a spectrum of p_{wf} and α value pairs going from both small to both large that could define a weighting curve for that radiance value. Thus, to satisfy a set of spectral radiances with instrument noise the empirical routine will usually tend to err in the same direction for both p_{wf} and α. For the most part, Figures 24 and 28, and Figures 26 and 30 show this error characteristic.

Furthermore, the bias figures show errors due principally to boundary conditions. The physical constraints of the system force the instrument noise error to show bias errors when $p_{wf} \rightarrow 1000$ mb. In this case radiating surfaces below 1000 mb are not allowed causing the p_{wf} bias error to be negative (bias = calculated - given). At this boundary α bias errors are also generally negative. Figures 24 and 28 show the same effect as $\alpha \rightarrow 0$. By necessity the bias is toward larger α values and as a consequence larger p_{wf} values (positive bias). Figures 26 and 30 show this effect to a lesser degree. Overall this analysis shows the retrieval is highly unbiased due to instrument noise except as $\alpha \rightarrow 0$ and $p_{wf} \rightarrow 1000$ mb. As stated previously, when α is near zero and p_{wf} is near the surface the broadband weighting curve is only

slightly changed from the clear sky case. Thus, these error effects are minimized.

Figures 25, 27, 29 and 31 give the RMS error due to system noise of p_{wf} and α for a mid-latitude and tropical atmosphere. The more gradual increase in RMS errors for p_{wf} and α as $\alpha \to 0$ and $p_{wf} \to 1000$ mb indicates that the RMS error is probably related closely to signal to noise ratio which gradually decreases as $\alpha \to 0$ and $p_{wf} \to 1000$ mb. One also notices that RMS values are slightly larger for the mid-latitude case (Figures 25 and 29). This is probably due to the fact that the tropical atmosphere contains much more water vapor. The presence of water vapor may act as a buffer reducing the impact radiance errors have on the retrieval process. In conclusion, it appears that random noise effects produce p_{wf} and α retrieval errors that are in the mean quite small. Any specific case retrieval errors will be of the magnitude indicated by the RMS figures.

B. Profile error effects

Analysis of profile error effects is extremely difficult due to the computational time involved. Instead of adding random noise 60 times to sets of spectral radiance values (one for mid-latitude and another for tropical atmospheres), the sets of spectral radiance values have to be generated using profiles of temperature, humidity and CO_2 that are modified with errors. To run the spectral RTE for each wavenumber for 60 different error plagued profiles for each of the two basic atmospheres in an attempt to produce figures similar to Figures 24-31 requires a large amount of computer time. Instead of taking this route, a less descriptive but much faster approach is used and

outlined below. It is the same technique described at the end of Chapter IV.

Bias and RMS errors are calculated from 50 values. These values come from calculations made at the 5 effective cloud top levels within a 100's range (i.e. 200, 220, 240, 260 and 280 mb) for 10 fractional effective cloud amounts (i.e. 1.0, 0.9, ..., 0.1). The results given are only for the mid-latitude atmosphere although they are also representative of the tropical atmosphere case.

For example, Figure 32 which represents this approach using instrument noise, may be comprared to Figures 24, 25, 28 and 29. Notice that if the lines in Figure 32 are considered trends representing a single overall statistic, with no importance placed on variations between effective cloud top categories, they compare favorably with the trends indicated in Figures 24, 25, 28 and 29. Thus, the trends indicated in Figures 32-37, especially those trends neglecting the two end groupings are taken as representative of a mean value of bias or RMS. Remember that either end effective cloud category shows effects due to boundary conditions. Despite obvious limitations, these trend values are regarded as sufficiently descriptive for this analysis.

Figure 33 shows the bias and RMS of α and p_{wf} associated with a 2°C RMS and 50% water vapor profile uncertainty specified randomly and independently for each 20 mb layer. The distribution of errors is Gaussian with zero mean. Water mixing ratio errors are given as a percent of the correct mixing ratio at any given level. For this particular analysis instrument noise is set to zero.

For each plot in Figure 33 there are two curves. The dashed line represents the error when the specified climatological temperature and

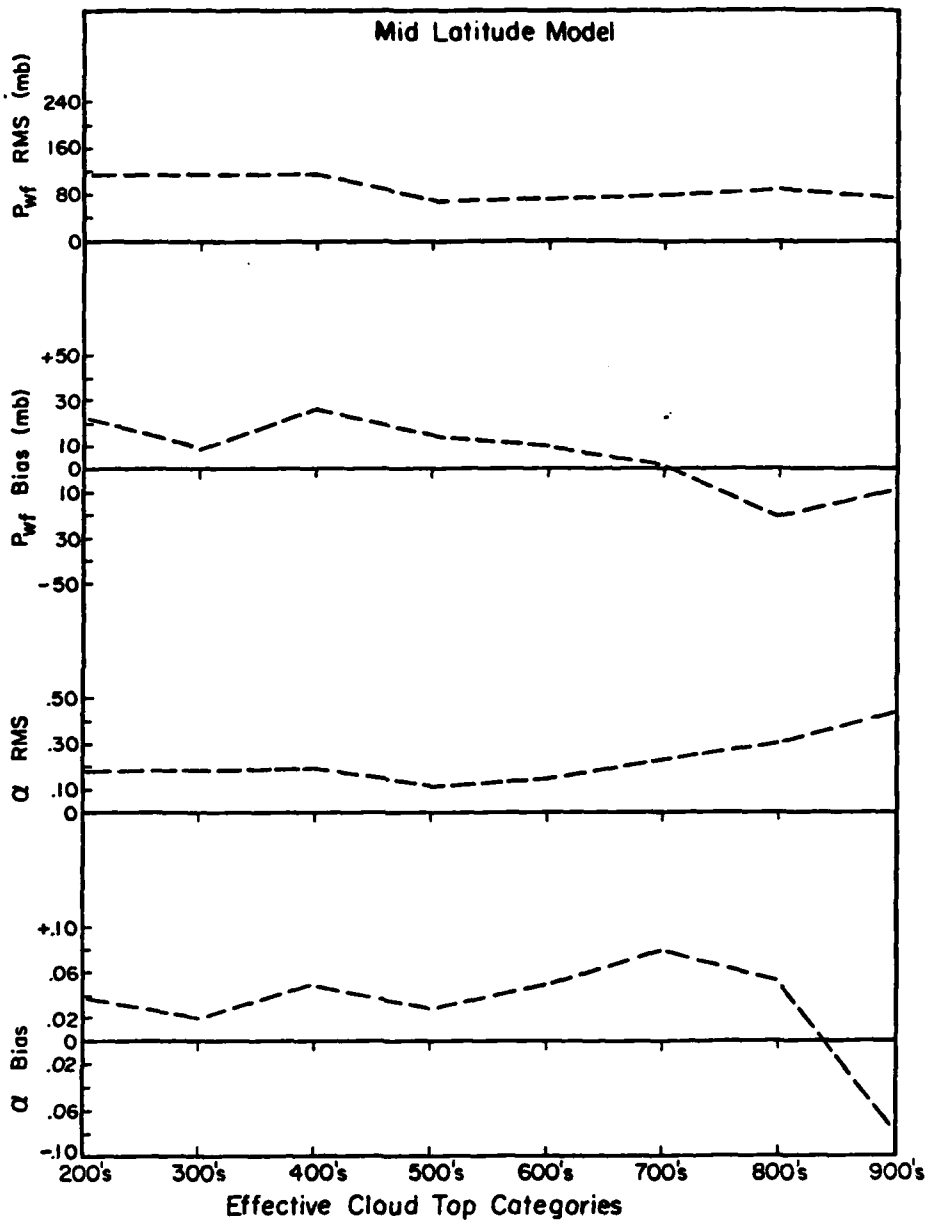

Figure 32. Random sensor error effect on shape parameter retrieval.

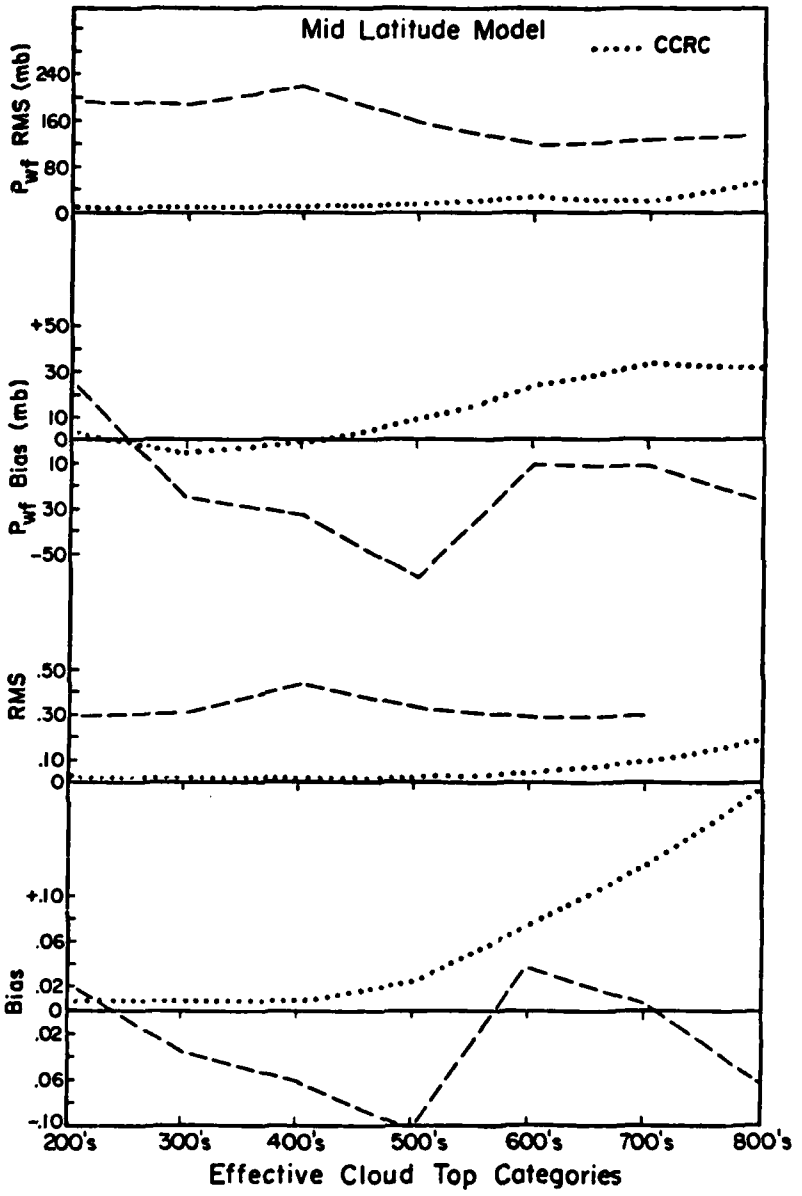

Figure 33. $\pm$ 2° RMS temperature and 50% humidity error effects on shape parameter retrieval.

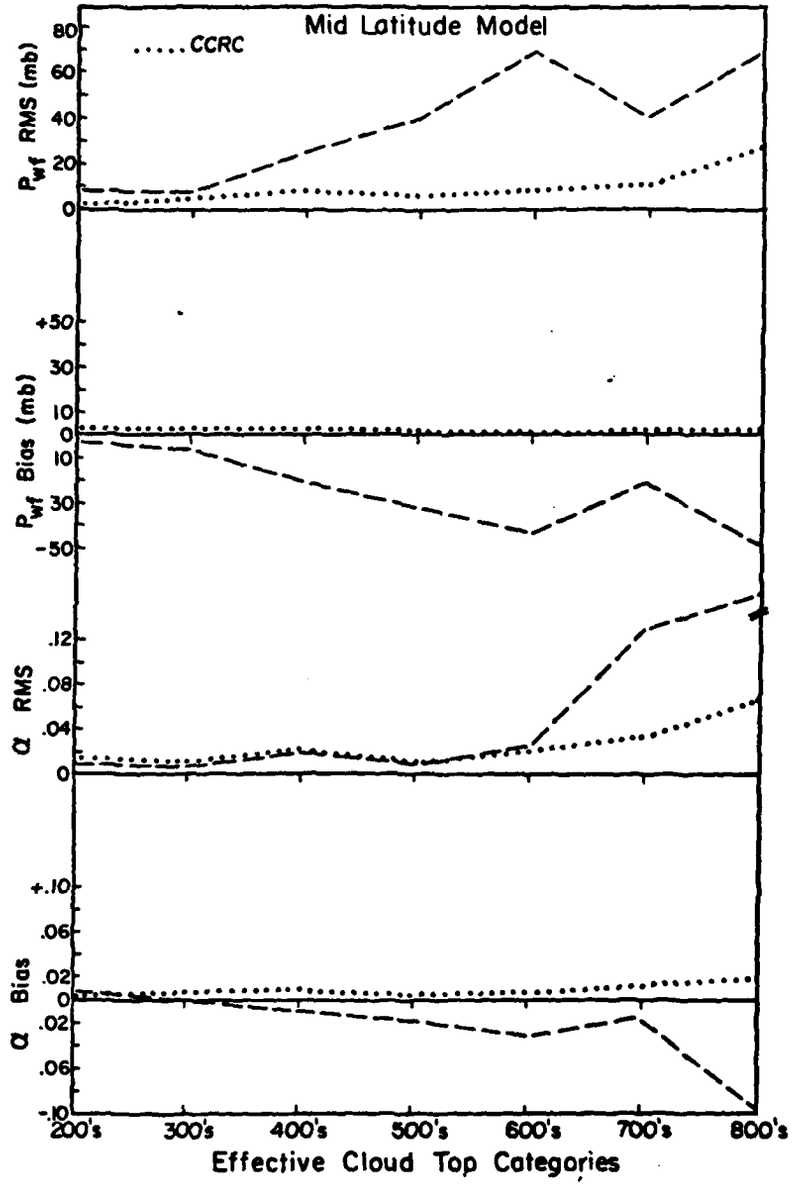

Figure 34. + 1% CO_2 profile error effect on shape parameter retrieval.

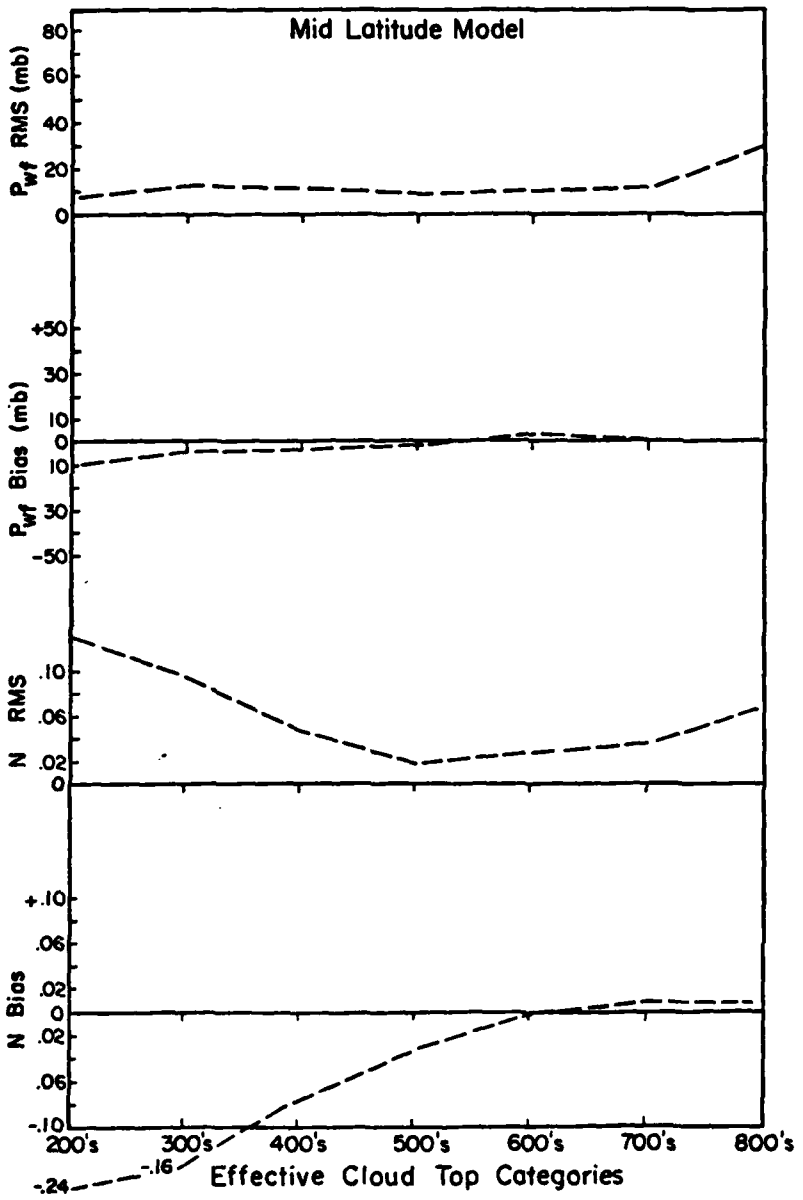

Figure 35. 80 mb cloud thickness error effect on shape parameter retrieval (20 mb vs. 100 mb).

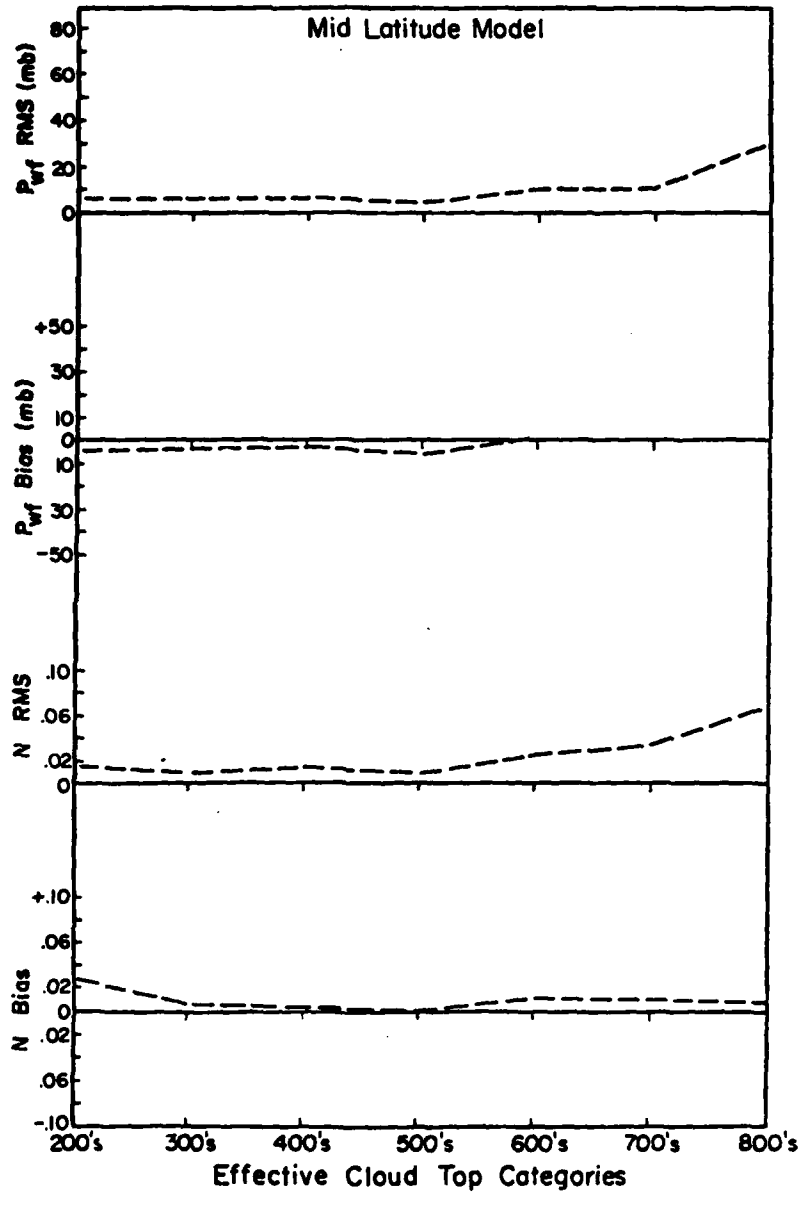

Figure 36. + 50% LWC error effect on shape parameter retrieval.

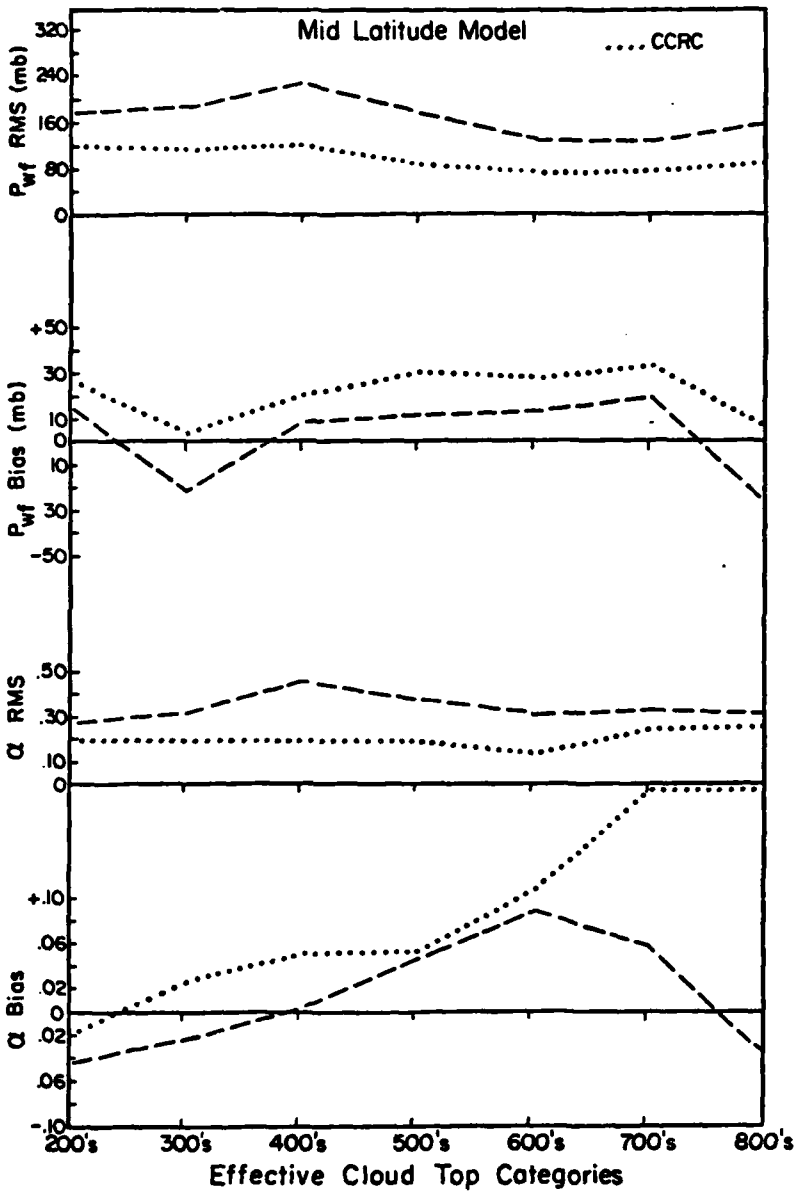

Figure 37. Combined errors effect on shape parameter retrieval.

humidity profile is used. The dotted line represents error analysis when a clear column radiance correction (CCRC) is applied. As can be seen in Figure 33, the application of CCRC, which simply adds one more piece of information ($L_{\nu cs}$), greatly reduces the RMS errors and seems to improve the bias error. The inclusion of the measured $L_{\nu cs}$ information is reasonable since in many cases this information will be available. Even in overcast situations, using the closest $L_{\nu cs}$ measurement should be an improvement over assuming the $L_{\nu cs}$ inferred from the climatological profile is correct.

The CCRC is applied in the following way. Let L_{csc} be the clear sky spectral radiance from a climatological profile. Let L_{csm} be the measured clear sky spectral radiance. Each spectral radiance value used in the retrieval procedure is then multiplied by a factor equal to $(L_{csc} \div L_{csm})_{\nu}$.

Figure 34 gives the RMS bias errors due solely to a + 1% error in the CO_2 profile. The error is not applied randomly but through the whole profile since CO_2 is well mixed in the troposphere. The magnitude represents $\frac{2}{3}$ of the seasonal maximum change in CO_2 observed. Again the CCRC technique eliminates the effect of the error almost entirely. The main effect of the CO_2 error is to change the p_{wf} value from true while α is calculated correctly. When there is more CO_2 than assumed the radiation surface is retrieved higher in the atmosphere that it really is. Notice a change of scale in the RMS plots. Even without the CCRC applied to the CO_2 error the temperature and humidity as well as instrument errors are far more important in terms of RMS error.

C. Effective cloud radiative properties effect

As stated previously, because the empirical RTE retrieval method solves for an α value, theoretically the emittance for the radiating surface being retrieved may be arbitrarily specified. The accuracy of this statement is tested in this section. Errors due to both over and under specifying emittance will be examined by neglecting all other error sources.

Figure 35 shows the effect of assuming effective cloud depths of 100 mb when they are actually 20 mb thick. In other words the emittance is assumed to be much larger than it really is. By comparing Figure 35 to Figures 13 and 14 one can see the RMS and bias errors for p_{wf} are essentially alike. The same is true for α errors which are not plotted. Instead the errors for N are plotted to illustrate that if emittance is assumed too large the N value is simply decreased to give the correct α value ($\alpha = \varepsilon N$). Notice that below 600 mb, 20 mb thick effective clouds behave much like 100 mb thick ones.

Figure 36 gives an analysis of the situation where the emittance is actually greater than specified. This error occurs only at higher levels since emittance below 300 mb is specified at its maximum value. Again N statistics are plotted instead of α statistics. Since emittance is assumed too small at the upper tropospheric levels, the N value calculations are biased positive to give the correct α value. In this case the curves show small variations from those plotted in Figures 13 and 14.

Figure 37 shows the results of combining errors. The errors used are a random 2°C RMS temperature profile error with 50% variation in humidity as explained in Section B. Also included is random

instrument noise as explained in Section A. Furthermore, true cloud depth is allowed to vary randomly from 20 to 180 mb and LWC is allowed to vary randomly from $\pm$ 50% of the specified value.

The consistency of the RMS error from one effective cloud top category to another suggests that the limited sample analyzed gives a typical value of RMS. However, confidence in the bias errors cannot be as high using the consistency argument. It appears that the CCRC procedure reduces the RMS. However, it also seems to add to the bias error. It must be remembered that the error characteristics (level by level independent randomness) used are the severest test of CCRC. For a more trend characteristic error as opposed to random error the CCRC works better as evidenced by the CO_2 values in Figure 34.

In conclusion, this analysis has shown the RMS and bias errors of p_{wf} and α to be of the order of magnitude given in Table 7. These values represent acceptable levels when matched with the approach of using weighting function curves defined by the shape parameters p_{wf} and α as an indication of climatological cloudiness. As pointed out above, a great advantage is gained due to the fact that maximum curve shape parameter errors occur as $p_{wf} \rightarrow 1000$ mb and as $\alpha \rightarrow 0$ and for these values of p_{wf} and α the broadband weighting curve shape remains nearly as it is for the clear sky case.

D. Single p_{wf} level effect

The nature of this error effect, due to errors in the assumption that the satellite sensor is viewing a scene with a single p_{wf} level, requires a different analysis approach. Figure 38 illustrates the effect of two radiating surfaces on the spectral weighting function for

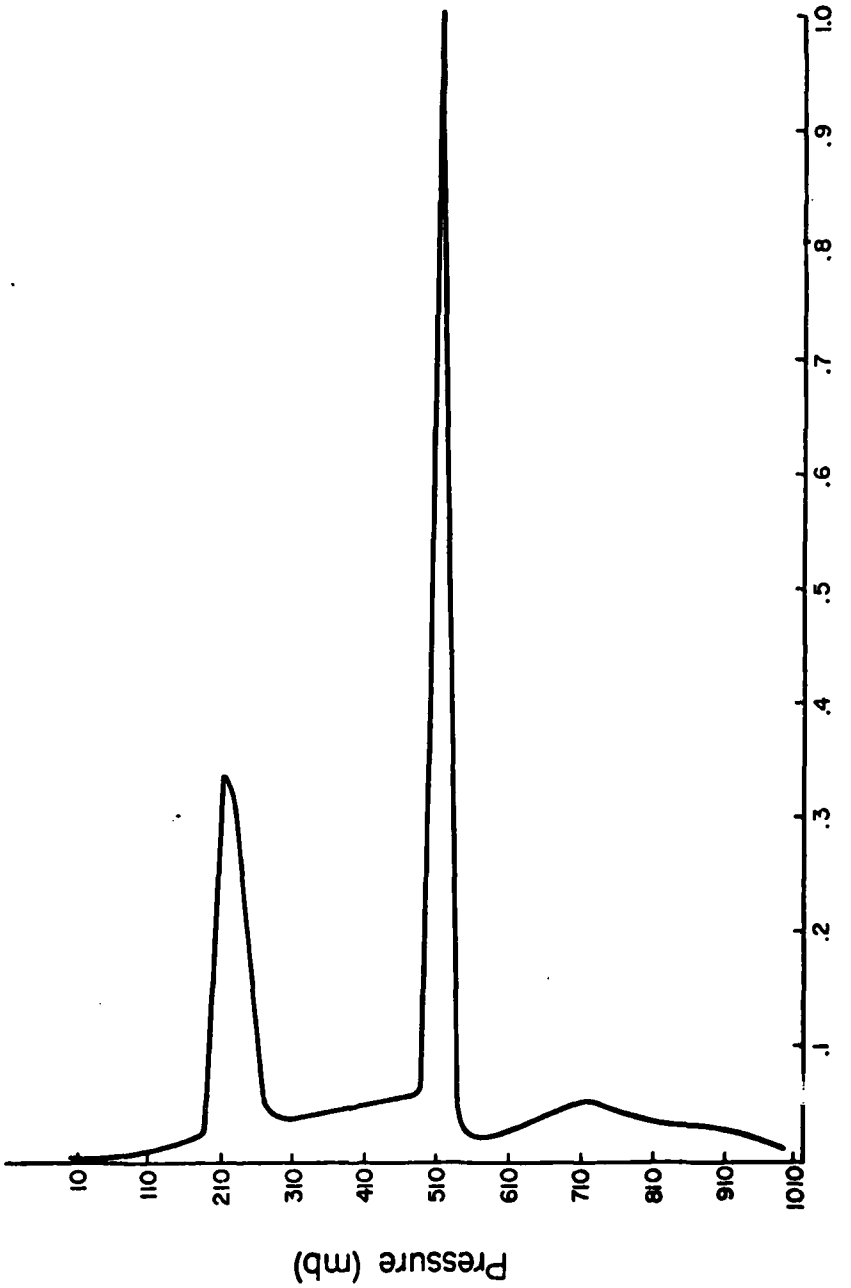

Figure 38. Spectral weighting curve for a case of two separate radiating surfaces in the same scene.

wavenumber 727.5 cm^{-1} using a tropical atmosphere. The values of p_{wf1} and p_{wf2} are 210 and 510 mb respectively. The α values are 0.35 and 0.40 respectively. It is clear that to describe the shape of this weighting function profile takes 4 curve shape parameters. What sort of errors are obtained when the set of spectral radiance values that correspond to these four shape parameters are used in the 2 parameter retrieval program? This problem of two radiating surfaces versus one radiating surface is addressed. To slightly simplify further, α values are restricted to 1.0 for a single specified known scene which when paired translates into a specified known scene that is described by α's of 0.5 and 0.5.

As pointed out in Figure 1 the ultimate objective is to composite broadband weighting curves for purposes of a climate index. Specific scene retrievals are only a secondary consideration. Therefore, the particular source of error described in this section is related to the final composite weighting curve product. To judge error effects, the true versus retrieved composite curves are compared. The composite can be thought of as representing either time or space averages. The experiment most closely resembles a space average.

To do this comparison the following experimental procedure is followed. Assign an effective radiating surface to a simulated spot scene. Do this for many spots ($\sim$ 200 spots) using different p_{wf} values with $\alpha = 1$. There is a set of spectral radiance values for each spot. A composite of curves ($\sim$ 200) described from the spot scenes spectral radiances gives the true weighting curve. Assume the satellite sensor views two scenes at once. In other words, the satellite is assumed to view two effective radiating surfaces instead of one. Thus, each of

the true spot scenes are paired off ($\sim$ 100 pairs). There is a set of spectral radiances for each pair of spot scenes which represent an average of the two separate radiance sets. From this set of spectral radiances, p_{wf} and α values are retrieved and all the resulting weighting curves ($\sim$ 100) are composited to give the retrieved composite weighting function curve. This is done for three separate groups of $\sim$ 200 spot values.

Tables 16 and 17 give the effective cloud top distributions in detail for the three groupings. The flat distribution (FLATS) is modeled after 20 day average GATE B-array cloud data (Cox and Griffith, 1978). The other two distributions (BIMOS and 1PK35) are specified to resemble alternate scenarios. BIMOS represents a specified bimodal distribution, while 1PK35 represents a specified one peak distribution at the 200 mb layer. There are 5 levels within each effective cloud top category (i.e. 400, 420, 440, 460 and 480 mb). The spots are paired off as realistically as possible by category. Within each pair the difference between tops vary according to the values at the bottom of Table 8. For example, if 200 and 300 mb category tops are paired off together their tops may differ between 20 and 180 mb; a 280 mb top may be paired with a 300 mb top or a 200 mb top may be paired with a 380 mb top. Once the top categories are chosen, the exact top differences are determined randomly. The exact specified distribution of top difference values is largely dependent on the total distribution of effective cloud tops. Notice that two 120 pair models of the flat distribution are specified in order to judge result sensitivity to differences in pair separation distributions.

Effective Cld. Top Cat. P_{wf}	240 Spot[1] Freq/%	120 Pair[2] Freq/%	120 * Pair[2] Freq/%	230 Spot[1] Freq/%	115 Pair[2] Freq/%	200 Spot[1] Freq/%	100 Pair[2] Freq/%	20-day GATE B-array %	Effective Cld. Top Cat. P_{wf}
100's	20/8	11/9	10/8	10/4	4/3	10/5	3/3	8	100's
200's	29/12	17/14	18/15	20/9	17/15	25/12.5	19/19	11	200's
300's	32/13	18/15	19/16	60/26	30/26	75/37.5	38/38	11	300's
400's	26/11	12/10	14/12	20/9	13/11	30/15	14/14	13	400's
500's	26/11	11/9	15/13	10/4	9/8	20/10	12/12	13	500's
600's	23/10	15/13	12/10	10/4	3/3	10/5	3/3	13	600's
700's	28/12	14/12	10/8	20/9	8/7	10/5	4/4	11	700's
800's	25/10	23/19	21/18	60/26	29/25	10/5	5/5	10	800's
900's	31/13	0/0	1/1	20/9	2/2	10/5	2/2	10	900's

Table 16. Model effective cloud top distributions by top category.

Paired Cloud Tops Within	120 Pair Model[1] Freq.	%	120 * Pair Model[1] Freq.	%	115 Pair Model[1] Freq.	%	100 Pair Model[1] Freq.	%
0 - 80 mb	0	0	27	22	47	41	33	33
20 - 180 mb	75	62	42	35	19	17	33	33
120 - 280 mb	34	28	20	17	17	15	23	23
220 - 380 mb	8	7	14	12	12	10	6	6
320 - 480 mb	1	1	11	9	6	5	2	2
420 - 580 mb	2	2	5	4	11	10	2	2
520 - 680 mb	0	0	1	1	3	3	1	1

1. specified values 2. retrieved values

Table 16. Model effective cloud top pair separation distribution.

Effective Cloud Top (mb)		240 Spot Freq.[1]	120 Pair Freq.[2]	120 * Pair Freq.[2]		230 Spot Freq.[1]	115 Pair Freq.[2]		200 Spot Freq.[1]	100 Pair Freq.[2]
100		4	0	0		2	1		2	1
120	(FLAT)	4	0	2	(BIMO)	2	0	(1PK3)	2	0
140		4	0	1		2	0		2	0
160		4	5	3		2	2		2	1
180		4	6	4		2	1		2	1
200		6	5	5		4	2		5	4
220		6	2	3		4	4		5	2
240		5	5	6		4	5		5	4
260		6	5	4		4	3		5	6
280		6	0	0		4	3		5	3
300		6	2	2		12	2		15	2
320		7	4	3		12	7		15	10
340		6	3	4		12	9		15	12
360		7	3	5		12	8		15	12
380		6	6	5		12	4		15	3
400		6	1	1		4	2		6	1
420		5	2	3		4	3		6	2
440		5	3	3		4	3		6	4
460		5	3	2		4	3		6	4
480		5	3	5		4	2		6	3
500		5	3	4		2	2		4	2
520		5	4	3		2	3		4	4
540		5	0	3		2	1		4	1
560		6	2	3		2	1		4	2
580		5	2	2		2	2		4	3

Table 17. (Page 1)

Effective Cloud Top (mb)	240 Spot Freq.[1]	120 Pair Freq.[2]	120 * Pair Freq.[2]	230 Spot Freq.[1]	115 Pair Freq.[2]	200 Spot Freq.[1]	100 Pair Freq.[2]
600	4	3	2	2	0	2	1
620	5	3	3	2	1	2	0
640	5	4	3	2	2	2	2
660	4	2	2	2	0	2	0
680	5	3	2	2	0	2	0
700	5	5	3	4	3	2	2
720	6	1	2	4	3	2	0
740	6	0	1	4	0	1	0
760	5	2	1	4	2	2	2
780	6	6	3	4	0	2	0
800	5	6	5	12	3	2	2
820	5	1	2	12	4	2	1
840	5	5	6	12	10	2	1
860	5	7	3	12	8	2	0
880	5	4	5	12	4	2	1
900	7	0	1	4	2	2	2
920	6	0	0	4	0	2	0
940	6	0	0	4	0	2	0
960	6	0	0	4	0	2	0
980	6	0	0	4	0	2	0

1. specified values

2. retrieved values

Table 17. Model effective cloud top distribution.

Because one would not expect each and every set of satellite radiance values to be influenced by a scene with two different radiating surfaces, this test set up may be extreme. On the other hand, occassional scenes with more than two radiating surfaces may be viewed. Overall one may consider this test of the single representative p_{wf} value error to be not quite a worse case situation.

Tables 16 and 17 give the effective cloud top retrieved distributions. Table 18 shows that kind of single p_{wf} and α values the retrieval program calculates from sets of spectral radiances containing the effects of two p_{wf} and α values. In most cases the results seem to provide a fortuitous average type value. Figure 39 gives a more informative summary of this process. Plot A shows the three effective cloud top distributions. Plot B compares the specified top distribution (240 spots) against the retrieved top distribution (120 pairs). Notice that the retrieved top distribution fails to match the specified one in the lower troposphere. This fault is minimized by considering that effective clouds at that level have little influence on the overall broadband weighting function. Notice that both pair models show the same general results. Plots C and D also show favorable comparison between the distribution of specified effective cloud tops and the retrieved ones.

Figures 40-42 show the broadband weighting curve composites for the three effective cloud top distributions. Specified (i.e. 240 spot) curves are compared to retrieved (i.e. 120 pair) curves. In Figure 40 the 120 pair model weighting cuve is not plotted in order to make visual comparison between the two plotted curves easier. All three figures show only minor differences between the specified and retrieved

Effective Cloud Top Pairings	Retrieved Cloud Top	LWC	Retrieved Fraction	Effective Cloud Top Pairings	Retrieved Cloud Top	LWC	Retrieved Fraction
380 - 340	360	.075	1.0	820 - 860	840	1.0	1.0
300 - 340	320	.055	1.0	800 - 840	820	1.0	1.0
360 - 340	340	.064	1.0	200 - 220	220	.025	1.0
380 - 320	340	.064	1.0	240 - 260	240	.029	1.0
380 - 380	360	.075	.96	200 - 220	240	.029	1.0
360 - 360	360	.075	1.0	400 - 480	440	.124	1.0
380 - 380	340	.064	1.0	460 - 440	440	.124	1.0
340 - 320	340	.064	1.0	420 - 480	440	.124	1.0
360 - 300	320	.055	1.0	700 - 780	720	.628	.92
320 - 300	320	.055	1.0	760 - 740	760	.792	1.0
360 - 320	340	.064	1.0	720 - 760	720	.628	.94
320 - 320	320	.055	1.0	940 - 960	900	1.0	.44
300 - 340	320	.055	1.0	980 - 920	900	1.0	.44
360 - 340	340	.064	1.0	900 - 900	880	1.0	.82
300 - 380	340	.064	1.0	100 - 120	100	.010	.90
880 - 860	880	1.0	1.0	540 - 500	520	.197	1.0
880 - 840	860	1.0	1.0	640 - 620	640	.395	1.0
880 - 820	860	1.0	1.0	340 - 240	280	.040	.96
820 - 860	840	1.0	1.0	380 - 280	320	.055	1.0
860 - 860	860	1.0	1.0	300 - 260	280	.040	1.0
880 - 840	860	1.0	1.0	320 - 200	260	.034	1.0
820 - 800	820	1.0	1.0	360 - 260	300	.047	1.0
800 - 880	840	1.0	1.0	360 - 240	280	.040	.92
840 - 860	860	1.0	1.0	380 - 400	380	.087	.98
800 - 860	840	1.0	1.0	380 - 460	360	.075	.92
840 - 840	840	1.0	1.0	340 - 420	360	.075	.94
820 - 840	840	1.0	1.0	820 - 700	720	.628	.84
880 - 800	840	1.0	1.0	800 - 720	760	.792	1.0
800 - 820	820	1.0	1.0	860 - 740	800	1.0	1.0
800 - 880	840	1.0	1.0	800 - 960	840	1.0	.78

Table 18. (Page 1.)

Effective Cloud Top Pairings	Retrieved Effective Cloud Top	LWC	Retrieved Fraction	Effective Cloud Top Pairings	Retrieved Cloud Top	LWC	Retrieved Fraction
880 - 920	880	1.0	.80	400 - 720	500	.175	.88
840 - 980	860	1.0	.66	440 - 780	540	.221	.84
820 - 940	860	1.0	.86	420 - 700	520	.197	.92
860 - 900	880	1.0	.94	480 - 720	580	.279	.94
800 - 980	840	1.0	.70	920 - 640	700	.559	.84
820 - 940	860	1.0	.86	540 - 220	260	.034	.68
300 - 520	380	.087	.90	480 - 160	200	.021	.74
380 - 580	460	.139	1.0	800 - 420	520	.197	.80
340 - 560	420	.110	.96	820 - 400	480	.156	.74
320 - 160	220	.025	.98	300 - 780	340	.064	.58
300 - 180	240	.029	1.0	340 - 760	420	.110	.72
360 - 140	200	.021	.88	520 - 960	560	.248	.62
320 - 100	160	.016	.86	580 - 180	220	.025	.64
340 - 120	180	.018	.88	860 - 360	400	.100	.62
880 - 600	640	.395	.68	800 - 380	460	.139	.74
840 - 660	700	.559	.92	820 - 320	360	.075	.60
880 - 680	700	.559	.78	840 - 340	380	.087	.62
440 - 200	240	.029	.80	880 - 300	320	.055	.54
480 - 280	360	.075	.92	860 - 320	360	.075	.58
460 - 260	340	.064	.94	840 - 360	420	.110	.64
920 - 740	800	1.0	.82	900 - 440	500	.175	.66
960 - 780	820	1.0	.76	700 - 240	260	.034	.56
980 - 760	800	1.0	.64	740 - 280	300	.047	.58
380 - 600	480	.156	1.0	680 - 140	160	.016	.54
360 - 660	460	.139	.90	940 - 380	400	.100	.54
300 - 620	380	.087	.82	820 - 200	220	.025	.56
860 - 560	620	.352	.74	880 - 220	240	.029	.56
840 - 500	580	.279	.78				

Table 18. Satellite Spot to Pair Value Conversion Example.

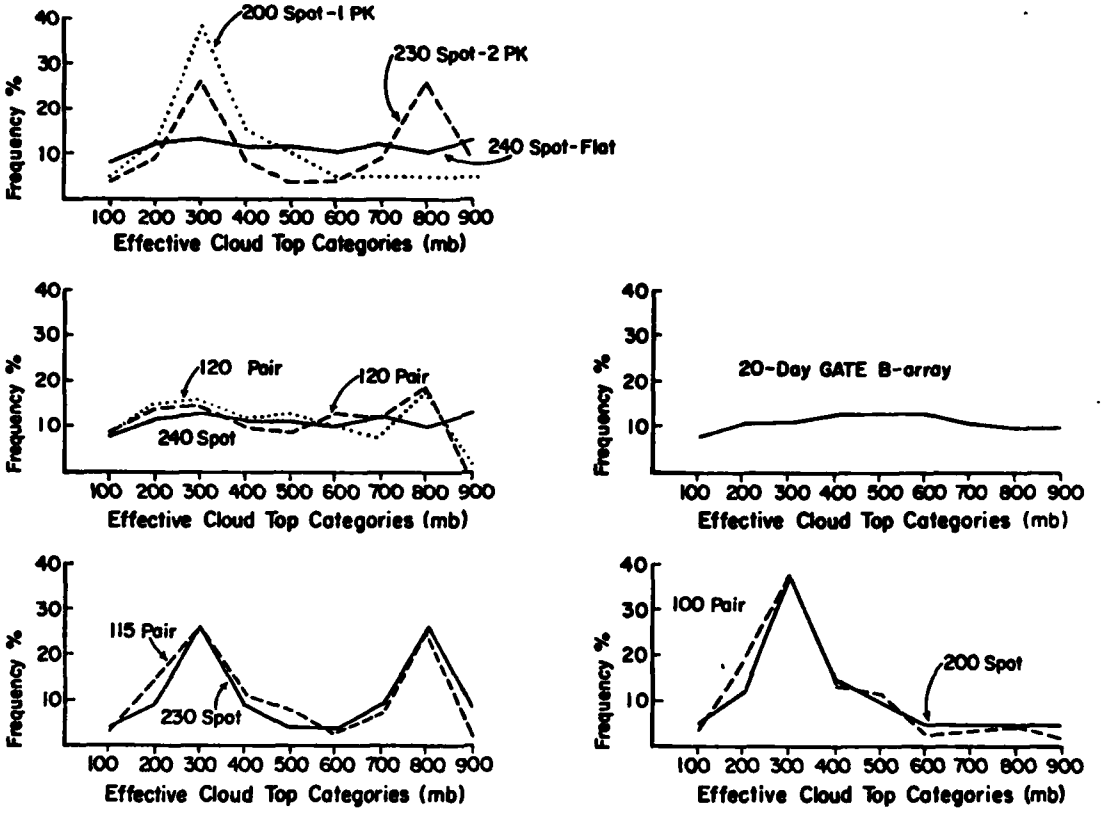

Figure 39. Plots showing comparison between specified effective cloud top distributions and the respective retrieved distributions.

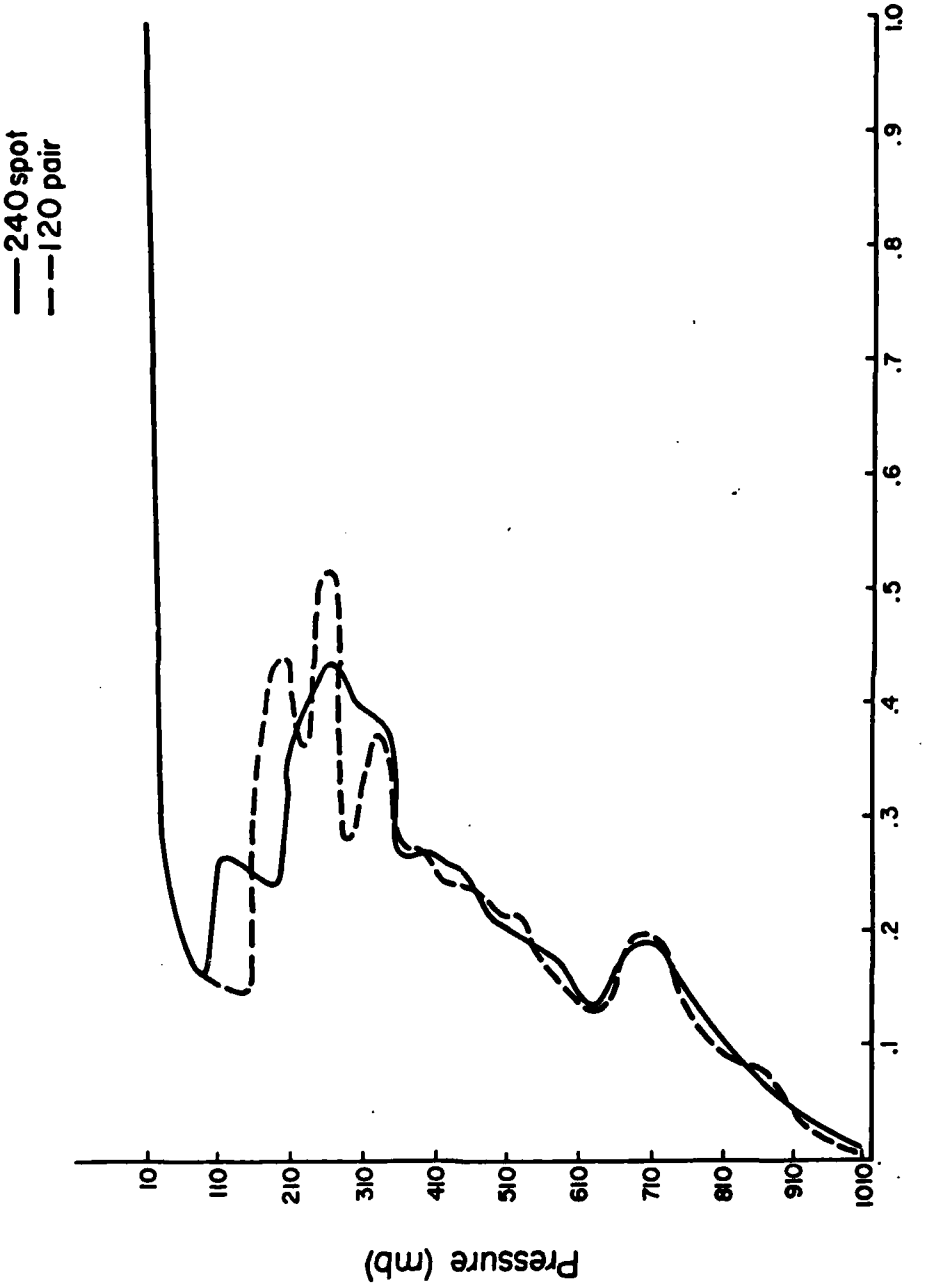

Figure 40. Broadband weighting curves for specified and retrieved flat effective cloud top distribution.

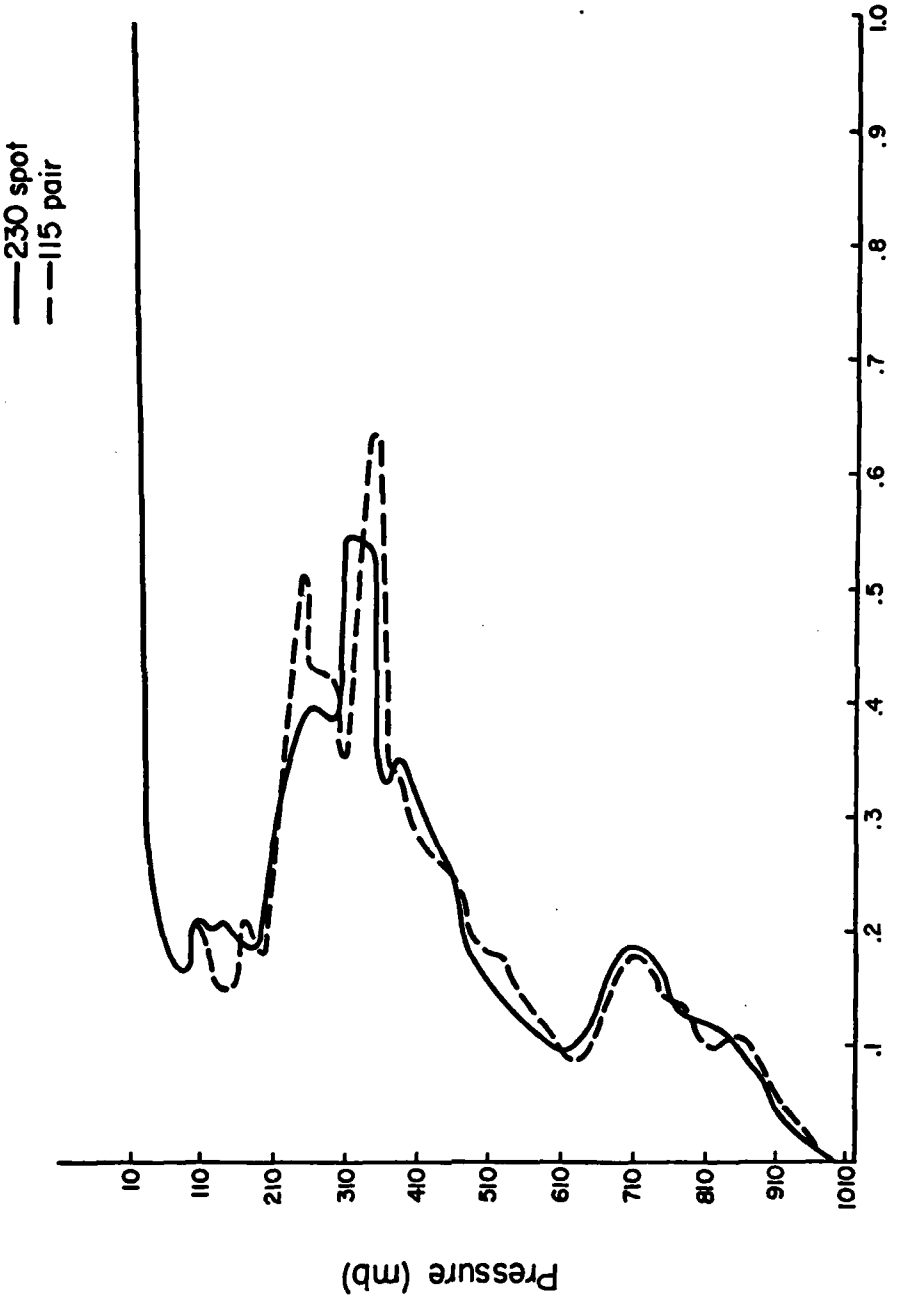

Figure 41. Broadband weighting curves for specified and retrieved two peaked effective cloud top distribution.

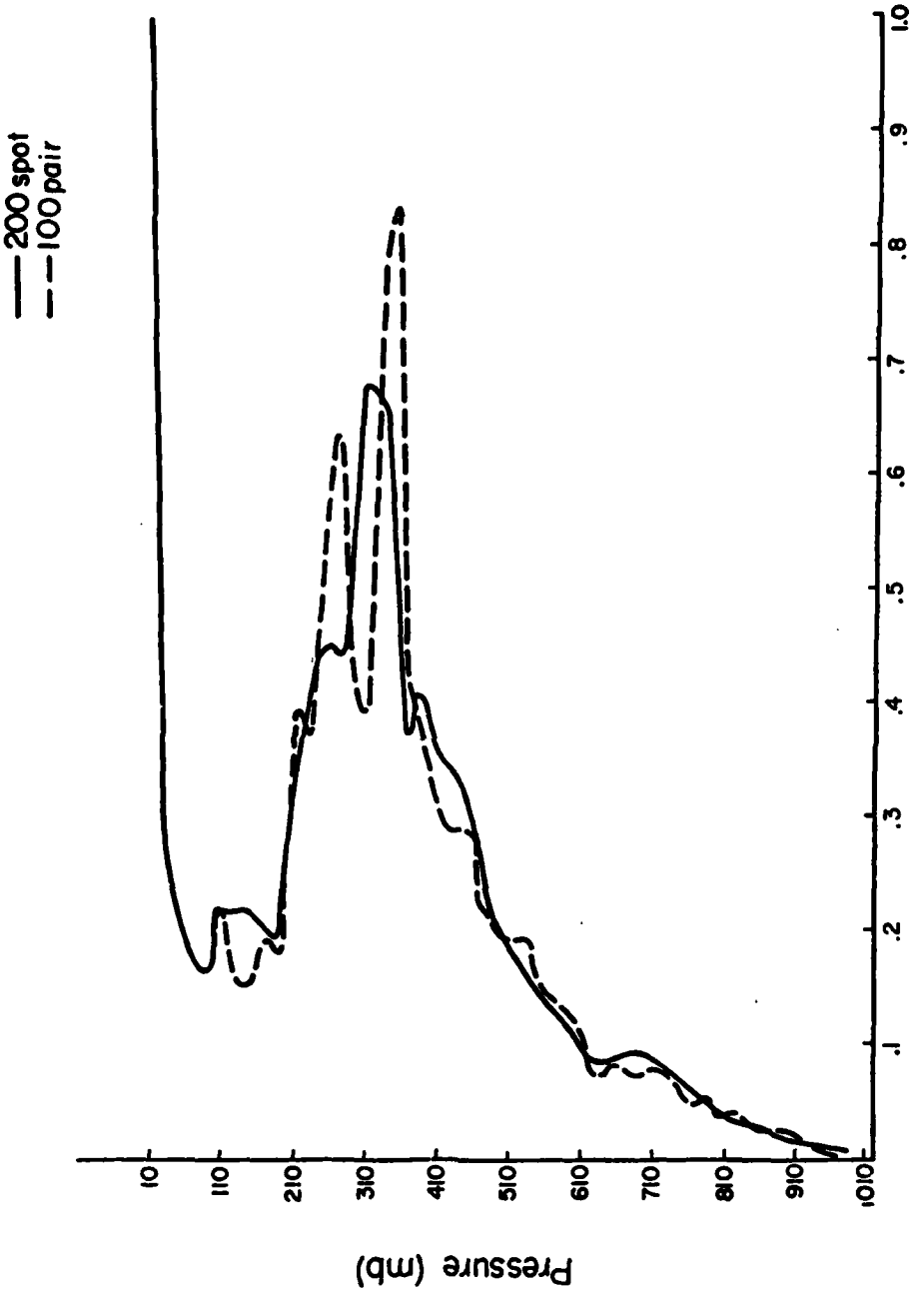

Figure 42. Broadband weighting curves for specified and retrieved one peak effective cloud top distribution.

curves. Notice that errors associated with u-per tropospheric radiating surface retrievals are the greatest. Figure 41 allows direct comparison between high and low atmospheric radiating surfaces and their effect on the weighting curve. Consequently Figure 42, which is the upper tropospheric single peak distribution plot, is taken to represent the severest test case. If retrieval errors are acceptable for this case, then one would expect them to be acceptable for nearly all other effective cloud top distributions.

Table 8 gives the results of a statistical analysis of the differences between the plotted curves in Figures 40-42. The statistical test is fully explained in Chapter VI. The values in Table 8 indicate that for all cases including the so-called worse case there is a high probability that the specified versus retrieved curves are not different.

From this experiment it appears that the assumption of one representative p_{wf} level in the radiometer field of view leads to only small errors when considered for the case of compositing weighting function curves. Of course for the single retrieval case, calculating a single set of p_{wf} and α values can lead to a retrieved weighting curve that is much different from the true one. There may be a question of the representativeness of the effective cloud top distributions specified. Figure 16 gives distribution plots of window radiances which for the most part relate directly to the cloud top distribution. Each plot represents over 900 measurements from a 200 x 200 km section for a specific time from a geostationary satellite. Notice the large number of 1 peak distributions. Although errors in this window radiance data analysis tend to broaden the peaks, they are still quite steep peaks.

It appears from an examination of Figure 16 that the experimental distributions specified above represent nearly a worse case consideration. In other words, steep peaked distributions imply that the assumption of a single radiating surface is for many cases nearly true. The tests above address the problem of the assumption always being false.

E. Minimizing the errors

Throughout this Appendix different techniques have been used to minimize retrieval weighting function errors (sometimes in the form of p_{wf} and α) due to the shortcomings of the basic approach assumptions. These methods include using a clear column radiance correction (CCRC) and stressing the use of composite weighting curves instead of single scene retrievals. The treatment of boundary conditions explained in the Chapter V introduction may also be viewed as a device to limit retrieval errors.

It is also important to view the general approach of using weighting function curves as a major way of minimizing errors. Used as a representation of the atmosphere's vertical infrared radiative emitting structure (VIRES), the composite broadband weighting curves are a measure of climatological cloudiness that is most complimentary to the satellite radiative measurements. As a result, the conditions under which the retrieval of weighting function curve shape parameters is weakest is exactly the condition under which the error effect is least. An advantage important to the approach of averaging over time is the ability to use this retrieval technique day or night with equal reliability.

Finally, to minimize errors further one uses the best information possible. This includes using retrieved clear sky radiance values. A disadvantage of this technique is that to use retrieved temperatures and humidity profiles would mean solving for the C and D values again. Of course sets of C and D values for different scenarios could be precalculated. Then the set corresponding closest to the measured profiles could be used. However, for most applications simple season values of C and D for specific areas should be sufficient when used with CCRC.

In summary, this Appendix examined the errors associated with retrieval of the weighting curve shape parameters or with the weighting curve composites. As indicated by Tables 7 and 8 the empirical RTE technique gives results that in the mean represent small errors. Of course only a sample of reasonable simulated error source values are used in the analysis. Nevertheless, the results indicate that the empirical RTE retrieval technique gives usefully accurate results.

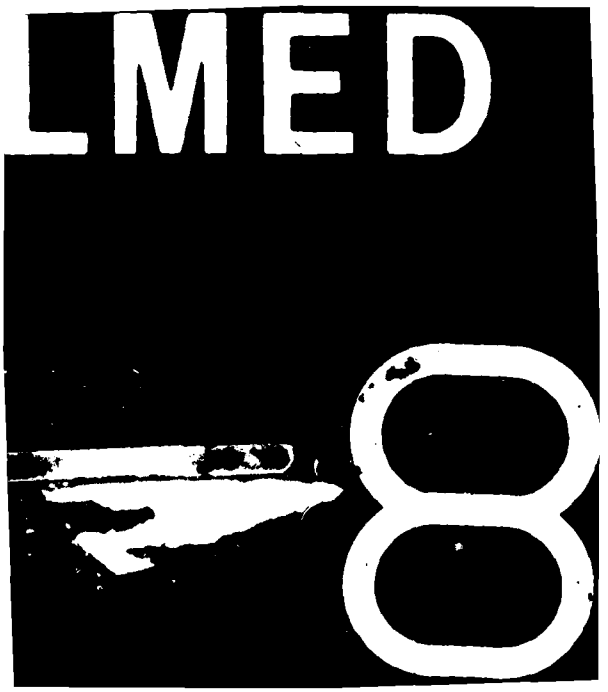
LMED
8